CHALMERS
UNIVERSITY OF TECHNOLOGY

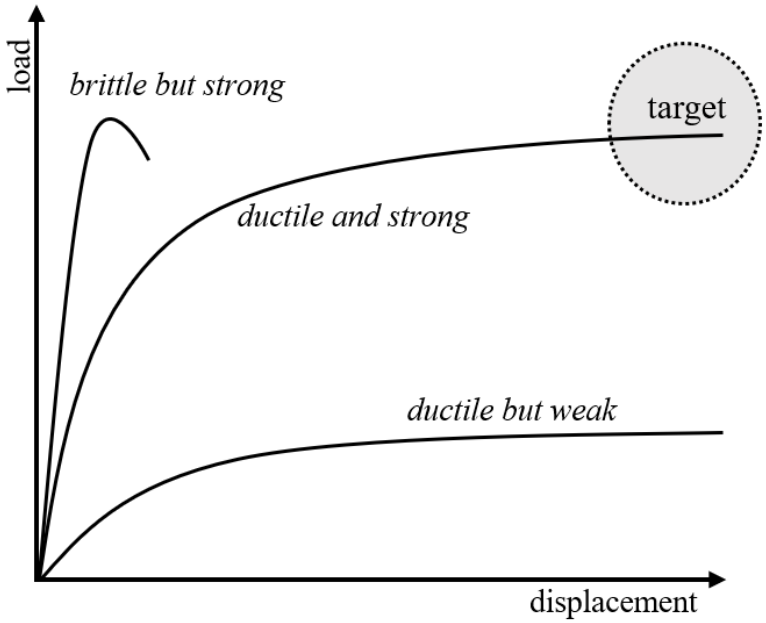

Impact of connections on the system behaviour and reliability of timber structures

Nonlinear Finite Element analyses of laterally loaded CLT wall systems

Master's thesis in Structural Engineering and Building Technology

MICHAELA HENRIKSSON
ANNA ROSENBERG

Department of Architecture and Civil Engineering
Division of Structural Engineering
Group for Light-Weight Structures
CHALMERS UNIVERSITY OF TECHNOLOGY
Master's thesis ACEX30-19-34
Gothenburg, Sweden 2019

MASTER'S THESIS ACEX30-19-34

Impact of connections on the system behaviour and reliability of timber structures

Nonlinear Finite Element analyses of laterally loaded CLT wall systems

Master's thesis in Structural Engineering and Building Technology

MICHAELA HENRIKSSON
ANNA ROSENBERG

Department of Architecture and Civil Engineering
Division of Structural Engineering
Group for Light-Weight Structures
CHALMERS UNIVERSITY OF TECHNOLOGY

Gothenburg, Sweden 2019

Impact of connections on the system behaviour and reliability of timber structures
Nonlinear Finite Element analyses of laterally loaded CLT wall systems
MICHAELA HENRIKSSON
ANNA ROSENBERG

Master's thesis ACEX30-19-34
Department of Architecture and Civil Engineering
Division of Structural Engineering
Group for Light-Weight Structures
Chalmers University of Technology
SE-412 96 Gothenburg
Sweden
Telephone: +46 (0)31-772 1000

Cover:
Illustration of load-displacement curves, describing the relationship between strength and ductility.

Chalmers Reproservice
Gothenburg, Sweden 2019

Impact of connections on the system behaviour and reliability of timber structures
Nonlinear Finite Element analyses of laterally loaded CLT wall systems
Master's thesis in Structural Engineering and Building Technology
MICHAELA HENRIKSSON
ANNA ROSENBERG
Department of Architecture and Civil Engineering
Division of Structural Engineering
Group for Light-Weight Structures
Chalmers University of Technology

ABSTRACT

Current design of timber structures is usually based on an element-by-element approach, mostly for simplicity and due to lack of knowledge of the exact structural behaviour of the connections. For Cross Laminated Timber (CLT) structures, the behaviour of the applied connections, i.e. stiffness and strength, is of high importance in terms of global structural behaviour. Improved knowledge about the stiffness properties and the load-deformation behaviour of connections is therefore crucial for a more efficient and reliable design of CLT systems.

The aim is to develop guidance for a more robust and reliable design of CLT structures, focusing on the stiffness and load-deformation behaviour of connections in laterally loaded CLT wall systems. The reliability of CLT wall structures is evaluated by accounting for the variability of the properties of the applied connections, including; load-carrying capacity, initial stiffness and ductility. Initially, a linear analysis is carried out for two types of connections, hold-downs and angle brackets, where wall systems consisting of two, four and eight connections are studied. When the linear behaviour is verified through comparison of the global wall stiffness between the FE-analysis and linear-elastic hand calculations, a nonlinear FE-analysis is performed, this time only for wall systems with hold-downs. Here, the global load-carrying capacity and the load distribution in the systems are studied. The analysis is based on; already existing theories regarding load-deformation, test data and coefficients of variability provided in published reports. To take the variability of the connections into consideration to be able to evaluate the structural reliability of an entire structure, Monte Carlo simulations were applied on the nonlinear FE-analyses. Additionally, the ductility ratio in the connections is varied, to make it possible to study the influence of the ductility on the global load-carrying capacity.

In general, both the nonlinear analyses and the design approach according to Eurocode 5 show that the first connection in the wall system is the most important one in terms of global load-carrying capacity. The nonlinear analyses show that when the maximum load is reached in the first connection, the load is redistributed to the other connections through parallel action, and the global load-carrying capacity of the wall system is not reached until several of the connections have come across their maximum point. While, in Eurocode, the global load-carrying capacity of the wall system is attained when the load-carrying capacity of the first connection is reached. Further, the effects of the variation of the material properties decrease with an increase of number of elements in the structure, provided that sufficient ductility of the connections can be guaranteed. For insufficient load-redistribution between the elements, however, the variation of the connections can lead to unpredictable global failure. This also needs to be accounted for in Eurocode 5.

Keywords: CLT wall system, Cross Laminated Timber structure, variability of connection properties, structural reliability, global load-carrying capacity, load-displacement curve, Eurocode 5, ductility

Impact of connections on the system behaviour and reliability of timber structures
Nonlinear Finite Element analyses of laterally loaded CLT wall systems
Examensarbete inom Structural Engineering and Building Technology
MICHAELA HENRIKSSON
ANNA ROSENBERG
Instutitionen för Arkitektur- och Samhällbyggnadsteknik
Avdelningen för Konstruktionsteknik
Lättviktskonstruktioner
Chalmers tekniska högskola

SAMMANFATTNING

Nuvarande design av träkonstruktioner är vanligtvis baserad på en element-för-element metod, huvudsakligen för enkelhetens skull men även på grund av bristande kunskap kring det strukturella beteendet hos träförband. När det kommer till konstruktioner av korslimmat trä (KL-trä) så är anslutningarnas egenskaper, dvs. styvhet och hållfasthet, av stor betydelse gällande det globala strukturella beteendet. Fördjupad kunskap angående styvhetsegenskaper och last-deformationsbeteende hos träförband är därför avgörande för, en i framtiden mer effektiv och pålitlig design av KL-träsystem.

Syftet med detta examensarbete är att utveckla riktlinjer för en mer robust och pålitlig design av KL-träsystem, med fokus på styvhet och last-deformationsbeteende hos träförband i en väggkonstruktion av KL-trä som utsätts för en horisontell punktlast. Tillförlitligheten hos väggkonstruktioner av KL-trä utvärderas genom att ta hänsyn till variabiliteten av anslutningarnas egenskaper, gällande; hållfasthet, initial styvhet och duktilitet. Inledningsvis utförs en linjär analys för två olika typer av vinkelbeslag, där väggsystem bestående av två, fyra och åtta anslutningar studeras. När det linjära beteendet har verifierats genom jämförelse av den globala väggstyvheten mellan FE-analysen och linjär-elastiska handberäkningar, så genomförs en ickelinjär FE-analys, denna gång enbart för väggsystem med den ena typen av vinkelbeslag. Här studeras den globala hållfastheten samt lastfördelningen i de tre väggsystemen. Analysen bygger på; redan befintliga teorier gällande last-deformation, data från utförda tester samt variationskoefficienter som tillhandahållits ur publicerade rapporter. För att ta hänsyn till variabiliteten hos anslutningarna för att vidare kunna utvärdera den strukturella tillförlitligheten för ett helt system, används Monte Carlo simuleringar vid de ickelinjära FE-analyserna. Dessutom varieras duktilitetsnivån i anslutningarna, detta för att göra det möjligt att studera duktilitets inverkan på den globala bärförmågan.

Generellt påvisar resultaten, både från de ickelinjära analyserna och utifrån designmetoden enligt Eurokod 5, att den första anslutningen i väggsystemet är den mest viktiga med avseende på global bärförmåga. De ickelinjära analyserna visar att när den maximala lasten är uppnådd i det första träförbandet, omfördelas lasten till de andra anslutningarna via parallell verkan, och den globala bärförmågan hos väggsystemet är inte nådd förrän flera av anslutningarna har överskridit sin maximala punkt. I Eurokod däremot, uppnås den globala bärförmågan för väggsystemet när den första anslutningen når sin bärförmåga. Vidare ses att effekterna till följd av variationen av materialegenskaper minskar med ökat antal träförband i väggstrukturen, förutsatt att tillräcklig duktilitet hos anslutningarna kan säkerställas. För bristfällig lastfördelning mellan elementen däremot, kan variationen hos träförbanden leda till en oförutsägbar global kollaps. Detta bör också beaktas i Eurokod 5.

Nyckelord: KL-trä väggkonstruktion, Korslimmat träsystem, variabilitet av egenskaper hos träförband, strukturell tillförlitlighet, global bärförmåga, last-deformationskurva, Eurokod 5, duktilitet

CONTENTS

List of Figures

List of Tables

PREFACE

This master's thesis was carried out at the Division of Structural Engineering, department of Architecture and Civil Engineering at Chalmers University of Technology, Sweden. The thesis has been performed from January 2019 to June 2019.

We would like to thank our supervisor Robert Jockwer, Assistant Professor at the division of Structural Engineering at Chalmers University of Technology, for his expertise during this thesis work. Without your contribution and excellent guidance, we would not have been able to carry out this thesis. We would also like to thank our examiner Associate Professor Mohammad Al-Emrani for his guidance throughout this thesis.

Finally, we would like to thank our opponents Simon Nilsson and Petter Öhman for their great feedback.

Michaela Henriksson and Anna Rosenberg

Gothenburg, June 2019

Acronyms

cdf Cumulative Distribution Function. 18

CLT Cross Laminated Timber. 4

CoV Coefficient of Variation. 19

LVL Laminated veneer lumber. 47

pdf Probability Density Function. 18

PoR Point of Rotation. 59

SLS Serviceability Limit State. 51

std Standard Deviation. 19

ULS Ultimate Limit State. 51

Nomenclature

Subscripts

AB	angle bracket
ax	axial
CLT	Cross Laminated Timber
con	connection
eff	effective
el	elastic
HD	hold-down
ini	initial
max	maximum
pl	plastic
R	resistance
S	loading
u	ultimate
y	yield

Greek letters

α, β	angles
γ_m	partial safety factor
σ	standard deviation
μ_f	coefficient of friction
ν	poisson ratio (-), lateral displacement (mm)
ν_{bn}	bending deformation (mm)
ν_{CLT}	deformation of CLT (mm)

v_{max} displacement corresponding to F_{max} (mm)
v_{rg} lateral displacement due to rocking (mm)
v_{sh} shear deformation (mm)
v_{sl} lateral displacement due to sliding (mm)
v_{tot} total lateral deflection (mm)
v_z vertical displacement due to rocking (mm)
ϕ rotation angle of CLT wall element
ρ density (kg/m^3)

Roman lower case letters

d diameter (mm)
f_c compression strength (kN)
f_h embedment strength (kN/mm)
h height (mm)
k_{mod} modification factor (-)
l length (mm)
l_p length of compression zone (mm)
n number of elements (-)
n_P compression strength for a connection (kN)
q uniformly distributed vertical load acting on wall system (kN/mm)
t thickness (mm)
v_{max} displacement at maximum load (mm)
v_{max} displacement at maximum loading (mm)
v_u ultimate displacement (mm)
v_y yield displacement (mm)

Roman capital letters

A Area (mm^2)
D Ductility (-)
E Modulus of Elasticity (kN/mm^2)
F Load (kN)
$F_{ax,Rk}$ Characteristic withdrawal capacity of the fastener (kN)
F_{max} Maximum load-carrying capacity of connection (kN)
F_t Point of intersection between the asymptote and the ordinate (kN)
$F_{v,Rd}$ Design load-carrying capacity (kN)
$F_{v,Rk}$ Characteristic load-carrying capacity (kN)
$F_{v,R}$ Load-carrying capacity per connection (kN)
G Shear modulus (kN/mm^2)
K_{ini} Initial stiffness (kN/mm)
K_p Post elastic stiffness (kN/mm)
K_{ser} Slip modulus (kN/mm)
M_y Yield moment (kN/mm)
P_f Probability of failure (-)
R_m Bending strength (kN/mm^2)

1 Introduction

1.1 Background

Current design of timber structures is usually based on an element-by-element approach, mostly for simplicity and due to lack of knowledge of the exact structural behaviour of the connections. This approach is not suitable when looking at the global structural behaviour. The reliability of the entire structural system must be evaluated in dependency of the consequences of failure of individual members and connections, which may cause local or global failure.

In large timber structures, connections are highly important details. Joints are not only responsible for connecting timber elements and transferring loads but also to provide stiffness and ductility. The property ductility, intended for assessing the plastic capacity of a joint, is barely mentioned in Eurocode 5. Effect of deformations has so far been applied mostly in seismic design of structures (Eurocode 8) whereas Eurocode 5 mainly considers the load-carrying capacity of connections.

Static models are usually assumed where joints are considered as simply pinned or rigid. This approach is appropriate and leads to proper results when designing structures with several linear shaped elements with a relatively high slenderness (Flatscher, 2017, p. 1). The actual behaviour of the joints, however, lies somewhere in between pinned and rigid, also known as semi-rigid. Flatscher (2017, p. 1) writes;

"As a rule of thumb, it can be stated that as compact timber elements are, as important connections' stiffness and ductility for a well-tempered behaviour of the structure gets. This particularly applies to cross-laminated timber (CLT) structures exposed to lateral loads, i.e. earthquakes or heavy wind loads."

Considering only the load-carrying capacity of a connection when designing a structure is straight forward only with statically determinate structures. In case of statically indeterminate structures, the deformation capacity of the connection is of high importance. Better knowledge about the stiffness properties and the load-deformation behaviour of connections is crucial for a more efficient and reliable design of connections in structural systems.

1.2 Aim

The aim of the proposed master's thesis is to develop guidance for a more robust and reliable design of high-performance structures enabling a more efficient use of timber as construction material, focusing on the stiffness and load-deformation behaviour of connections in Cross Laminated Timber. The goal is to evaluate the impact of connections on the performance of laterally loaded CLT wall elements, connected to the floor, and to evaluate the reliability of the entire structural system accounting for the variability of the properties of the connections, including; load-carrying capacity, initial stiffness and ductility.

1.3 Limitations

The study is limited to two systems, where both systems consist of a CLT wall connected to a concrete foundation. The load case is narrowed down to one lateral load, acting at the upper corner of the CLT wall system, ignoring the self-weight of the CLT element and uniform loads from a possible roof. In the first system, hold-downs are used as connections, limited to only act in tension as it is the primary area of use for hold-downs. The second system have angle brackets as connection between the CLT wall and the concrete foundation. These can resist load both vertically and horizontally but with the simplification that the stiffness is equally large in both directions. The number of connections studied in each system is limited to 2, 4 and 8, resulting in a total of six different set-ups of the model.

The type of CLT that will be studied is limited to CLT panels with three layers where the layers are glued together. The thickness of the CLT wall element is kept constant and parameters such as moisture is not considered. Only the deformations of the CLT wall system, i.e. the CLT wall and the applied connections are of interest in this thesis. Thus, the concrete floor, which the CLT wall is connected to, is assumed to be rigid.

For the connections, the steel plate could get subjected to bending at the corner of the plate. The behaviour of the plate could be nonlinear. The analysis is not going to address the nonlinear behaviour of the steel plate but will be limited to capacity of the fasteners and focus on the connection of the fasteners to the timber and the steel plate. The properties of the steel plate for angle brackets and hold-downs are neglected, whereas the fasteners' properties will represent the behaviour of the connections. In particular, the stiffness of each connection is represented by the total stiffness of the applied fasteners in the connection.

There is a strive to make the model no more complex than necessary. The model will therefore be designed with spring elements that represent the connections, as the simplification with the fasteners allow. The system will be simplified even further by creating symmetry, if the connections are applied on both sides of the CLT wall element. In this way, the effects of eccentricity can be neglected. The nonlinear springs are limited to only depend on force and relative displacement. Dependency of temperature and other field variables are be out of the scope and are thereby not included.

For verification of the finite element analysis, the results will be compared with hand calculations which will be carried out according to Eurocode 5. No other standard documentation will be considered in the comparison since the thesis will be published within Europe where Eurocode is the official standard.

1.4 Method

The project will be carried out in three phases where the first phase consists of a literature study of timber connections and their reliability. The material properties of different timber materials are studied, and the variability of the data is analysed. Furthermore, the literature study is focused on gaining a better understanding of different types of connections and their application as well as how the design of fasteners in timber structures are approached in Eurocode 5. Great emphasis is placed on examining the load-deformation behaviour of connections and analysing different proposed models of load-displacement curves for determining the different parameters of the connections.

In the second phase of the thesis a Finite Element model of the CLT wall connected to the floor with hold-downs and another with angle brackets is developed in Abaqus/CAE. Initially, a linear analysis is established and then a nonlinear, where the behaviour of the fasteners is analysed regarding deformation under loading. Furthermore, a Monte Carlo simulation is performed where the input data of the material properties, such as stiffness and load-carrying capacity are varied. Here, also the variation of ductility ratio is considered.

In parallel with the finite element analyses, a numerical analysis based on hand calculations using Eurocode 5 is carried out in order to obtain reference values for the load-carrying capacity of the connections. An evaluation of the results and a comparative analysis between the results obtained from the simulations and the calculated reference values is conducted in the third phase.

2 Theory

This chapter presents the reader with a theoretical background of CLT systems and their structural reliability. First, an overview of the material and the connections studied are presented, followed by the variability of the studied material and connections. Further, different load deformation curves and methods to determine these are described. This is followed by a short explanation of analytical approximations for load-displacements curve. After that, the two different types of modelling CLT elements are presented; force-based and displacement-based models. Finally, a brief description of calculations according to the European standard Eurocode 5 are presented.

2.1 CLT - Cross Laminated Timber

Cross Laminated Timber (CLT) is a building product composed of an uneven number of layers of boards, made of sawn timber, crosswise arranged with an angle of 90° and glued together. CLT is commonly manufactured with three, five or seven layers and the thickness of the layers varies. In Figure 2.1, a CLT panel with five glued layers is shown. Some CLT boards are manufactured using nails or screws instead of adhesive but those products do not dominate the market. (Swedish Wood, 2016, p.60)

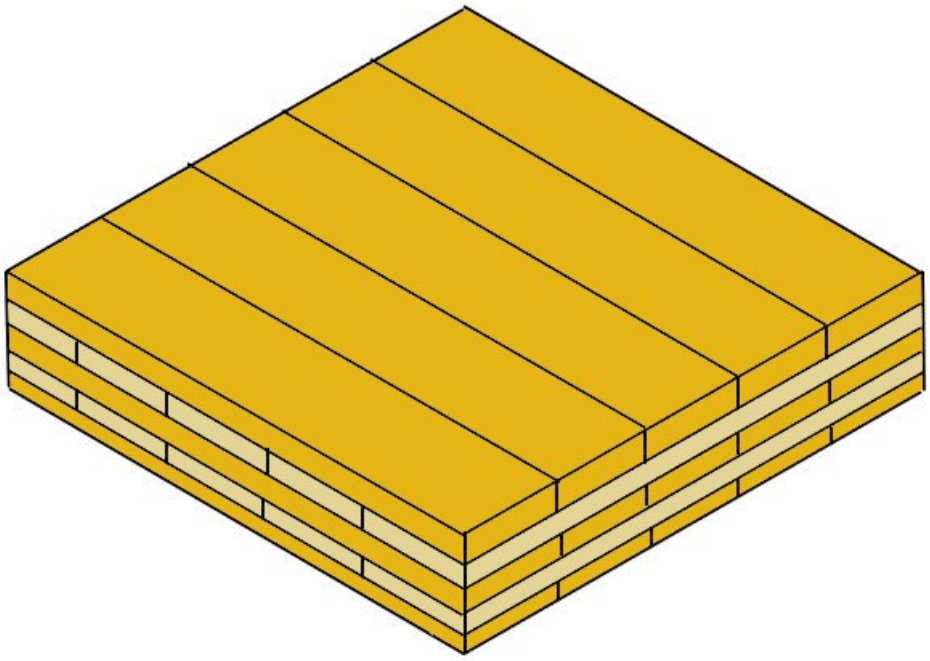

Figure 2.1: *Cross Laminated Timber panel with five layers.*

The uneven number of layers gives an element where the outer layers are oriented in the same grain direction whereby an increase in strength of the element is obtained. The large-sized building product gets the structural ability of bearing loads both in- and out-of-plane. Due to its load bearing properties, CLT could be used as floor elements where it is acting as a plate, or as wall elements where it is bearing loads through panel action. Its thickness allows it to be used as a stand-alone structural element with good properties when it comes to strength and stiffness. (Sigrist, 2018, p.128)

CLT is a young timber building product, that since its commercial introduction 20 years ago is increasing in popularity in multi-storey buildings as well as in commercial buildings. This because of not only the advantageous properties previously mentioned but also due the fact that the industrial production processes of CLT is relatively straightforward and the final products are easily assembled. Furthermore, the variability in the physical and mechanical properties is reduced thanks to its homogeneous character. (Ringhofer, Brandner, & Blass, 2018)

2.2 Connections

The behaviour of the connections in CLT structures have a large influence on the entire system (Lukacs, Björnfot, & Tomasi, 2018, p.203). This chapter covers some commonly used fasteners in CLT systems. The fasteners presented below are all included in SIMPSON Strong-Tie (2019), a product catalogue of connectors and fastenings for use with CLT and glulam.

2.2.1 Screws, nails and threaded Rods

In this section, the screws, nails and threaded rods that are recommended by the earlier mentioned product catalogue will be presented. The fasteners included are either suitable for CLT or concrete, and the fasteners are intended to be used in combination with either a hold-down, see Section 2.2.2, or an angle bracket, see Section 2.2.3.

CSA - Structural Connector to Timber Screw

The CSA is a self-drilling flat head screw that has a type 17 point tip. Since the type 17 point tip is a sharp tip that is fluted, see Figure 2.2, chips are captured and the screw penetrates quickly through a CLT panel. The screw is available in both carbon steel and stainless steel and comes in several different dimensions. The different dimensions and the characteristic performance values are presented in Table 2.1. To better understand Table 2.1, an illustration of CSA screws with measurements and load direction is shown in Figure 2.2.

Table 2.1: *Dimensions and Characteristic Performance Values of CSA Screws (values obtained from SIMPSON Strong-Tie (2019, p.56)).*

Model Reference	Steel type	Dimensions [mm]				Axial [kN]
		d	l	d_h	l_g	$F_{ax,Rk}$
CSA4.0x30	Carbon	3.9	30	7.3	24	1.28
CSA5.0x25		4.9	25	8.3	19	1.38
CSA5.0x35		4.9	35	8.3	29	2.11
CSA5.0x40		4.9	40	8.3	34	2.47
CSA5.0x50		4.9	50	8.3	44	3.20
CSA5.0x25S	Stainless	4.9	25	8.3	19	1.38
CSA5.0x35S		4.9	35	8.3	29	2.11
CSA5.0x40S		4.9	40	8.3	34	2.47

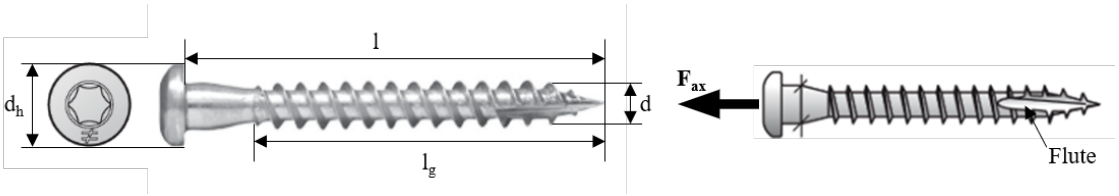

Figure 2.2: *Illustration of CSA screws with measurements and load direction.*

CNA - Ring Shank Nail

The CNA is an annular ring shank available in several different dimensions. The nail is made in both carbon steel and stainless steel, but carbon steel is for interior applications only according to SIMPSON Strong-Tie (2019). The grade 304 stainless steel nails are intended for exterior applications and corrosive environments. In Table 2.2 the dimensions and the characteristic performance values for CNA ring shank nails are presented. An illustration of CNA ring shank nails with measurements and load direction is shown in Figure 2.3 in order to complement the data given in Table 2.2.

Table 2.2: *Dimensions and Characteristic Performance Values of CNA Nails (values obtained from SIMPSON Strong-Tie (2019, p.57)).*

Model Reference	Steel quality	Dimensions [mm]				Axial [kN]
		d	l	d_h	l_g	$F_{ax,Rk}$
CNA4.0x35	Carbon	4.0	35	8	19	0.64
CNA4.0x40		4.0	40	8	24	0.76
CNA4.0x50		4.0	50	8	34	1.01
CNA4.0x60		4.0	60	8	44	1.25
CNA4.0x35S	Stainless	4.0	35	8	19	0.64
CNA4.0x50S		4.0	50	8	34	1.01
CNA4.0x60S		4.0	60	8	44	1.25

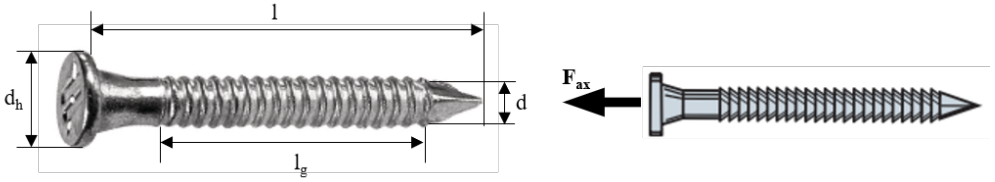

Figure 2.3: *Illustration of CNA ring shank nails with measurements and load direction.*

LMAS - Threaded Rod

It is suggested by Simpson Strong-Tie that a LMAS threaded rod is used as anchorage of hold-downs and angle brackets to concrete. In Table 2.3 the different LMAS products available at Simpson Strong-Tie together with the dimensions are displayed. An illustration of a LMAS threaded rod with measurements are shown In Figure 2.4 to clarify the dimensions in Table 2.3.

Table 2.3: *LMAS threaded rods and dimensions available at Simpson Strong-Tie.*

Product	d	l [mm]
LMAS M8 x 95	M8	95
LMAS M8 x 110	M8	110
LMAS M10 x 110	M10	110
LMAS M10 x 130	M10	130
LMAS M10 x 150	M10	150
LMAS M12 x 120	M12	120
LMAS M12 x 150	M12	150
LMAS M12 x 185	M12	185
LMAS M16 x 170	M16	170
LMAS M20 x 200	M20	200
LMAS M24 x 310	M24	310

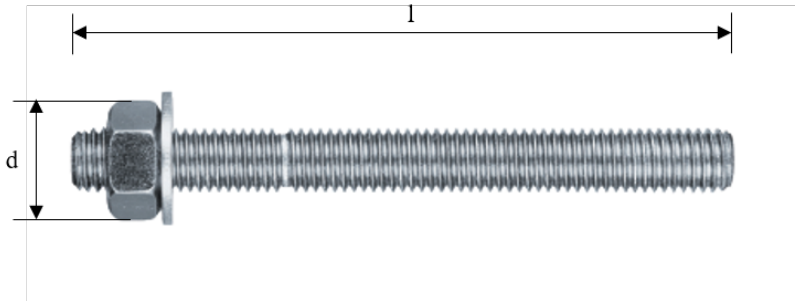

Figure 2.4: *Illustration of LMAS threaded rod with measurements.*

Intended to be used in conjunction with the LMAS threaded rod, is the high performance resin AT-HPBN380-UK. This resin is also a product of Simpson Strong-Tie and it is suitable for use with threaded rod into concrete and is specially designed for construction uses.

2.2.2 Hold-downs

Hold-downs are a type of connection that is designed to carry tensions (i.e., uplift forces) (Pozza, Ferracuti, Massari, & Savoia, 2018, p.96). Simpson Strong-Tie developed connections for use with Cross Laminated Timber and their two hold-downs of model HTT; the HTT5 and the HTT22E can connect a CLT wall with a concrete floor to resist the uplift forces acting on the wall element. As stated in SIMPSON Strong-Tie (2019), the material of the hold-downs is pre-galvanised mild steel and the dimensions are presented in Table 2.4 and Figure 2.5.

Dimensions [mm]	Modal Reference	
	HTT5	HTT22E
A	404	558
B	62	61
C	64	64
t	3.0	3.0
t_{base}	11.0	12.0

Table 2.4: *Dimensions of the hold-downs HTT5 and HTT22E (values obtained from SIMPSON Strong-Tie (2019, p.16)).*

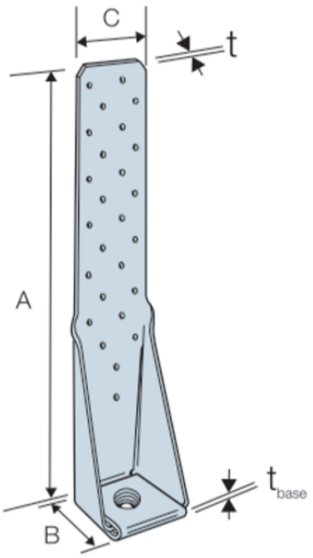

Figure 2.5: *Illustration of a hold-down connection (SIMPSON Strong-Tie, 2019, p.16).*

The different characteristic capacities of the hold-downs HTT5 and HTT22E are listed in Table 2.5 and the force direction is depicted in Figure 2.6. For the characteristic capacities to be valid, a M16 bolt should be used for anchorage of the HTT5 and the HTT22E to the concrete floor and for anchorage to the CLT wall panel, 14 fasteners should be used for the HTT5, 24 fasteners for the HTT22E. It is regulated in SIMPSON Strong-Tie (2019) that the lower 10 nail holes for the HTT22E must always be filled. For the HTT5, there are also rules regarding which holes that always need to be filled. Figure 2.7 shows the nailing pattern of the two types of hold-downs and the holes highlighted in red are the ones that must be filled with relevant fasteners.

Table 2.5: *Characteristic capacities of the hold-downs HTT5 and HT22E connecting CLT wall to concrete floor, with one hold-down on each side of the wall (values obtained from SIMPSON Strong-Tie (2019, p.16) and multiplied with two).*

Force direction	Type of fastener	Characteristic capacity [kN]	
		HTT5	HTT22E
R_1	CNA 4.0x40 mm	37.2	75
	CNA 4.0x50 mm	46.6	84.6
	CNA 4.0x60 mm	49.6	96.8
R_1	CSA 4.0x40 mm	-	91
	CSA 4.0x50 mm	-	104.6

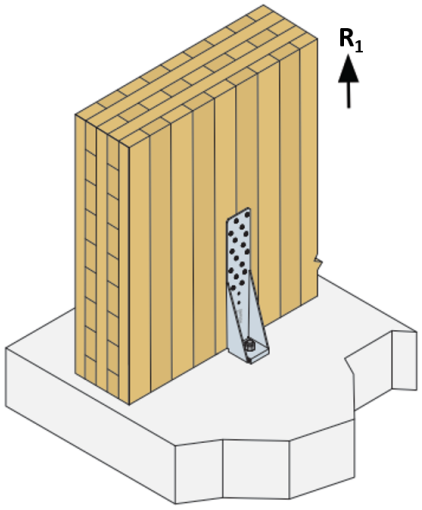

Figure 2.6: *Illustration of a hold-down connected to a CLT wall and a concrete floor, showing the load-carrying direction (redrawn from SIMPSON Strong-Tie (2019, p.16)).*

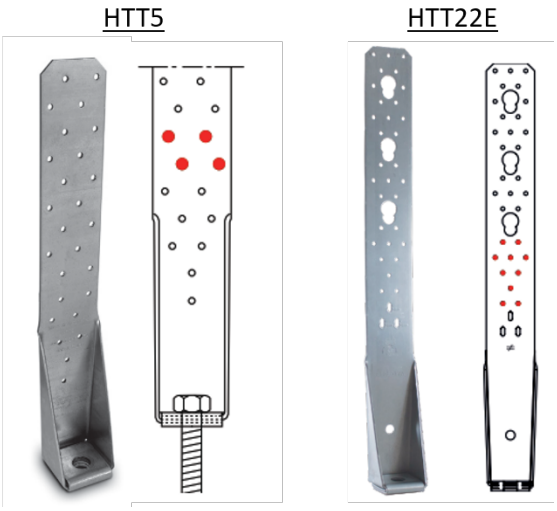

Figure 2.7: *A HTT5 hold-down and the fixing patter of timber to concrete connection (to the left). A HTT22E hold-down and the fixing pattern of timber to concrete connection (to the right). The red circles mark the holes that need to be filled with the recommended fasteners (redrawn from SIMPSON Strong-Tie (2019, p.16)).*

2.2.3 Angle brackets

Angle brackets are used for connecting walls to floors. To carry shear forces is described by Pozza et al. (2018) to be the main purpose of angle brackets, even though some angle brackets have the ability to carry both horizontal and vertical loads. A selection of angle brackets available in SIMPSON Strong-Tie (2019) is presented in this chapter. All the angle brackets included are suitable for connecting CLT walls with concrete floors. The fasteners that are being used have already been treated in Chapter 2.2.1.

BNV33 - Shear Angle Bracket

The BNV33 shear angle bracket is made of pre-galvanised mild steel and is according to SIMPSON Strong-Tie (2019) primarily designed to connect CLT walls with concrete floors. The BNV33 has a small height but a large width as can be seen in Table 2.6 and Figure 2.8. The width of the bracket allows for large spacing between the fasteners along the length of the wall and floor elements which gives good shear resistance. This type of angle bracket only carries horizontal shear forces and is therefore ideally combined with hold-downs that carries the vertical uplift forces in the system.

	Dimensions [mm]
A	63
B	35
C	180
t	1.5

Table 2.6: *Dimensions of the BNV33 shear angle bracket (values obtained from SIMPSON Strong-Tie (2019, p.20)).*

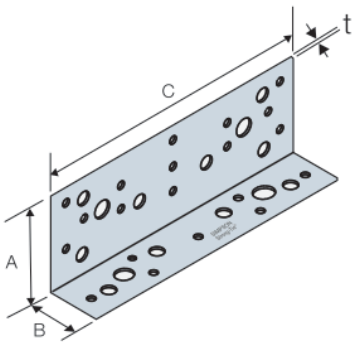

Figure 2.8: *Illustration of a BNV33 shear angle bracket with measurements (SIMPSON Strong-Tie, 2019, p.20).*

Fasteners of the previously mentioned type CNA is recommended by SIMPSON Strong-Tie (2019) to use for fastening the upper flange to the CLT wall. For anchorage of the lower flange to the concrete, LMAS threaded rods with the dimension M12 of the bolts are recommended, together with the high performance resin AT-HP. The characteristic capacity in shear of the BNV33 angle bracket is displayed in Table 2.7, where Figure 2.9 illustrates the force direction. The characteristic capacity presented in the table is based on two angle brackets, one on each side of the CLT wall. The value applies for the type of fastener that is stated in Table 2.7 and the set up according to the timber to concrete nailing pattern shown in Figure 2.10.

Table 2.7: *Characteristic capacity of the BNV33 shear angle bracket connecting CLT wall to concrete floor, with one bracket on each side of the wall (capacity obtained from SIMPSON Strong-Tie (2019, p.20) and multiplied with two).*

Force direction	Type of fastener	Characteristic capacity [kN]
R_2=R_3	CNA 4.0x40 mm	21.4

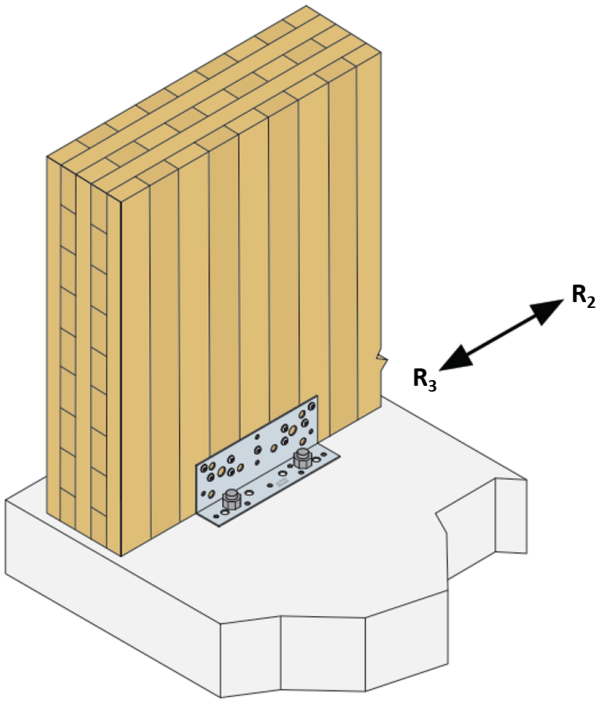

Figure 2.9: *Illustration of a BNV33 shear angle bracket connected to a CLT wall and a concrete floor, showing the load-carrying directions (redrawn from SIMPSON Strong-Tie (2019, p.20)).*

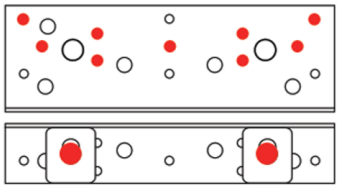

Figure 2.10: *The fixing pattern of timber to concrete where the red circles mark the holes that need to be filled with nails for the upper flange and bolts for the bottom flange (SIMPSON Strong-Tie, 2019, p.20).*

AE116 - Reinforced Angle Bracket

There are also some angle brackets that carry loads in both x and y direction. Several of these angle brackets together can be used as connections in a wall-to-floor system. The reinforced angle bracket of model AE116, available in the Simpson Strong-Tie catalogue fulfils structural requirements in timber to concrete connections. The AE116 reinforced angle bracket is made of pre-galvanised mild steel and have dimensions according to Table 2.8 and Figure 2.11.

	Dimensions [mm]
A	90
B	48
C	116
t	3

Table 2.8: *Dimensions of the AE116 reinforced angle bracket (values obtained from SIMPSON Strong-Tie (2019, p.21)).*

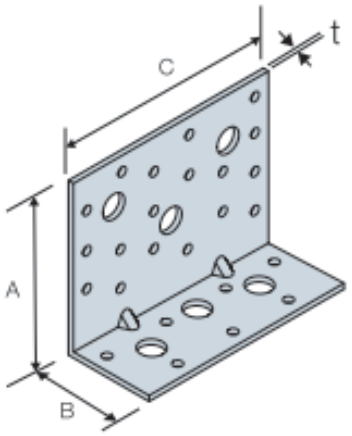

Figure 2.11: *Illustration of an AE116 reinforced angle bracket with measurements (SIMPSON Strong-Tie, 2019, p.21).*

According to Simpson Strong-Tie's product catalogue, CNA ring shank nails should be used for fastening the upper flange to the CLT wall. For the bottom flange, LMAS threaded rods of dimension M12, in combination with the high performance resin AT-HP is recommended. The characteristic capacities of the angle bracket AE116 is presented in Table 2.9, where Figure 2.12 illustrates the force direction. Note that the product capacities in Table 2.9 are based upon two angle brackets per connection, one on each side of the CLT panel. The values apply for the timber to concrete fixing pattern in Figure 2.13.

Table 2.9: *Characteristic capacities of AE116 reinforced angle bracket connecting CLT wall to concrete floor, with one bracket on each side of the wall (values obtained from SIMPSON Strong-Tie (2019, p.21)).*

Force direction	Type of fastener	Characteristic capacity [kN]
R_1	CNA 4.0x40 mm	12.6
	CNA 4.0x60 mm	12.8
R_2=R_3	CNA 4.0x40 mm	12.8
	CNA 4.0x60 mm	13.8

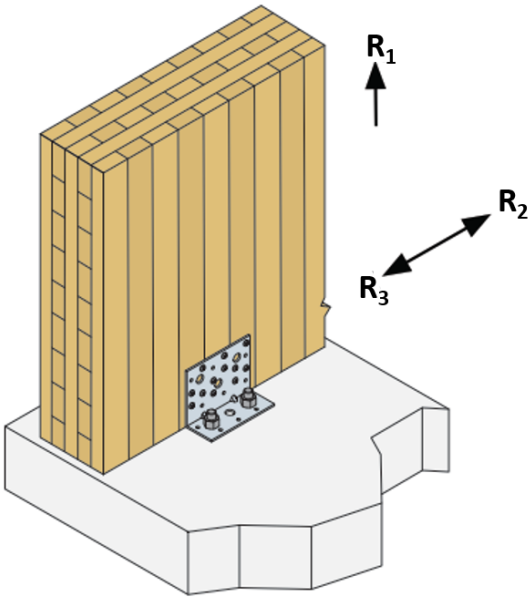

Figure 2.12: *Illustration of an AE116 reinforced angle bracket connected to a CLT wall and a concrete floor, showing the load-carrying directions (redrawn from SIMPSON Strong-Tie (2019, p.21)).*

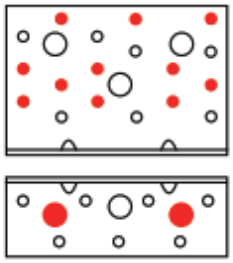

Figure 2.13: *The fixing pattern of timber to concrete connection using AE116 reinforced angle bracket. The red circles mark the holes that need to be filled with nails for the upper flange and bolts for the bottom flange (SIMPSON Strong-Tie, 2019, p.21).*

ACRL10520 - Reinforced Angle Bracket

Another angle bracket that carries both vertical and horizontal loads is the reinforced angle bracket of model ACRL10520. This angle bracket is also designed for fixing CLT walls to concrete floors and is made of pre-galvanised mild steel (SIMPSON Strong-Tie, 2019, p.31). Table 2.10 together with Figure 2.14 gives the dimensions of the ACRL10520.

	Dimensions [mm]
A	105
B	105
C	90
t	2

Table 2.10: *Dimensions of the ACRL10520 reinforced angle bracket (values obtained from SIMPSON Strong-Tie (2019, p.31)).*

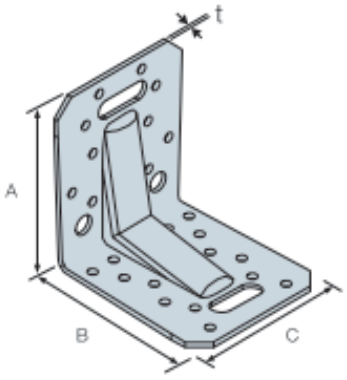

Figure 2.14: *Illustration of an ACRL10520 reinforced angle bracket with measurements (SIMPSON Strong-Tie, 2019, p.31).*

CNA ring shank nails are recommended by Simpson Strong-Tie as fasteners for connecting the upper flange to the CLT wall. For the connection of the bottom flange to the concrete floor, the LMAS threaded rods with the dimension M10 is recommended, together with the high performance resin AT-HP mentioned in Chapter 2.2.1. The product capacities of the ACRL10520 is shown in Table 2.11 where the performance values are based upon two ACRL10520 angle brackets per connection, one on each side of the CLT wall. The force directions are illustrated in Figure 2.15 and the values in Table 2.11 applies for two M10 bolts connected to the concrete, see Figure 2.15, and 14 CNA ring shank nails connected to the CLT wall panel.

Table 2.11: *Characteristic capacities of ACRL10520 reinforced angle bracket connecting CLT wall to concrete floor, with one bracket on each side of the wall (values obtained from SIMPSON Strong-Tie (2019, p.31)).*

Force direction	Type of fastener	Characteristic capacity [kN]
R_1	CNA 4.0x35 mm	24.1
	CNA 4.0x50 mm	28.5
R_2=R_3	CNA 4.0x35 mm	10.8
	CNA 4.0x50 mm	14.2

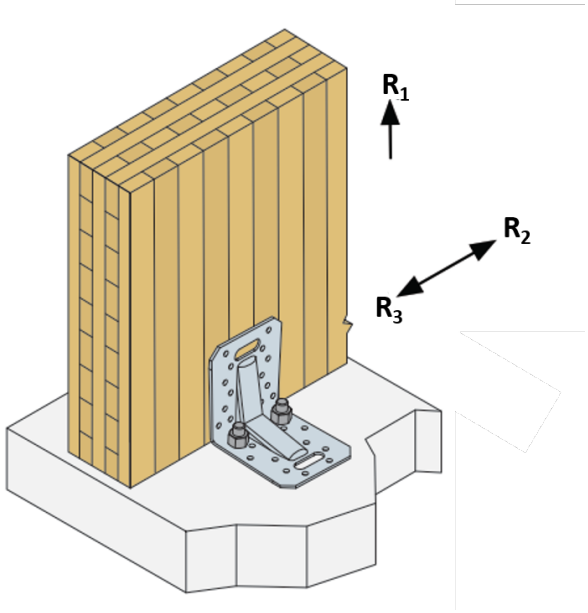

Figure 2.15: *Illustration of an ACRL reinforced angle bracket connected to a CLT wall and a concrete floor, showing the load-carrying directions (redrawn from SIMPSON Strong-Tie (2019, p.31)).*

2.2.4 Summary of connections

A summary of the characteristic capacity for the different types of connections described earlier in this chapter are illustrated in Figure 2.16. The different hold-downs can carry a significant higher load than the angle brackets in vertical direction. However, the hold-downs cannot take any load in horizontal direction and therefore the angle brackets are beneficial when taking load in more than one direction.

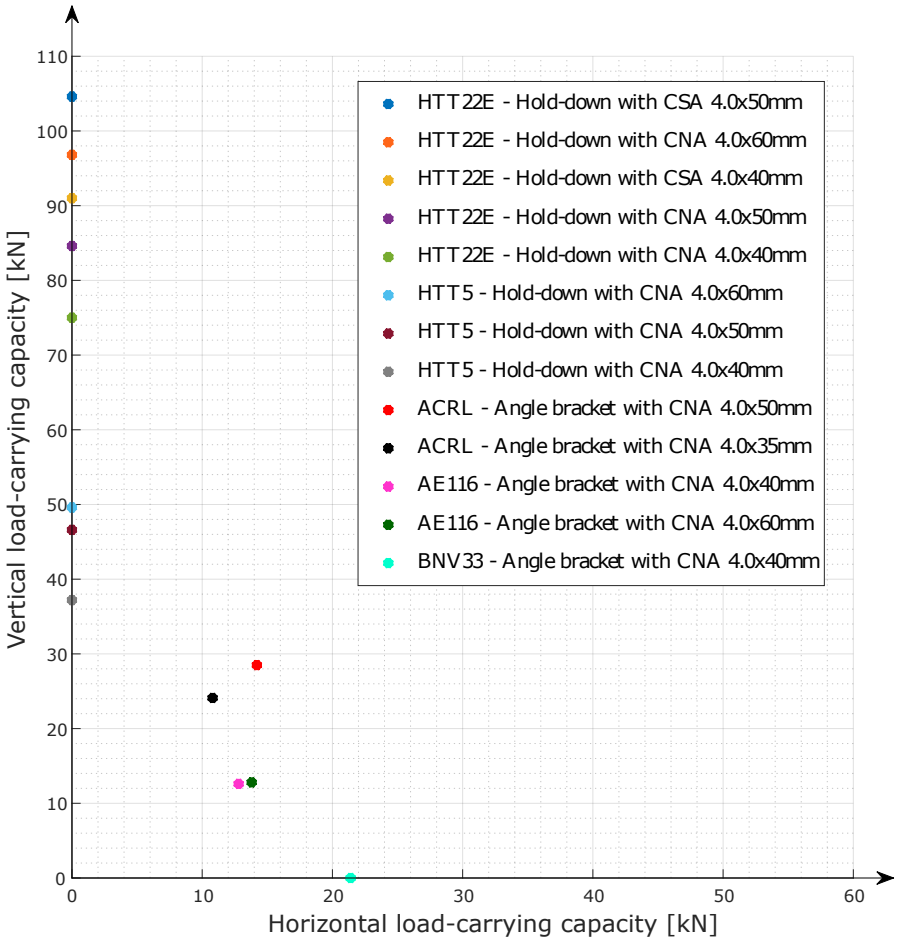

Figure 2.16: *Vertical and horizontal load-carrying capacity for different connections.*

2.3 CLT systems

The stiffness and the load bearing capacity in-plane and out-of-plane makes CLT panels structurally ideal in both single-family houses and multi-storey residential buildings, but also in tall office buildings, commercial buildings and even for wide-span structures such as bridges (Brandner, 2013). Currently, the potential of CLT is seen in medium and high-rise buildings. For low-rise single-family houses, CLT is not an economical choice of material (Brandner, 2013). The load bearing abilities makes CLT suitable in multi-storey buildings as floor elements and wall elements for load bearing walls, facades and shear walls.

2.3.1 CLT as shear walls

In multi-storey buildings, CLT panels are well capable of transferring lateral loads to the foundation while stabilising and reducing uplifting, which makes them suitable as shear walls. (Lukacs, Björnfot, & Tomasi, 2018)

A single CLT shear wall commonly consists of a CLT panel with 3 or 5 layers in general and connections to floor or foundation. Normally, the connections used are; hold-downs which take vertical loads, and angle brackets which resist horizontal shear forces (Lukacs, Björnfot, & Tomasi, 2018). A shear wall could be subjected to a uniform vertical load from a roof but it could also be loaded with a lateral load, representing a wind load. When the shear wall is subjected to a lateral load on the top of the CLT wall, a total lateral deflection v_{tot} occurs. The total lateral deflection is the sum of four types of deformations; sliding v_{sl} (rigid body translation), rocking v_{rg} (rigid body rotation), shear v_{sh} (deformation of the CLT panel) and bending v_{bn} (deformation of the CLT panel), all of which are included in Figure 2.17 and Equation 2.1. The sliding and rocking deformations mainly depend on the type of connections, their stiffness and their positions, while the shear and bending deformations are influenced by the different properties of the CLT element (Flatscher, 2017, p.107). The sliding and bending deformations are therefore often summarised as v_{CLT}.

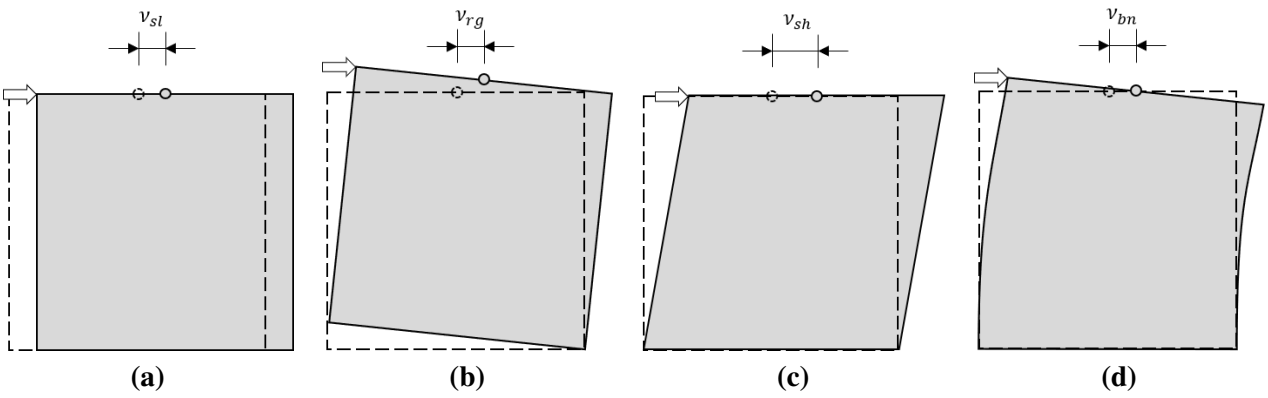

Figure 2.17: *Contributions to total lateral deflection of CLT wall system - (a) sliding v_{sl}, (b) rocking v_{rg}, (c) shear deformation of CLT panel v_{sh}, (d) bending deformation of CLT panel v_{bn}.*

$$v_{tot} = v_{sl} + v_{rg} + v_{sh} + v_{bn} = v_{sl} + v_{rg} + v_{CLT} \tag{2.1}$$

According to Flatscher (2017), experimental tests show that, for wall systems where the length and the height of the CLT panel are equal, the contribution from the CLT deformation to the total lateral deflection is usually less than 10 %. Furthermore, simulations reveal that for CLT wall systems where the length-to-height ratio is below 1.5, rocking is the primary deflection that is taking place. For systems that exceeds a ratio of 1.5, i.e longer walls, sliding is the dominant deflection.

As can be noticed by looking at Figure 2.17b, the horizontal displacement is somewhat different than for the other types of displacements shown in Figure 2.17. How to calculate the lateral displacement caused by rocking is described in Figure 2.18 together with Equation 2.2.

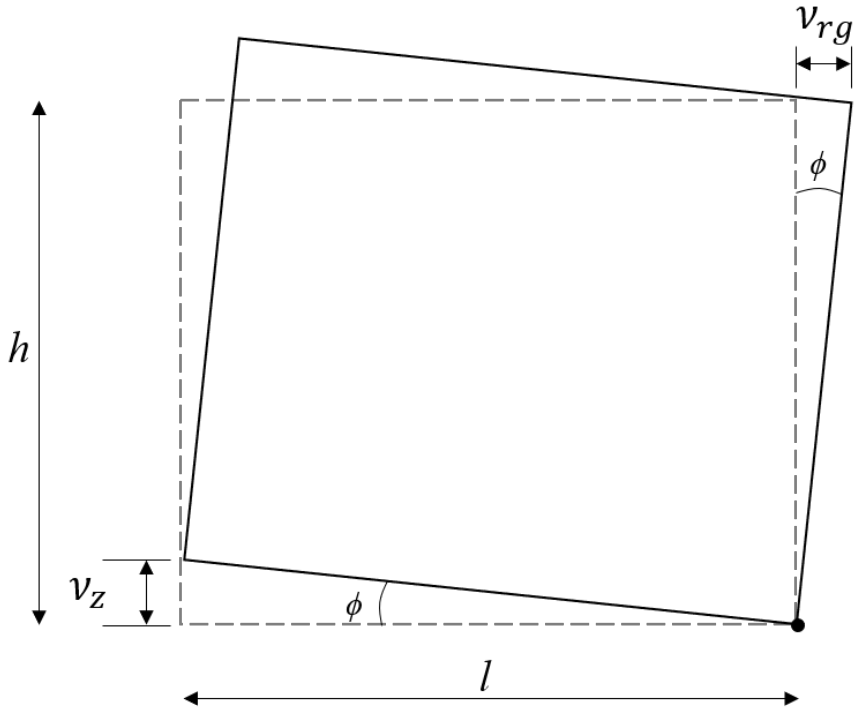

Figure 2.18: *Illustration of lateral deflection due to rocking* v_{rg}.

$$v_{rg} = h \cdot \frac{v_z}{l} = h \cdot \phi \tag{2.2}$$

where:

v_{rg} = lateral displacement due to rocking
v_z = vertical displacement due to rocking
ϕ = rotation angle of CLT wall element

2.3.2 CLT as floor diaphragm

The semi-rigid composition of CLT makes it fit for using as horizontal floor diaphragms. A floor diaphragm is the result of connecting the sides of floor panel elements into a plate. This continuous diaphragm contributes to the horizontal load distribution to the vertical shear walls located below the floor diaphragm. Diaphragms also contribute to lateral support, embracing out-of-plane forces and in-plane stiffness. (Lukacs, Pradel, Björnfot, & Tomasi, 2018)

For CLT diaphragms the most common load distribution method is the envelope force method. In this method the worst case of either rigid or flexible is used. However, Chen, Chui, Ni, Doudak, and Mohammad (2014) points out some issues with this model. In some situations, the semi-rigid stiffness were larger than both flexible and rigid stiffness when shear walls were loaded. (Lukacs, Pradel, et al., 2018)

2.4 Material property distribution

There is always some relative uncertainty when dealing with material properties. Most construction material properties lie within an area and is not always the same value. Therefore, different statistical measures can be used and illustrated with different distribution functions, such as probability density functions or cumulative density functions.

Probability density function

Material properties are sometimes illustrated with a Probability Density Function (pdf). The characteristic of the curve depends on the mean and the standard deviation. Standard deviation is defined as how dispersed the distribution is about the mean and are often denoted with σ and equal to the square-root of the variation. The smaller the standard deviation is the larger the spike on the curve will be. The sum underneath the graph is equal to one, with data on the x-axis and probability density on the y-axis. The curve can follow several different probability density distributions, such as normal, lognormal, Weibull or exponential distribution. In Figure 2.19 an example of a normal probability density distribution is illustrated.

Cumulative distribution function

Another way to show distribution is with a Cumulative Distribution Function (cdf). The cumulative distribution function is the integral of the probability density function. Therefore, it differs from the probability density function with the fact that the values go from zero to one. The median value occurs when the y-axis is 0.5 and, in some distribution, also is the mean. Likewise, the 0.95-quantile is equal to when the y-axis is 0.95 and then the value on the x-axis. A cumulative distribution function, in the same way as a probability density function, be differently distributed, such as normal, lognormal, Weibull or exponential distribution. In Figure 2.20 an example of a normal cumulative distribution function is illustrated.

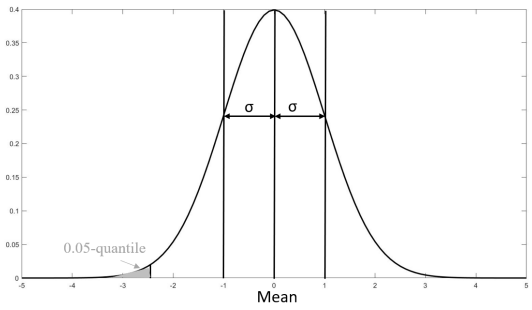

Figure 2.19: *Normal probability density function with 0 as mean and 1 as standard deviation. Also, the standard deviation and the 0.05-quantile marked out in the figure.*

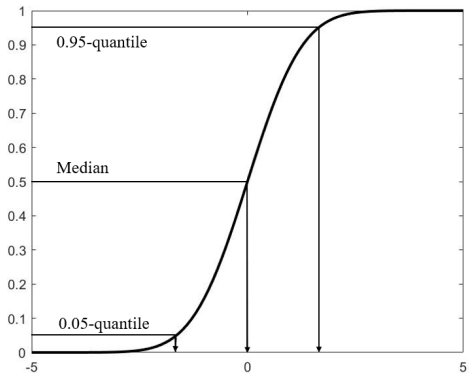

Figure 2.20: *Normal cumulative distribution function with 0 as mean and 1 as standard deviation. Also, the 0.05-quantile and 0.95-quantile marked out in the figure.*

Quantiles

From probability distributions it is common to use quantiles, which represent all values below the specific quantile. For example, the 0.5-quantile represent the values which lies below 50 % of samples in the probability density function and therefore also is the mean value of the distribution. In Figure 2.19 and 2.20 some different quantiles in a lognormal probability density function distribution are marked out. Within two standard deviation from the mean value, 95 % of the distribution lies. In structural engineering especially the 0.05-quantile is frequently used. This represent the values which lies below 5 % of samples in the probability density function. The 0.05-quantile is often defined as the characteristic value of a material property, e.g. modulus of elasticity in stability calculations.

Coefficient of Variation

Relative uncertainty can be measured with the Coefficient of Variation (CoV) and is only used for positive quantities. The CoV is defined as the ratio between the Standard Deviation (std) and the mean:

$$\text{CoV} = \frac{\text{std}}{\text{mean}} = \frac{\sigma}{E} \tag{2.3}$$

A lower CoV gives a more precise estimate with small variations, and therefore a small CoV is to prefer. Furthermore, if the CoV is smaller this leads to a less differences between the 0.05-quantile and the mean value, which is to prefer. If the mean and the 0.05-quantile is close in value this could reduce the need for using both values and simplify calculations.

2.4.1 Correlation between timber material properties

Timber properties are assessed by it is grading. Therefore, are material properties correlated with some control scheme, where only reference material properties are considered. The reference material properties are the bending strength R_m, bending modulus of elasticity E_m and the density ρ_{den}. The other material properties are determined from the reference material properties. The other material properties include among other tension and compression strength, as well as tension and compression modulus of elasticity and shear modulus. If the expected value (mean) and coefficient of variation is known for the reference material properties all the other material properties can be calculated according to Table 2.12. (Joint Committee on Structural Safety, 2006)

Table 2.12: *Relations between reference material properties and other material properties in structural timber.*

Property	Expected value E[X]	CoV[X]
Tension strength $R_{t,0}$	$0.6\mathrm{E}[R_m]$	$1.2\mathrm{CoV}[R_m]$
Tension strength $R_{t,90}$	$0.015\mathrm{E}[\rho_{den}]$	$2.5\mathrm{CoV}[\rho_{den}]$
MoE $E_{t,0}$	$\mathrm{E}[E_m]$	$\mathrm{CoV}[E_m]$
MoE $E_{t,90}$	$\mathrm{E}[E_m]/30$	$\mathrm{CoV}[E_m]$
Compression strength $R_{c,0}$	$5\mathrm{E}[R_m]^{0.45}$	$0.8\mathrm{CoV}[R_m]$
Compression strength $R_{c,90}$	$0.008\mathrm{E}[\rho_{den}]$	$\mathrm{CoV}[\rho_{den}]$
Shear modulus G_v	$\mathrm{E}[E_m]/16$	$\mathrm{CoV}[E_m]$
Shear strength R_v	$0.2\mathrm{E}[R_m]^{0.8}$	$\mathrm{CoV}[R_m]$

In Table 2.13 the correlation between all main material parameter in timber are illustrated. The higher the value is the higher is also the correlation between material properties. Therefore, 0.8 indicates high correlation, 0.6 indicate medium correlation, 0.4 indicate low correlation and 0.2 indicate very low correlation. The values are according to quantified judgement performed by Köhler, Sørensen, and Faber (2007).

Table 2.13: *Correlation matrix between different material properties.*

	E_m	ρ_{den}	$R_{t,0}$	$R_{t,90}$	$E_{t,0}$	$E_{t,90}$	$R_{c,0}$	$R_{c,90}$	G_v	R_v
R_m	0.8	0.6	0.8	0.4	0.6	0.6	0.8	0.6	0.4	0.4
E_m		0.6	0.6	0.4	0.8	0.4	0.6	0.4	0.6	0.4
ρ_{den}			0.4	0.4	0.6	0.6	0.8	0.8	0.6	0.6
$R_{t,0}$				0.2	0.8	0.2	0.5	0.4	0.4	0.6
$R_{t,90}$					0.4	0.4	0.2	0.4	0.4	0.6
$E_{t,0}$						0.4	0.4	0.4	0.6	0.4
$E_{t,90}$							0.6	0.2	0.6	0.6
$R_{c,0}$								0.6	0.4	0.4
$R_{c,90}$									0.4	0.4
G_v										0.6

From this table it is clear which properties that relay highly on each other, such as bending moment of elasticity E_m and bending strength R_m. Obviously, tension strength in different direction should have a low impact on each other which is also shown in Table 2.13.

2.4.2 Timber property distribution

As previously mentioned timber is a complex building material, which is anisotropic and contains deviations. Because of its anisotropic the properties of timber vary depending which direction one is interested in. Deviation in timber can among other come from knots, warping, moisture content and fungi.

Cross Laminated Timber

Since CLT is homogeneous material the properties of CLT has a lower variability than structural timber in most cases. This leads to a lower CoV and therefore a more precise value of properties with smaller diversity. Therefore, CLT is preferred to rather than structural timber regarding variation of material properties. Furthermore, if the CoV is low this can be led to a lower partial safety factor. Table 2.14 describes how the partial safety factor can vary depending on the CoV of the resistance. (Köhler, Fink, & Brandner, 2016)

Table 2.14: *Partial safety factors for the resistance for different CoV with constant γ_G and γ_Q, and a lognormal distribution.*

CoV of the resistance	γ_m
0.15	1.20
0.2	1.24
0.25	1.33

Statistics regarding material properties for CLT varies depending on source. Data from Köhler et al. (2016) are presented in Table 2.15 and statistics from Jockwer, Fink, and Köhler (2017) in Table 2.16.

Table 2.15: *CLT material properties distribution from Köhler, Fink, and Brandner (2016).*

Property	CoV
Bending strength (elements)	0.08-0.16
Net-shear strength (in-plane; elements)	0.06
Rolling shear (board segments)	0.13-0.22
Compression strength perpendicular to grain (basic value; prism)	0.08
Density	0.007-0.026

Table 2.16: *CLT material properties distribution from Jockwer, Fink, and Köhler (2017).*

Property	Distribution	Mean	CoV
Tension perpendicular to grain strength $f_{t,90}$ [kN/mm^2]	Weibull	0.002	0.3
Modulus of Elasticity E_0 [kN/mm^2]	Lognormal	11.5	0.23
Density ρ_{den} [kg/m^3]	Lognormal	420	0.1

Comparison between CLT, glulam and structural timber

Structural timber has larger variation than CLT and glulam since it is a non-homogeneous material, as presented in Table 2.17. As long as the thickness of CLT is not too small, the mean density of CLT would be the same as for the base material (Köhler et al., 2016). However, CLT has a lower variability in density than the base material, because of averaging effects in the CLT elements. Therefore, since the mean density is the same and CLT has an lower variation the CLT of density would be much lower in the CLT case than the structural timber case. The same reasoning as for density also applies to the bending strength, where the CLT decreases the more layer it consists of.

Table 2.17: *Comparison in material properties of CLT, glulam and structural timber. Glulam and structural timber from Joint Committee on Structural Safety (2006)*

Property	Distribution	CLT	GL	ST
Bending strength R_m	Lognormal	0.08-0.16	0.15	0.25
Bending MoE E_m	Lognormal	-	0.13	0.13
Density ρ_{den}	Normal	0.007-0.026	0.1	0.1

2.4.3 Connections

Since steel is an isotropic material the variability in steel properties is much lower than in timber properties. However, deviations in steel properties can come from different steel quality, hardening properties and other treatments.

Hold-downs

There exist not many tests on hold-downs and angle brackets that present the variability of material properties. However, tests on hold-downs connections between CLT wall element and foundation have been performed by Gavric, Fragiacomo, and Ceccotti (2015) and parts of the strength properties results are presented in Table 2.18. The test was made with two different types of hold-down connections tested under cyclic loading separately in shear and tension.

Table 2.18: *Mechanical properties of hold-down connections in a wall CLT element connected to foundation loaded in tension.*

Property	Unit	Mean	CoV
F_{max}	[kN]	48.33	0.0537
D	-	2.76	0.1621

Angle brackets

Angle brackets mainly carries the load in shear, however according to tests performed by Gavric et al. (2015) it also has relatively good capacity in tension. The results from these tests are presented in Table 2.19.

Table 2.19: *Mechanical properties of angle brackets connections in a wall-floor CLT element loaded in tension and in shear.*

		Tension		Shear	
Property	Unit	Mean	CoV	Mean	CoV
F_{max}	[kN]	23.47	0.0432	26.85	0.0315
D	-	3.21	0.0686	2.63	0.0603

Angle brackets has a lower CoV than hold-downs, however it also has a significant lower mean in all the properties. The overstrength factor is also lower for angle brackets than for hold-downs.

2.5 Structural reliability

Probability of failure for a structure is difficult to determine. Often are the failure probability described with an uncertain resistance R and an uncertain loading S. Thus the failure of probability can be determined by Equation 2.4, where the resistance is modelled by random variable x with a probability density function f_R and the loading likewise with the probability density function f_S.

$$P_F = P(R \leq S) = P(R - S \leq 0) = \int f_R(x) f_S(x) dx \tag{2.4}$$

The probability functions for resistance and loading in Equation 2.4 are illustrated in Figure 2.21. The curve for resistance is always further to the right than the load. Since both curves are a probability density function the area underneath each curve is one.

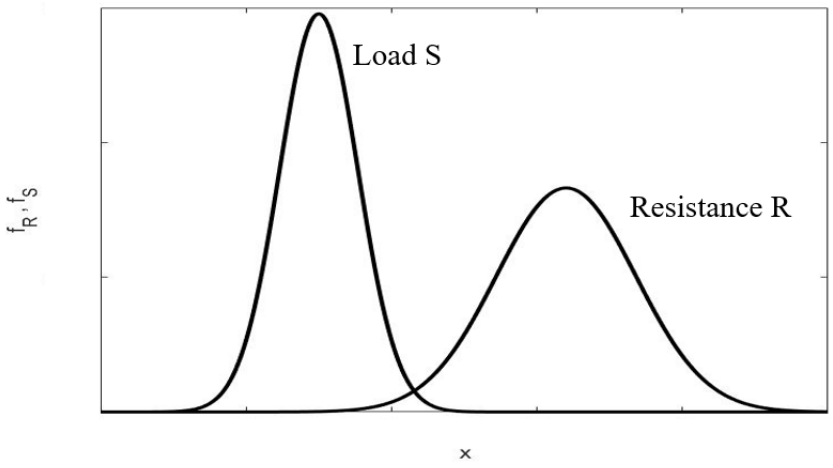

Figure 2.21: *Structural reliability with uncertain resistance R and uncertain loading S.*

The area of overlap between the two curves are not the same as the probability of failure. However the integral of this area is the probability of failure P_F. Therefore, to minimise the probability of failure the area should be as small as possible. However, if there are not any overlapping area there are a chance that the structure is over dimensioned. Often there is a target reliability that is correlating to the optimisation of the structure.

Since the probability function for resistance and loading can be different distributed, calculating the failure probability according to Equation 2.4 can be difficult. However, if both have the same distribution some special cases can be derived. For example if both are normal distributed the probability of failure can be determined by a safety margin M, which is a random variable and equal to $M = R - S = g(x)$. Where $g(x)$ is often referred to as the limit state function, meaning which state the considered element has. If $g(x)$ is smaller or equal to zero, the element is considered in a state of failure and if it is larger than zero it is in a safe state. Therefore, the new probability of failure is:

$$P_F = P(R - S \leq 0) = P(M \leq 0) = \int_{g(x)\leq 0} f_x(x)dx \tag{2.5}$$

where $f_x(x)$ is the joint probability density function for the random variable x and the integral is determined when the limit state function is less than zero, e.g. in the state of failure. The solution to this equation is non-trivial and several different methods to solve this integral has been developed. The most commonly methods to calculate the probability of failure according to Joint Committee on Structural Safety (2000) can be divided into either asymptotic approximate methods or simulation methods. Examples of methods are Monte Carlo simulations, numerical integration techniques and asymptotic Laplace expansions (Faber, 2005). Today, different softwares are often used to calculate the probability of failure.

2.6 Load-displacement

Currently in the standards that are being applied, only the linear elastic behaviour of fasteners is considered (Brandner, Ringhofer, & Dietsch, 2017). In seismic design, for ductile structures, plastic deformations are allowed (Muñoz, Mohammad, Salenikovich, & Quenneville, 2008). For a nonlinear behaviour, the load-displacement behaviour of the fasteners becomes relevant (Brandner et al., 2017). To be able to determine the limit between elastic and plastic behaviour, the so-called yield point is important to define (Muñoz et al., 2008). It is also crucial to have knowledge about the ductility, how much plastic deformation the system can undergo without a substantial reduction in strength (Muñoz et al., 2008).

For determining the yield point and ductility, the mechanical properties such as stiffness and load-carrying capacity are examined in a load-deformation diagram. These diagrams show load-displacement curves based on experimental tests. (Flatscher, 2017, p.5)

This chapter is divided into subsections where the first subsection explains the characteristics of load-displacement curves. The second subsection is covering the parameters initial stiffness and yield point. There, some of the most commonly used analysis methods for determining the initial stiffness and estimating the yield point are briefly described. These methods are based on typical load-displacement curves that have been derived from laboratory tests on timber connections. Finally, the parameter ductility is concisely treated.

2.6.1 Characteristics of load-displacement curves

A load-displacement curve visualises the behaviour of the investigated specimen. It is a common tool in several fields of science for analysing the material and structural properties. Here, the focus lays on the field of timber engineering and the load-displacement relationships relevant for that field. (Flatscher, 2017, p.5)

To be able to obtain mechanical properties from experimental load-displacement curves, one must have the knowledge in interpreting the curves. Figure 2.22, which is illustrating a typical load-displacement curve of a single nail loaded in tension will work as an example when explaining the characteristics of a load-displacement curve.

In general, load-displacement diagrams are separated into three parts; a linear increasing part (I), a nonlinear increasing part (II) and a nonlinear decreasing part (III). Additionally, until the system is "stable", an initial slip may occur, represented by an initial sector (S). The different regions can be seen in Figure 2.22, where also the initial sector (S) is shown, even if that region will not be further discussed. Region (I) represents the elastic part in the load-displacement curve. That part ranges between the origin (0) and the yield point (Y). The enlarged part of the elastic range presented in Figure 2.22b shows a more detailed curve where the proportional limit (P), the elastic limit (E) and the plastic limit (Y), also known as the yield point, is included. Here it can be seen that there is an ideal linear elastic behaviour of the specimen up to the proportional limit (P). It is the inclination of the line between (0) and (P) that is defined as the initial stiffness (K_{ini}), a parameter that is of interest in this thesis. After reaching the proportional limit (P), the nonlinear behaviour starts, but as long as the elastic limit (E) is not reached, the deformations are reversible. The yield point (Y) is the point which separates the elastic behaviour from the plastic behaviour, it is therefore also called the plastic limit. (Flatscher, 2017, p.6-7)

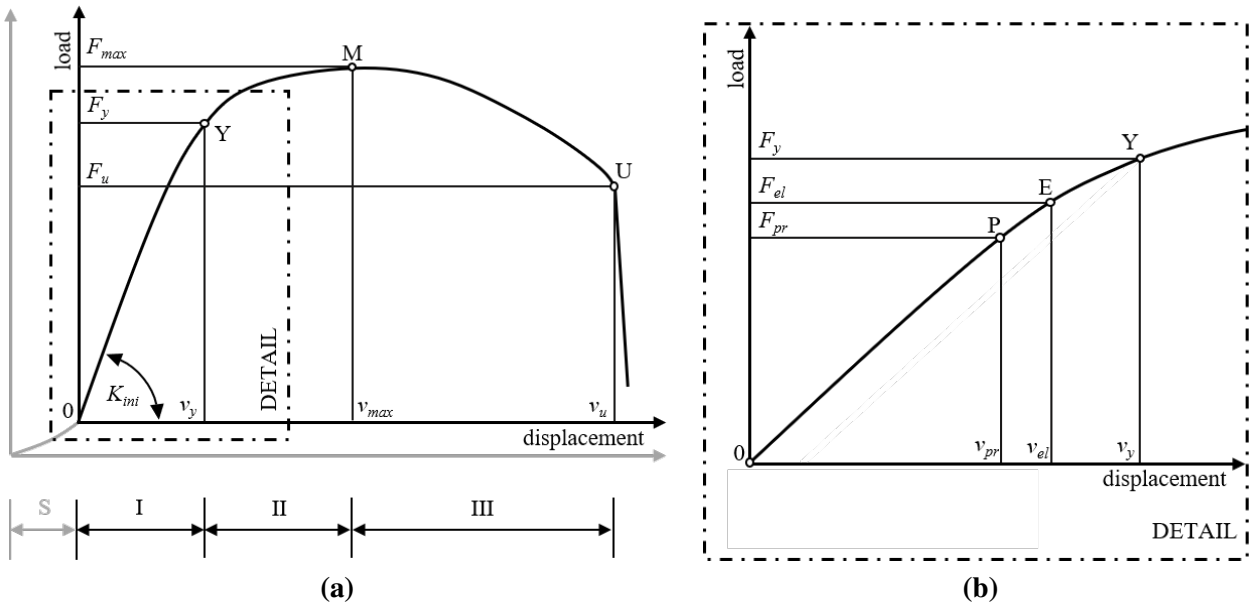

Figure 2.22: *Illustration of a typical load-displacement curve of a single nail loaded in tension.*

2.6.2 Initial stiffness, Yield Point and test methods to determine them

When studying the nonlinear behaviour, one of the most important parameters is the yield point, which separates the elastic behaviour from the plastic behaviour and represents the limit where plastic deformations start to occur (Brühl & Kuhlmann, 2017, p.32). There are several existing methods to determine the yield point and the method that is applied in each country and region differs. Nevertheless, each method, in some way uses the initial stiffness in order to define the yield point. The initial stiffness is in all methods defined somewhere in the elastic range and is expressed as the slope, measured by the ratio of the resisted load F_i and the corresponding displacement v_i (ISO/TC165, 2018).

Some of the common analysis methods for determining initial stiffness and yield point that are being used in North America, Japan and Europe are briefly described below.

ASTM E2126 - EEEP model

One method that is being used in North America is the so-called equivalent energy elastic-plastic (EEEP) curve. This curve was originally applied on concrete and steel systems but was adopted by the American standard ASTM E2126 to be used also for analysis of shear walls (Muñoz et al., 2008). In particular, studying resistance of shear walls in buildings, subjected to lateral force.

The bilinear curve in Figure 2.23 is representing the ideal elastic-plastic behaviour of the specimen. The model is built around the dissipation of energy, striving towards equal dissipation between the bilinear curve and the test curve. The bilinear curve is therefore approximated in such way that it covers the same area as the original test curve. The initial stiffness corresponds to the straight line in Figure 2.23 that is passing through the origin and the point where 40 % of the peak load F_{max} is reached and the ultimate displacement v_u is defined at 80 % of F_{max}.

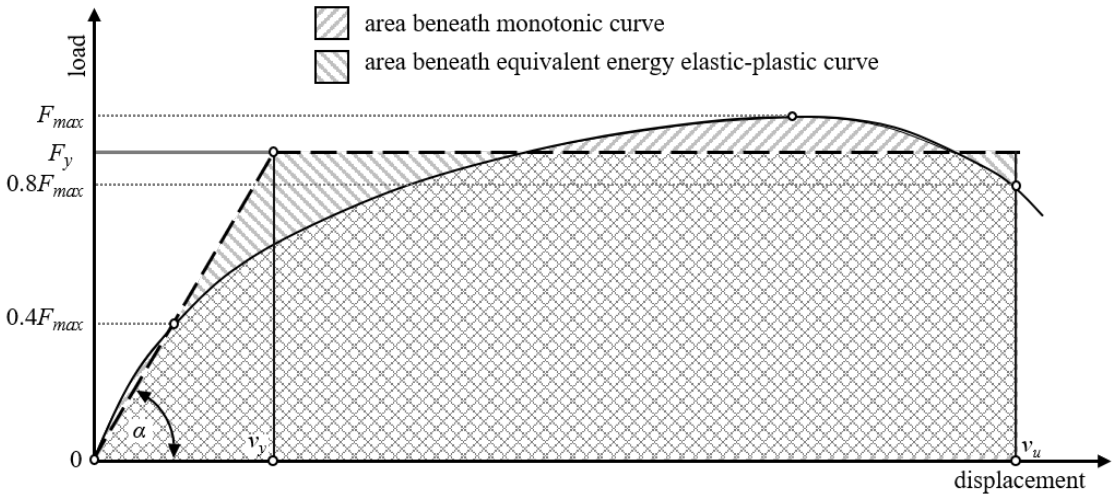

Figure 2.23: *Illustration of equivalent energy elastic-plastic (EEEP) curve according to ASTM E2126.*

The yield load can be determined by using Equation 2.6, where K_{ini} is the initial stiffness and A corresponds to the area under the test curve between the origin and the ultimate displacement v_u. The yield displacement v_y that corresponds to the yield load can be defined once the yield load is solved for.

$$F_y = \left[v_u - \sqrt{\left(v_u\right)^2 - \frac{2 \cdot A}{K_{ini}}} \right] \cdot K_{ini} \tag{2.6}$$

ASTM D5764 and ASTM D5652 - 5 % diameter model

In the two American standards, ASTM D5764 and ASTM D5652, the 5 % diameter offset line is used to decide the dowel-bearing capacity of wood (Muñoz et al., 2008). As described in ISO/TC165 (2018), the standard test methods are based on single-bolt connections in building elements made of timber. In these methods, a line, representing the initial stiffness is drawn in the load-displacement curve illustrated in Figure 2.24. The line has a slope between 0 % and 40 % of the peak load. A line parallel to the initial stiffness line is drawn on the right-hand side. The offset of this line equals to 5 % of the diameter of the connector. The yield point F_y is defined as the point where the line to the right intersect with the load-displacement curve. According to American Forest & Paper Association (1999) the yield load value denotes the nominal embedment resistance of the wood and the bending resistance of the connector in the *National Design Specification*. (Muñoz et al., 2008)

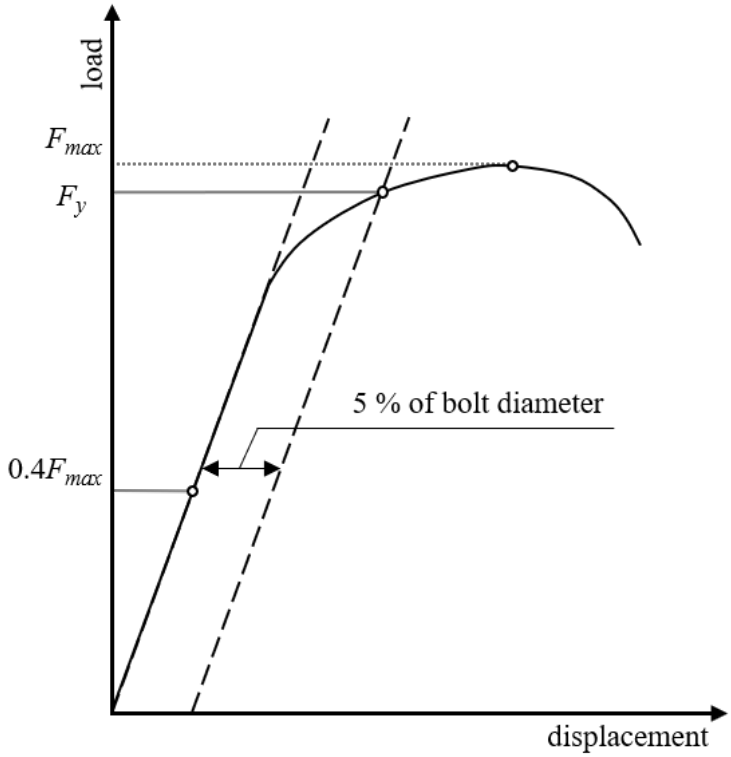

Figure 2.24: *Illustration of load-displacement curve based on the 5 % diameter model, according to ASTM D5764 and ASTM D5652.*

Yasumura and Kawai model

Yasumura and Kawai from Japan proposed a method in 1997. The method was initially developed for describing the behaviour of laterally loaded wood-framed shear walls. Parts of already existing methods were combined with a new theory for finding the parameters of yielding (Flatscher, 2017, p.15). Even though timber buildings represent 50 % of the constructions in Japan, the method is not yet standardised. The method is, however, frequently used in design of CLT constructions in Japan. (Sassu, Puppio, Awad, Giresini, & Koshihara, 2017, p.224)

In this method, the initial stiffness is defined according to Figure 2.25, with a straight line between 10 % and 40 % of the peak load (Muñoz et al., 2008, p.2). Then the inclination of the second line is determined by the points on the test curve corresponding to 40 % and 90 % of the peak load F_{max}. The point where the two lines intersect is where the yield load F_y is found. The yield displacement v_y is obtained by horizontally project the point of the yield load towards the original load-displacement curve. (Flatscher, 2017, p.15)

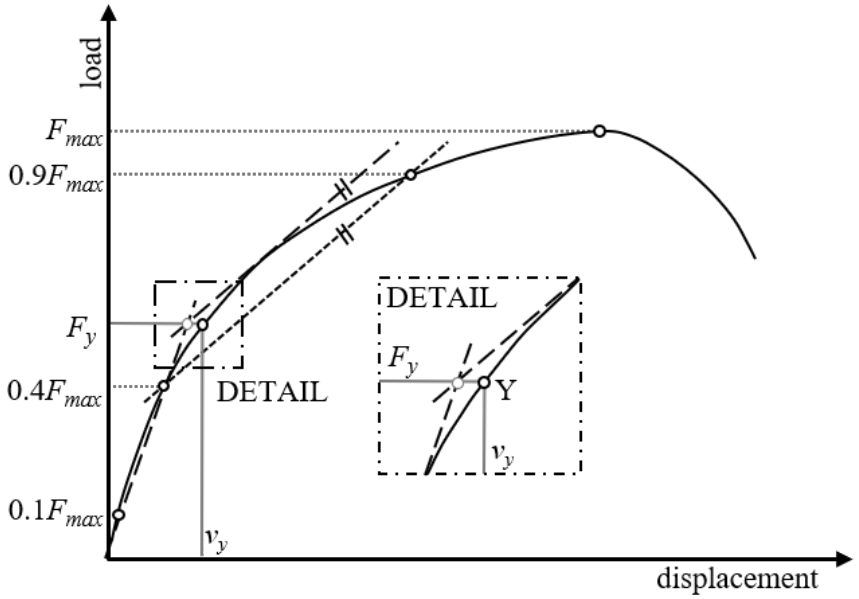

Figure 2.25: *Illustration of load-displacement curve according to the Yasumura and Kawai model.*

European standard

In the European standard ON EN 12512, the cyclic experiments of connections in timber are handled. To determine the joint slip that corresponds to the yield load, that is later needed as input parameter for the cyclic loading protocol, monotonic pretests are performed and then one of two methods is applied. (Flatscher, 2017, p.10)

The first method applies for the case where the load-displacement curve takes on the appearance of two delineated linear segments. The yield load F_y and the yield displacement v_y are determined in the point where these two lines intersect, as illustrated in Figure 2.26.

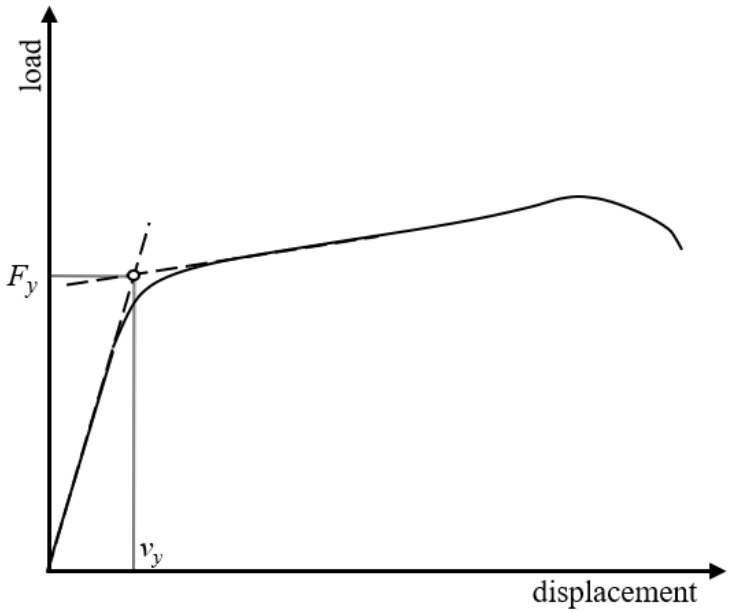

Figure 2.26: *Illustration of load-displacement curve according to ON EN 12512 - for the case with two defined linear segments.*

In the case where there are no clear linear segments, the second method is applied. There, the yield values are defined by the intersection of the two dashed lines depicted in Figure 2.27. That is, the lines where; the first line is drawn through the points corresponding to 10 % of F_{max} and 40 % of F_{max}, and the second line is drawn as a tangent with an inclination of 1/6 of the first line (ON EN 12512, 2002). As interpreted by Flatscher (2017), the initial stiffness K_{ini} is represented by the inclination of the secant of the first dashed line seen in Figure 2.27, i.e. $\tan(\alpha)$.

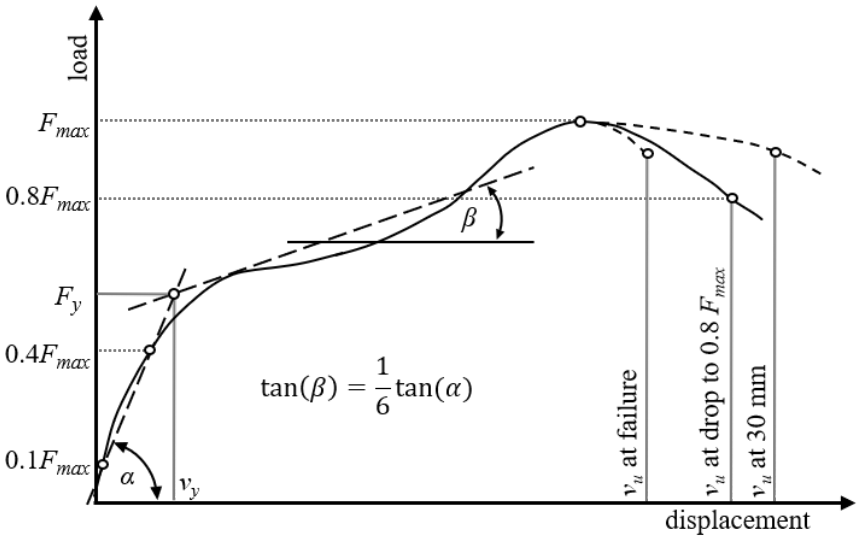

Figure 2.27: *Illustration of load-displacement curve according to ON EN 12512 - for the case without the two defined linear segments.*

As can be seen in Figure 2.27, the ultimate displacement v_u is marked in three different places in the curve. According to ON EN 12512 (2002), the ultimate displacement v_u and the corresponding ultimate load F_u are defined in one of the three points; the point of failure, the point where the load has decreased to 80 % of F_{max}, or at the point where the displacement is 30 mm. Whichever event that occurs first is the one that decide the ultimate parameters.

2.6.3 Ductility

Ductility is a material, connection or structure's ability to attain large displacements without experiencing significant loss in strength. In timber structures the timber members often have a linear elastic behaviour and therefore the level of ductility depends mostly on the connections in the structure. To achieve a effective connection in timber structures it is important to achieve high strength and stiffness, but also high ductility as illustrated in Figure 2.28. (Flatscher, 2017, p.56)

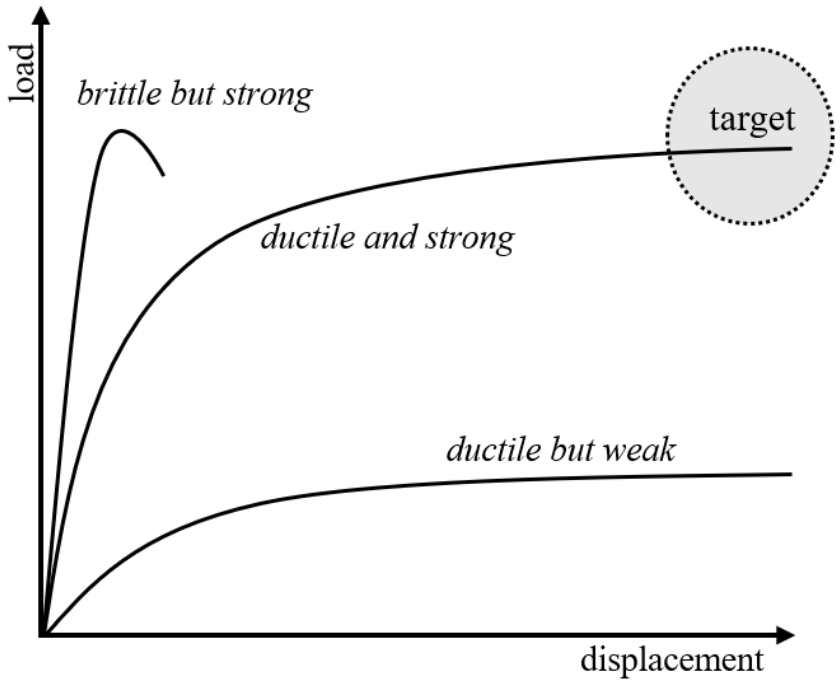

Figure 2.28: *Different load-displacement curves with varying strength and ductility level.*

Ductility is usually divided into one of four classifications; brittle, low ductility, moderate ductility and high ductility. How ductility is determined differs and is not always clear but according to SIA 265 (2012) it is generally defined as the ratio between ultimate displacement and yield displacement, like described in Equation 2.7. This way of calculating ductility does come with some issues. The ductility level can be equal but have completely different load-displacement curves.

$$D = \frac{v_u}{v_y} \tag{2.7}$$

where:

v_u = ultimate displacement
v_y = yield displacement

Even though the classification of ductility is mostly the same in different references, the limits of these classifications have considerable differences. These limits are presented in Table 2.20. From this, it is clear that Eurocode 8 has twice as high limits in all different classifications compared to Swiss standard SIA 265 (2012). Otherwise, the first two references are similar, and the two last ones are similar.

Table 2.20: *Different classifications of ductility.*

Classification	SIA 265 (2012)	Smith et al. (2015)	Eurocode 8	Smith et al. (2006)
brittle	$1 \leq D$	D=1	-	$D \leq 2$
low ductility	$1 < D \leq 2$	D=1.25	$D < 4$	$2 < D \leq 4$
moderate ductility	$2 < D \leq 3$	$1.25 < D \leq 3$	$4 \leq D < 6$	$4 < D \leq 6$
high ductility	$3 < D$	$3 < D$	$6 \leq D$	$6 < D$

In Eurocode 5 there is not much information about ductile behaviour of timber structures. It only states:

5.1 (3): For structures able to redistribute the internal forces via connections of adequate ductility, elastic-plastic methods may be used for the calculation of the internal forces in the members.

After this Eurocode 5 does not mention anything more about ductility. However, Swiss standard SIA 265 (2012) presents that when the ductility is larger than 3.0 this should mean a reduction in the safety factor from 1.7 to 1.5. In Eurocode 5 the calculation is independent on the ductile behaviour of the timber structure and its connections.

2.7 Analytical approximations for load-displacement curves

In general, there are two different types of analytical approximations; piecewise and continuous. Where piecewise approximations often are linear models while the continuous are mathematical functions. The continuous models are often divided into three subgroups; power and polynomial functions; exponential and logarithmic functions; rational functions. (Flatscher, 2017)

The most commonly used analytical approximation model in Timber engineering is the exponential model proposed by Foschi in 1974 which is illustrated in Figure 2.29. This model is commonly used since it includes a post-elastic stiffness K_p.

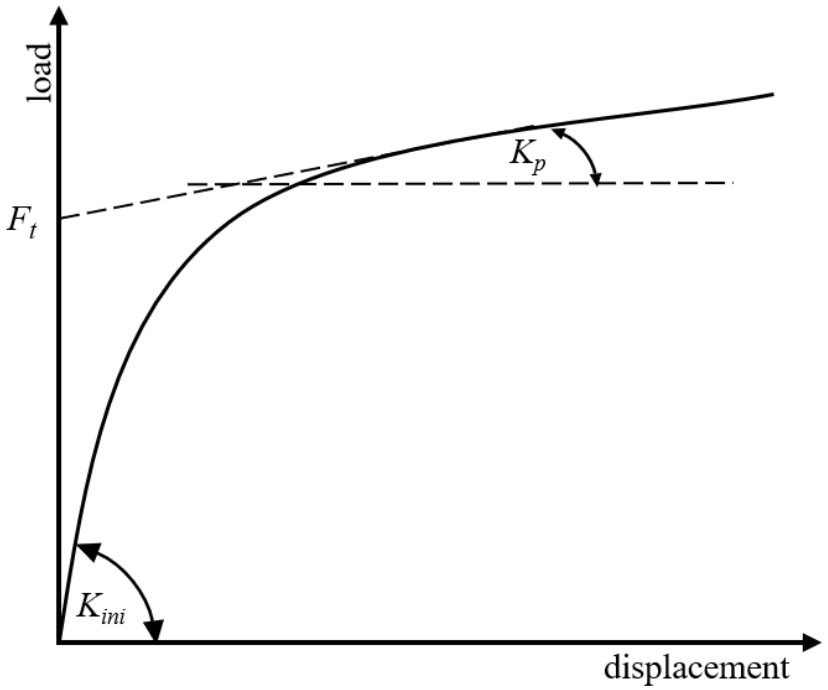

Figure 2.29: *Foschi's exponential approximation model from 1974.*

The downside to the model proposed by Foschi in 1974 is that it does not have a softening branch. Therefore, there are several evolved models from this one. In this thesis, the evolved model by Foschi (2000), which is illustrated in Figure 2.30 where used.

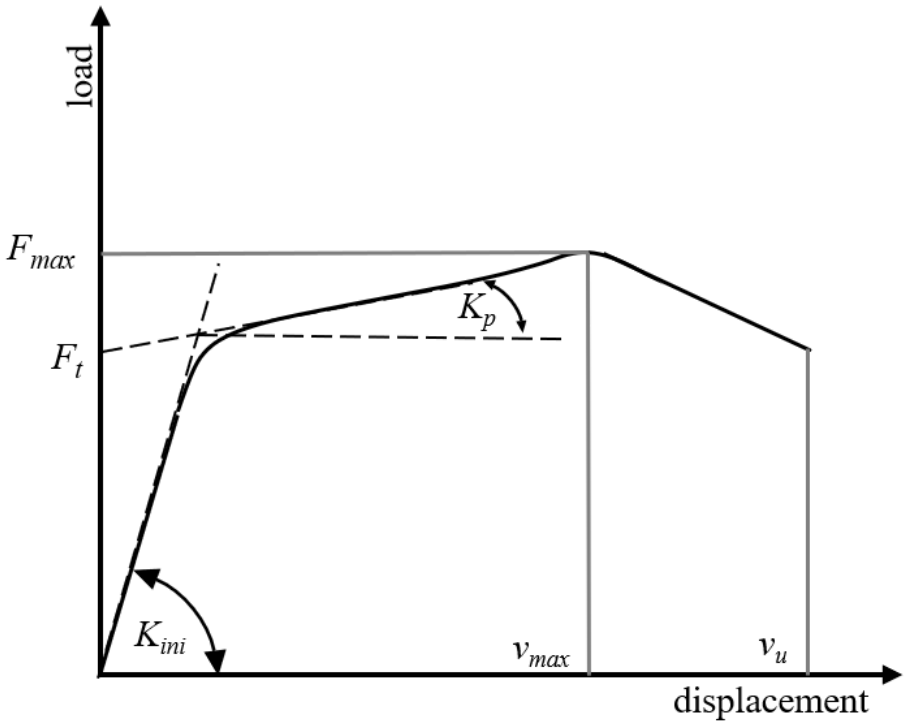

Figure 2.30: *Foschi's approximation model from 2000.*

This model consists of five independent input parameters; the maximum load F_{max}, displacement at maximum load v_{max}, initial stiffness K_{ini}, point of intersection between the asymptote and the ordinate F_t and the displacement at ultimate load capacity v_u. The equations used in this model are described as:

$$K_p = \left(\frac{F_{max}}{1 - e^{-\frac{K_{ini}}{F_t} \cdot v_{max}}} - F_t \right) \cdot \frac{1}{v_{max}} \tag{2.8}$$

$$F_u = 0.8 \cdot F_{max} \tag{2.9}$$

$$C = \frac{ln\left(\frac{F_u}{F_{max}}\right)}{\left(v_{max}\left(\frac{v_u}{v_{max}} - 1\right)\right)^2} \tag{2.10}$$

where the load dependent on the displacement v where calculated as follows:

$$F(v) = (F_t + K_p \cdot v)\left(1 - e^{-\frac{K_{ini}}{F_t} \cdot v}\right) \qquad \text{if } v \leq v_{max} \tag{2.11a}$$

$$F(v) = F_{max} \cdot e^{C(v - v_{max})^2} \qquad \text{if } v > v_{max} \tag{2.11b}$$

2.8 Modelling CLT wall systems

So far, there are no guidelines available in Eurocode 5 regarding design of CLT wall systems. The global behaviour of CLT wall systems are only covered in literature where analytical models are used to describe the load capacity and the stiffness of the systems. This section covers some of the approaches that are currently available when evaluating CLT wall systems. Two different types of models have been considered, force-based models and displacement-based models. First, some force-based models that are included in Flatscher (2017) are described, whereafter some displacement-based models are presented, of which also are included in Flatscher (2017). The models are presented in a chronological order and are named after the main person behind the model, together with the year it was introduced. Finally, the two different types of models are summarised.

2.8.1 Force-based models

Ceccotti 2006

Chapter 4-3.2.1 in Flatscher (2017) describes an elementary model for taking the behaviour of connections into consideration in the design of CLT systems. In the model, the overturning moment of the CLT wall is resisted solely by the hold-downs which are assumed to only carry vertical forces. The shear forces are assumed to entirely be taken by the angle brackets. When applying a lateral load in accordance with Figure 2.31, the lateral load per angle bracket F_{AB} could be calculated according to Equation 2.12 by the assumption that the load is equally distributed between the angle brackets. To calculate the axial load per hold-down, Equation 2.13 is used.

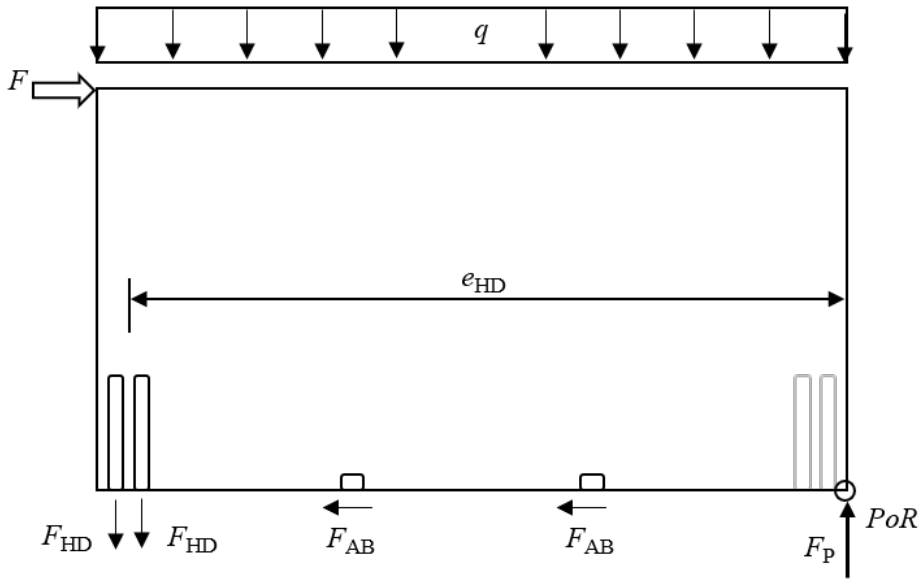

e_{HD} = distance between PoR and centre of considered hold-downs

F_P = compression (bearing) load

Figure 2.31: *Fundamental model for considering the connections in a CLT wall system according to the method Ceccotti 2006.*

$$F_{AB} = \frac{F}{n_{AB}} \tag{2.12}$$

$$F_{HD} = \frac{2 \cdot F \cdot h - q \cdot l^2}{2 \cdot e_{HD} \cdot n_{HD}} \tag{2.13}$$

where:

n_{AB} = number of applied angle brackets
n_{HD} = number of applied hold-downs

In Equation 2.14, the smallest of the values for the load-carrying capacity against sliding and rocking is the one that governs the load-carrying capacity of the CLT wall system.

$$R_{ges} = \min \begin{cases} R_{sliding} = R_{AB} \cdot n_{AB} \\ R_{rocking} = \dfrac{q \cdot l^2 + 2 \cdot R_{HD} \cdot e_{HD} \cdot n_{HD}}{2 \cdot h} \end{cases} \tag{2.14}$$

where:

R_{ges} = lateral load-carrying capacity of CLT wall system
$R_{sliding}$ = lateral load-carrying capacity against sliding
$R_{rocking}$ = lateral load-carrying capacity against rocking
R_{AB} = lateral load-carrying capacity per angle bracket
R_{HD} = axial load-carrying capacity per hold-down

The method Ceccotti 2006 focuses on each connection and assumes that the load is divided equally between the connections that are of the same type. It is a simple approach that is applied in practical design. Something that is not considered in this method, however, is the stiffness properties of the connections and the CLT panel itself.

Ringhofer 2010/2011

Based on a document from 2010, written by Ringhofer about seismic design of CLT structures, a model was established by Schickhofer and Ringhofer in 2011, a model that here is called Ringhofer 2010/2011 (Flatscher, 2017, p.113). In this model, the stiffness properties of angle brackets, hold-downs and screws as well as the CLT panel are included, something that have not been included in previous models. Like Ceccotti 2006, angle brackets are assumed to act parallel and only transmit lateral loads, which makes Equation 2.12 applicable for calculating the lateral load per angle bracket.

When determining the resistance against overturning of the CLT wall system, an approach commonly seen in the design of concrete is being used (Flatscher, 2017, p.113). Instead of using a triangular stress block, a rectangular stress block is applied from concrete design. The stress block, that is shown in Figure 2.32 is representing the compression loads that are taken. The point loads F_T and F_P included in Equation 2.25 are the hold-downs' contribution to resist the uplift forces. The dimensions of the stress block in terms of width l_P, calculated in Equation 2.16, and the distance $l_P/2$ from the edge to the centre of the block, is depending on the compression strength of the CLT. The compression strength of the CLT is separated into two cases, one with wall-to-foundation connection ($n_{P,eg,found}$) and one with wall-to-floor connection ($n_{P,eg,floor}$), where the first can be calculated via Equation 2.17 and the latter with Equation 2.18.

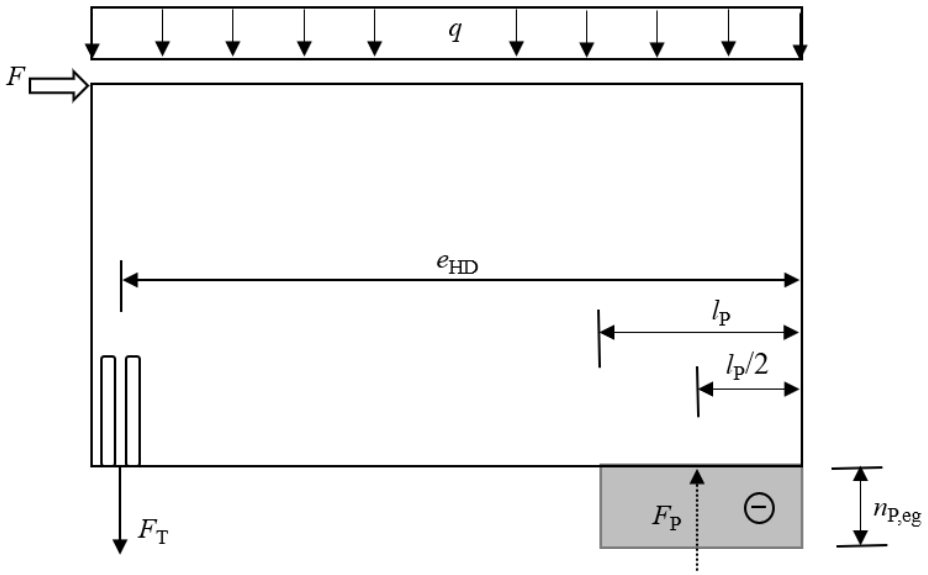

Figure 2.32: *Illustration of model with triangular stress block according to the method Ringhofer 2010/2011.*

$$F \cdot h + F_P \cdot \frac{l_P}{2} - \frac{q \cdot l^2}{2} - F_T \cdot e_{HD} = 0 \tag{2.15}$$

$$l_P = \frac{e_{HD} \cdot n_{P,eg} - \sqrt{n_{P,eg} \cdot \left(-2 \cdot F \cdot h + e_{HD}^2 \cdot n_{P,eg} - 2 \cdot e_{HD} \cdot l \cdot q + l \cdot q^2\right)}}{n_{P,eg}} \tag{2.16}$$

$$n_{P,eg,found} = t_{eff} \cdot f_{c,0} \tag{2.17}$$

$$n_{P,eg,floor} = t_{CLT} \cdot f_{c,90} \tag{2.18}$$

where:

$n_{P,eg,found}$ = compression strength for wall-to-foundation connection
$n_{P,eg,floor}$ = compression strength for wall-to-floor connection
t_{eff} = effective thickness of CLT wall panel (sum of thickness of vertical layers)
t_{CLT} = total thickness of CLT wall panel
$f_{c,0}$ = compression strength parallel to grain
$f_{c,90}$ = compression strength perpendicular to grain

The Ringhofer 2010/2011 model, developed within the field of seismic design, divides the wall system into components when studying the dynamic behaviour of the system. The CLT wall is considered as a bar while the connections are modelled as spring elements as depicted in Figure 2.33. The angle brackets are simplified into one lateral spring with a stiffness against the displacements caused by

sliding, expressed in Equation 2.19. The rotational spring represents the rocking behaviour as a sum of the vertical stiffness provided by the hold-downs. The stiffness of the rotational spring is expressed in Equation 2.20 where the deformations in the compression zone plays a role. In Equation 2.21 and 2.22, the stiffness representing those deformations are presented, the first one for a wall-to-foundation connection and the second one in case of wall-to-floor connection. In both of the last-mentioned equations, the stiffness properties of the CLT are implemented.

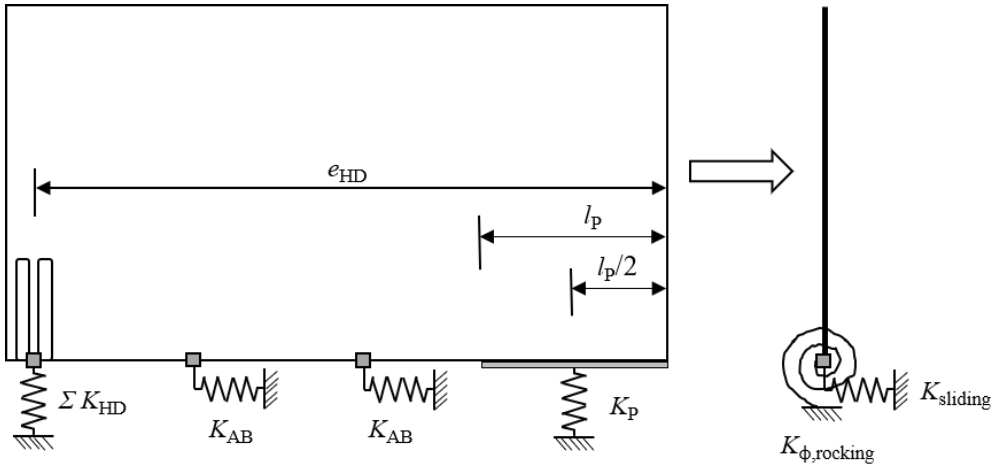

Figure 2.33: *Illustration of redefined model with connections modelled as springs according to the method Ringhofer 2010/2011.*

$$K_{sliding} = n_{AB} \cdot K_{AB} \tag{2.19}$$

$$K_{\phi,rocking} = \frac{\left(e_{HD} - l_P/2\right)^2}{\frac{1}{n_{HD} \cdot K_{HD}} + \frac{1}{K_P}} \tag{2.20}$$

$$K_{P,found} = \frac{2 \cdot E_{0,CLT} \cdot l_P \cdot t_{eff,wall}}{h_{wall}} \tag{2.21}$$

$$K_{P,floor} = \frac{2 \cdot E_{90,CLT} \cdot l_P \cdot t_{CLT,wall}}{t_{CLT,floor}} \tag{2.22}$$

where:

$K_{sliding}$ = stiffness of lateral spring resisting displacement caused by sliding
K_{AB} = stiffness of each angle bracket
$K_{\phi,rocking}$ = stiffness of rotational spring resisting displacement caused by rocking
K_{HD} = stiffness of each hold-down
K_P = stiffness representing the deformations in the compression zone, for either of the two types of joints: wall-to-foundation or wall-to-floor
$E_{0,CLT}$ = Modulus of Elasticity of CLT parallel to grain
$E_{90,CLT}$ = Modulus of Elasticity of CLT perpendicular to grain

Gavric 2011/2015

This model with its origin from 2011 is described in section 4-3.2.4 in Flatscher (2017) as the first detailed analytical model with the capacity to simulate the complete load-displacement relationship of a CLT wall system. The developed version of the model, published in 2015 by Gavric and other involved authors, includes the capacity of the applied connections regarding shear and uplift. The appearing lateral sliding deformation for a certain lateral load can be calculated using Equation 2.24, derived from Equation 2.23, where friction is included as an influencing coefficient.

$$F = \sum \left(K_{C,x,m}\right) \cdot v_{sl} + \mu_f \cdot q \cdot l \tag{2.23}$$

$$v_{sl} = \frac{F - \mu_f \cdot q \cdot l}{\sum \left(K_{C,x,m}\right)} \tag{2.24}$$

where:

v_{sl} = lateral displacement caused by sliding
μ_f = coefficient of friction
$K_{C,x,m}$ = lateral stiffness of connections

Flatscher (2017) states that this model differs from the previously mentioned models, especially when determining the rocking deformations. In this model, it is possible to take the uplift resistance of all connections into account and the stiffness of each connection is included. Another difference is that there is no compression zone defined in this model. Instead, the CLT panel is assumed to rotate around its lower corner as depicted in Figure 2.34, where the bearing load F_P is concentrated in the point.

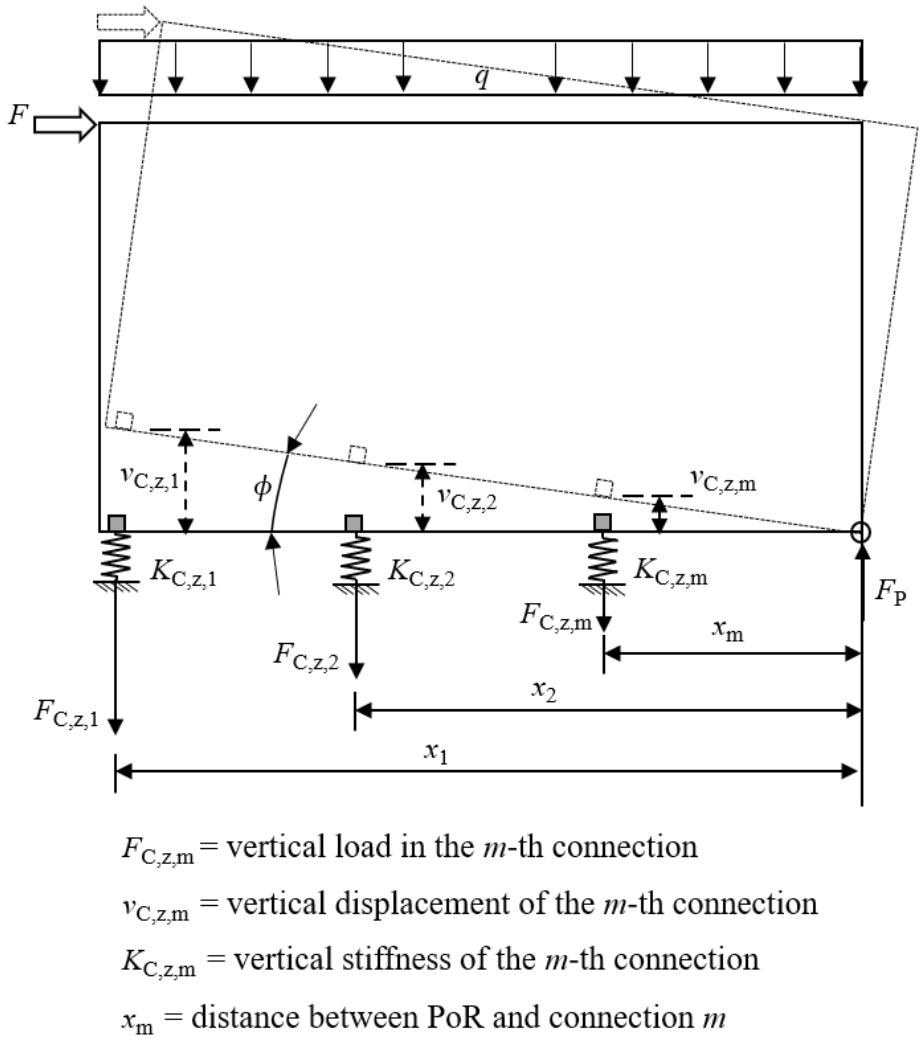

$F_{C,z,m}$ = vertical load in the m-th connection

$v_{C,z,m}$ = vertical displacement of the m-th connection

$K_{C,z,m}$ = vertical stiffness of the m-th connection

x_m = distance between PoR and connection m

Figure 2.34: *Illustration of CLT wall element with notations included for solving rocking deformations according to the method Gavric 2011/2015.*

When the wall system in Figure 2.34 is in equilibrium, Equation 2.25 represents the corresponding condition. The reacting loads per connection are expressed in Equation 2.26. For an actual load F, the rocking deformation is derived in Equation 2.27.

$$F \cdot h - \frac{q \cdot l^2}{2} - \sum \left(F_{C,z,m} \cdot x_m \right) = F \cdot h - \frac{q \cdot l^2}{2} - \frac{\nu_{rg}}{h} \cdot \sum \left(K_{C,z,m} \cdot x_m^2 \right) = 0 \tag{2.25}$$

$$F_{C,z,m} = K_{C,z,m} \cdot \nu_{C,z,m} = K_{C,z,m} \cdot x_m \cdot \phi = K_{C,z,m} \cdot x_m \cdot \frac{\nu_{rg}}{h} \tag{2.26}$$

$$\nu_{rg} = \frac{\left(F \cdot h - \frac{q \cdot l^2}{2} \right) \cdot h}{\sum \left(K_{C,z,m} \cdot x_m^2 \right)} \tag{2.27}$$

The Equations 2.24 and 2.27 are applicable when considering linear-elastic springs in the CLT wall system but are not appropriate for investigating nonlinear behaviour. To be able to also study the nonlinear behaviour, the method Gavric 2011/2015 offers an incremental loading procedure. An incremental load step ΔF_i is added to the load at the previous load step to receive the actual load at a certain incremental step F_i according to Equation 2.28. With the incremental displacement step Δv_i of the corresponding incremental load step ΔF_i, the displacement v_i that corresponds to the load F_i could be calculated by Equation 2.29.

$$F_i = F_{i-1} + \Delta F_i \tag{2.28}$$

$$v_i = v_{i-1} + \Delta v_i \tag{2.29}$$

Moreover, the Y-M-U model, a trilinear approximation of experimental test curves described in Chapter 2.6 is applied in the Gavric 2011/2015 method to further be able to consider nonlinear behaviour of connections. An illustration of the original test curve and the trilinear approximation is shown in Figure 2.35, where the dashed line is representing the original test curve and the trilinear approximation is showed with the solid line.

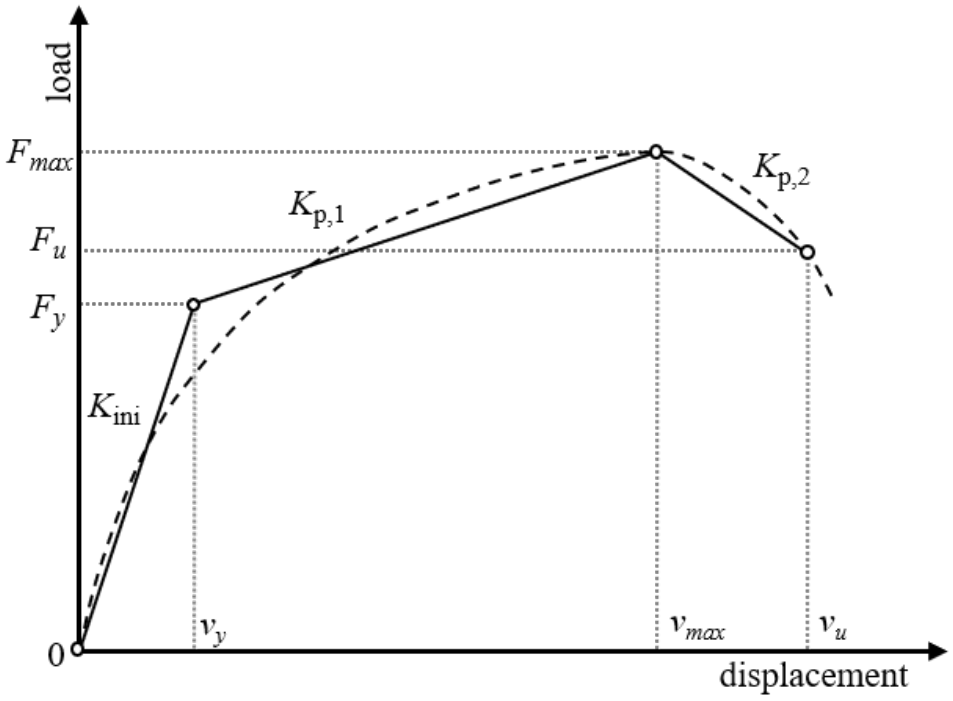

Figure 2.35: *Illustration of the trilinear test curve approximation, i.e. Y-M-U model as used in the method Gavric 2011/2015.*

Since the connections are loaded bi-directional, a quadratic interaction presented in Equation 2.30 is added to the method. There, the load-carrying capacity (R) correspond to the yield strength (F_y) in Figure 2.35. Lateral and vertical plastification is assumed to take place simultaneously when the condition in Equation 2.30 is overreached.

$$\left(\frac{F_{C,x}}{R_{C,x}}\right)^2 + \left(\frac{F_{C,z}}{R_{C,z}}\right)^2 \leq 1.0 \tag{2.30}$$

where:

$F_{C,x}$ = lateral load in connection
$R_{C,x}$ = lateral load-carrying capacity of connection
$F_{C,z}$ = vertical load in connection
$R_{C,z}$ = vertical load-carrying capacity of connection

In force-based models, it is usually difficult to determine a softening branch. This problem is dealt with in the Gavric 2011/2015 method by assuming that the incremental load step shift to being negative when one of the following two conditions is met; the maximum load-carrying capacity against uplift is reached in the most outer connection, or the load-carrying capacity against sliding is reached in any of the connections. Here, the load-carrying capacity corresponds to the respective maximum load (F_{max}) presented in Figure 2.35.

According to the method, before displacements in the connections are able to occur, the conditions in Equation 2.31 for sliding and 2.32 for rocking need to be fulfilled. This is due to the assumptions in the Gavric 2011/2015 method that is stated in Flatscher (2017, p.119) as, *"no sliding is possible as long as friction is higher than the acting lateral load, no rocking displacement occurs as long as the vertical load prohibits a rotation of the CLT panel"*.

$$F - \mu_f \cdot q \cdot l > 0 \tag{2.31}$$

$$F \cdot h - \frac{q \cdot l^2}{2} > 0 \tag{2.32}$$

When the load levels stated in Equation 2.31 and 2.32 are reached, the incremental growth of sliding and rocking that together contribute to the total head deflection can be calculated in Equation 2.33 and 2.34 respectively.

$$\Delta v_{sl} = \frac{\Delta F}{\sum \left(K_{C,x,m}\right)} \tag{2.33}$$

$$\Delta v_{rg} = \frac{\Delta F \cdot h^2}{\sum \left(K_{C,z,m} \cdot x_m^2\right)} \tag{2.34}$$

2.8.2 Displacement-based models

Felicetti 2012

According to Flatscher (2017), Felicetti introduced a semi-displacement-based approach in 2012 which was the first leap towards displacement-based modelling. In the model, every CLT wall system is assumed to be exposed to rocking deflection to some extent. Also, the deformations caused by sliding and CLT displacements are considered within the semi-displacement-based model presented by Felicetti in 2012 (Flatscher, 2017, p.121). The first step in this approach is to apply a lateral displacement with the assumption that only rocking deformations are appearing. The next step is to determine the load that is needed for the displacements to occur. Then, based on the actual load, the corresponding sliding and CLT deformations could be determined. These steps are then repeated until either the uplift capacity or the shear capacity of the connections are reached. It turned out, when comparing with experimental tests, that the assumption about the applied lateral displacement is only carried by rocking does not match well with test results. The model was therefore not suitable to use in practice.

Flatscher 2014/2016

Since the Felicetti 2012 method was not appropriate for practical use, Flatscher decided, in 2014 to develop a fully displacement-based model that predicts the behaviour of a CLT wall system. This model was in 2016 further developed and is in Chapter 4-4 in Flatscher (2017) introduced as "New displacement-based model", whereas in this thesis, the final model is called Flatscher 2014/2016.

The model is based on the approach with shear blocks. Some initial assumptions, similar to the Gavric 2011/2015 method are made, such as an assumption that the CLT panel is rigid. Furthermore, the CLT element is assumed to rotate around the lower corner (Flatscher, 2017, p.129).

While a displacement-based method uses, as the name indicates, a lateral displacement as input parameter instead of a lateral load, there is no direct way to determine how much sliding and rocking contribute individually to the total lateral displacement. To separate the total displacement into sliding and rocking, experimental results are used to fit a relation between the two types of displacements (Flatscher, 2017, p.121). To be able to perform wall analyses without being dependent on test results, an iterative process was added to the Flatscher 2014/2016 method in 2016. The process is based on equilibrium conditions and follows a six-step procedure that is presented below. To support the understanding and implementation of the method, a CLT wall system with some notations are visualised in Figure 2.36.

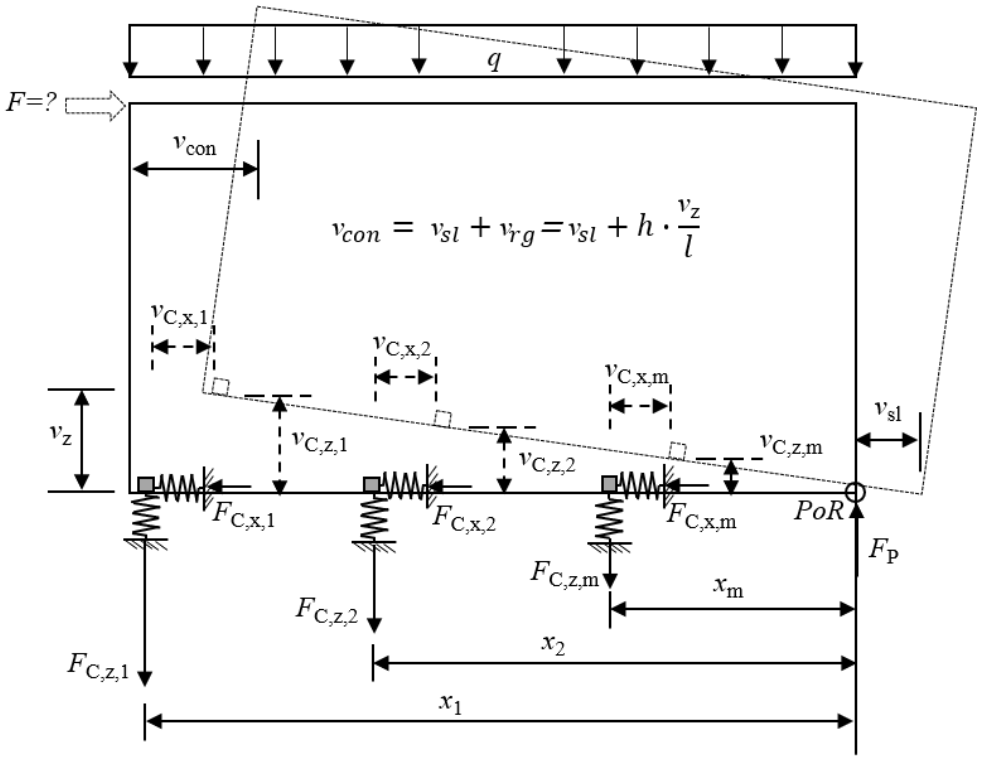

Figure 2.36: *Illustration of CLT wall system with notations included in the method Flatscher 2014/2016.*

Step 1:
Firstly, an estimation is made regarding how much the sliding and rocking are each contributing to the connection based lateral displacement v_{con}. To actualise this, a share parameter p, able to attend values between 0 and 1, is introduced in Equation 2.35 and 2.36 in which the lateral deflection caused by sliding and rocking is calculated, respectively.

$$v_{sl} = p \cdot v_{con} \tag{2.35}$$

$$v_{rg} = (1 - p) \cdot v_{con} \tag{2.36}$$

Step 2:
The second step is to compute the lateral and vertical displacements for every connection. The lateral displacement of a connection $v_{C,x,m}$ is expressed in Equation 2.37 and for the calculation of vertical displacement of a connection $v_{C,z,m}$, Equation 2.38 is used.

$$v_{C,x,m} = v_{sl} = v_{con} \cdot p \tag{2.37}$$

$$v_{C,z,m} = x_m \cdot \frac{v_{rg}}{h} = x_m \cdot \frac{(1 - p) \cdot v_{con}}{h} \tag{2.38}$$

Step 3:
Next, the appearing loads, corresponding to the calculated lateral and vertical displacements of each considered connection are determined. To determine the loads, the relationships presented in Equation 2.39, for lateral loads, and Equation 2.40, for vertical loads, are applied on a load-displacement model. Linear elastic, multi linear or any other method could be used when determining the loads, although the displacement-based model presented in Chapter 2.6 is recommended by Flatscher (2017).

$$F_{C,x,m} = f\left(v_{C,x,m}\right) \tag{2.39}$$

$$F_{C,z,m} = f\left(v_{C,z,m}\right) \tag{2.40}$$

Step 4:
Lateral loads, based on the estimated displacements, can now be calculated using Equation 2.41 and Equation 2.42, the first to determine the load responsible for sliding F_{sl} and the latter to calculate the load responsible for rocking F_{rg}. The potential effect of friction included in Equation 2.41 is taken into account by multiplying the coefficient of friction μ_f with the actual bearing load F_P. Based on equilibrium conditions, Equation 2.43, in which the actual bearing load F_P is calculated, is composed of the external vertical load q and the actual uplift loads acting in the connections $F_{C,z,m}$.

$$F_{sl} = \underbrace{\sum\left(F_{C,x,m}\right)}_{\text{connections}} + \underbrace{F_P \cdot \mu_f}_{\text{friction}} \tag{2.41}$$

$$F_{rg} = \underbrace{\frac{\sum\left(F_{C,z,m} \cdot x_m\right)}{h}}_{\text{connections}} + \underbrace{\frac{q \cdot l^2}{2 \cdot h}}_{\text{vertical load}} \tag{2.42}$$

$$F_P = \sum\left(F_{C,z,m}\right) + q \cdot l \tag{2.43}$$

Step 5:
Up until this point, the loads responsible for sliding and rocking have been studied separately. Physically, though, simply one lateral load F can act at the same time. Due to this, the sliding load F_{sl} need to be equal to the rocking load F_{rg}, to put it differently, the condition in Equation 2.44 shall be true.

$$F = F_{sl} = F_{rg} \tag{2.44}$$

The share parameter p assumed in the first step is correct if the condition in Equation 2.44 complies. If this is the case, the calculation can proceed to the next step. In the case where the condition is not satisfied, a new parameter p must be assumed in step 1 and the process needs to be repeated until equilibrium in Equation 2.44 is achieved. It is worth noting that the parameter p needs to be decreased if the sliding load F_{sl} exceeds the rocking load F_{rg}, otherwise p needs to be increased. For small deformations, one of the contributors to the total deflection might be prohibited by either sliding through high influence of friction or rocking via large vertical loads, see Equation 2.41 and

Equation 2.42 in step 4. If this occurs, the share parameter p could reach its minimum or maximum limit before the condition in Equation 2.44 is satisfied. The solution is then to take the load value as the minimum of F_{sl} and F_{rg}.

Step 6:
Now, when the actual load F is known, it is possible to determine the elastic CLT deformations if that is of interest. If so, the Equation 2.45 and Equation 2.46 are applied to calculate bending and shear, respectively.

$$v_{bn} = \frac{4 \cdot F \cdot h^3}{E_0 \cdot l^3 \cdot t_{eff}} \tag{2.45}$$

where:

E_0 = modulus of elasticity of raw material parallel to grain
t_{eff} = effective thickness of CLT element, considering thickness of vertical layers only

$$v_{sh} = \frac{1.2 \cdot F \cdot h}{G \cdot A_{eff}} = \frac{1.2 \cdot F \cdot h}{G \cdot t_{eff} \cdot l} \tag{2.46}$$

where:

G = shear modulus of timber element
A_{eff} = effective area of CLT element, considering area of vertical layers only
t_{eff} = effective thickness of CLT element, considering thickness of vertical layers only

The Flatscher 2014/2016 method also suggests a way to consider wall systems with openings but that will not be considered in this thesis.

2.8.3 Summary of force-based and displacement-based models

The majority of the models available are force-based since there is an advantage in being able to instantly calculate the displacement that agrees with the actual force. Although the force-based models enable a prediction similar to practical design, there are difficulties in defining the peak load and describing the subsequent softening branch.

Among the force-based models, Gavric 2011/2015 is the most advanced method but also the method that provides a simulation that fits well with various of load-displacement curves that have been collected from actual tests. The procedure of using incremental load steps gives a legitimate estimation of the load-displacement relationship, as long as being within the elastic area.

Similar to other force-based methods, the Gavric 2011/2015 method has problems with defining the maximum load-carrying capacity of the wall system and predicting the post peak softening area in the curve. The problem is dealt with in the method Gavric 2011/2015 by implementing the assumption of a shift from positive to negative incremental load steps when either the maximum load-carrying capacity against uplift is reached in the most outer connection, or the load-carrying capacity against sliding is reached in any of the connections. Notwithstanding the attempts to determine the maximum

capacity and the subsequent softening branch, an assumption still needs to be made in order to find where the negative load increments begins. The consequence of this is that the behaviour of the wall system, in the case where a weak connection is positioned at the most outer corner, would be markedly underestimated for systems where rocking is governing. Similar effects could be expected for wall systems where a single connection exhibits low shear resistance and sliding is the controlling mechanism.

Although the method of using deflection of the wall system as an input parameter instead of force, in general is considered to lack feasibility, displacement-based methods are actually superior to the force-based methods in defining the maximum load-carrying capacity and describing the softening branch that follows after the peak. This due to the augmented consideration of connections that a displacement-based approach enables, even after the connections have reached their maximum load-carrying capacity. Hence, making it possible to simulate the post peak behaviour of the connections without being required to make any additional assumptions.

2.9 Calculations according to Eurocode 5

To predict the strength of dowel-type connections according to the European standard Eurocode 5 (CEN, 2004) the Johansen theory is used. To calculate the strength of a fastener according to the Johansen theory in Eurocode 5 one needs to know the fastener geometry and material properties along with the embedment strength and the fastener yield moment.

2.9.1 Failure modes

A connection can fail in different ways depending on several different parameters. Different failure modes were presented by Johansen in 1949, where he identified failure modes relating to the number of plastic hinges occurred in the fastener. Johansen identified three different failure modes, illustrated in Figure 2.37. Where failure mode I has none plastic hinges in the fasteners, failure mode II has one plastic hinge and failure mode III has two plastic hinges in the fasteners. Eurocode 5 divides the fasteners if there are single shear or double shear. In this study, only double shear will be regarded.

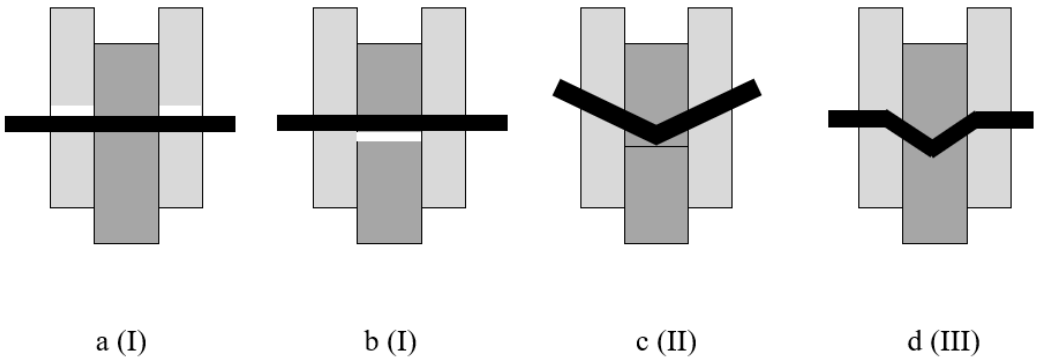

Figure 2.37: *Different failure modes for timber-to-timber fastener in double shear.*

2.9.2 Embedment strength

In Eurocode 5 the embedment strength is based on studies performed by Whale and Smith (1986) and Ehlbeck and Werner (1992) according to Leijten, Köhler, and Jorissen (2004). The variables in the formula for calculating the embedment strength are the timber density and diameter of the fastener.

According to Eurocode 5 the characteristic embedment strength $f_{h,k}$ for timber and Laminated veneer lumber (LVL) elements with fasteners up to 8 mm is determined as:

$$f_{h,k} = 0.082\rho_k d^{-0.3} \quad \text{without pre-drilled holes} \tag{2.47a}$$

$$f_{h,k} = 0.082(1 - 0.01d)\rho_k \quad \text{with pre-drilled holes} \tag{2.47b}$$

where:

ρ_k = characteristic timber density in kg/m^3
d = fastener diameter in mm

If the bolts are larger than 8 mm the embedment strength must be calculated with a factor depending on the timber product and fastener diameter.

In the case for other timber panel products with nails with head diameter of at least $2d$, the characteristic embedment strength is determined as:

$$f_{h,k} = 0.11\rho_k d^{-0.3} \quad \text{for plywood} \tag{2.48a}$$

$$f_{h,k} = 30d^{-0.3}t^{0.6} \quad \text{for hardfibre board (SS-EN 622-2)} \tag{2.48b}$$

$$f_{h,k} = 65d^{-0.7}t^{0.1} \quad \text{for particle board and OSB} \tag{2.48c}$$

where:

ρ_k = characteristic timber density in kg/m^3
d = fastener diameter in mm
t = panel thickness in mm

The way according to Eurocode 5 to calculate the embedment strength does not consider if it is loaded parallel or perpendicular to the grain. The direction will significantly influence the displacement behaviour according to Leijten et al. (2004), where the embedment strength is twice as high if it is loaded parallel to the grain instead of perpendicular to the grain. Since this way of calculating the embedment strength does not give a value that represent the reality, Leijten et al. (2004) has come up with an equation that has a better fit to match reality:

$$f_h = A\rho^B d^C \tag{2.49}$$

where:

ρ = timber density
d = nail diameter in mm is the material parameters

A, B and C are parameters derived from regression analysis. The regression parameters are presented in Table 2.21.

Table 2.21: *Parameters from regression analysis for embedment strength calculations according to Leijten, Köhler, and Jorissen (2004).*

Parameter	Distribution type	Mean	st. Dev
A	Normal	-2.33	0.23
B	Normal	1.07	0.04
C	Normal	-0.25	0.012
ϵ	Normal	0	0.11

The ϵ in Table 2.21 represent the error term with zero as mean value. The values for A, B and C are results from data analysis from many different research projects. Equation 2.49 is quantified for parallel to the grain loading in softwood with pre-drilled dowel fasteners.

2.9.3 Yield moment

The yield moment is the same as the plastic moment in the steel fastener and represent the moment needed for a plastic hinge to occur in the fastener. The yield moment is dependent on the fastener diameter and the strength of the fastener material in tensile. The characteristic yield moment $M_{y,Rk}$ for round bolts and dowels according to Eurocode 5 is determined as:

$$M_{y,Rk} = 0.3 f_u d^{2.6} \tag{2.50}$$

where:

f_u = characteristic tensile strength in N/mm^2
d = fastener diameter in mm

2.9.4 Partial and modification factor

In order to determine design values, a partial factor γ_M is used which is chosen from Table 2.22 for the material property that is being relevant.

Table 2.22: *Recommended partial factors γ_M for material properties and resistances.*

Fundamental combinations	γ_M
Solid timber	1.3
Glued laminated timber	1.25
LVL, plywood, OSB	1.2
Connections	1.3
Accidental combinations	1.0

Also, the modification factor k_{mod} is included in order to determine design values. This factor is taking the effect of moisture content and load-duration into account. The moisture content in the environment of the applied building element is decisive regarding the service class. The service class together with the load-duration class gives a modification factor k_{mod} which is listed in Table 2.23 for some selected materials.

Table 2.23: *Values of modification factor k_{mod}.*

Material	Service class	Load-duration class				
		Permanent action	Long term action	Medium term action	Short term action	Instanta-neous action
Solid timber	1	0.60	0.70	0.80	0.90	1.10
	2	0.60	0.70	0.80	0.90	1.10
	3	0.50	0.55	0.65	0.70	0.90
Glued laminated timber	1	0.60	0.70	0.80	0.90	1.10
	2	0.60	0.70	0.80	0.90	1.10
	3	0.50	0.55	0.65	0.70	0.90
LVL	1	0.60	0.70	0.80	0.90	1.10
	2	0.60	0.70	0.80	0.90	1.10
	3	0.50	0.55	0.65	0.70	0.90
Plywood	1	0.60	0.70	0.80	0.90	1.10
	2	0.60	0.70	0.80	0.90	1.10
	3	0.50	0.55	0.65	0.70	0.90
OSB	1	0.30	0.45	0.65	0.85	1.10
	2	0.40	0.50	0.70	0.90	1.10
	3	0.30	0.40	0.55	0.70	0.90

2.9.5 Load-carrying capacity

In Section 2.9.1 three different failure modes were described for fastener in double shear. Which one of these failure modes that will occur is determined by which has the lowest load-carrying capacity. Therefore, the characteristic load-carrying capacity in double shear for fastener is determined according to Eurocode 5 as:

$$F_{v,Rk} = \min \begin{cases} f_{h,1,k} t_1 d & \text{(2.51a)} \\ 0.5 f_{h,2,k} t_2 d & \text{(2.51b)} \\ 1.05 \dfrac{f_{h,1,k} t_1 d}{2+\beta} \left(\sqrt{2\beta(1+\beta) + \dfrac{4\beta(2+\beta) M_{y,Rk}}{f_{h,1,k} d t_1^2}} - \beta \right) + \dfrac{F_{ax,Rk}}{4} & \text{(2.51c)} \\ 1.15 \sqrt{\dfrac{2\beta}{1+\beta}} \sqrt{2 M_{y,Rk} f_{h,1,k} d} + \dfrac{F_{ax,Rk}}{4} & \text{(2.51d)} \end{cases}$$

where:

t_i = timber board thickness or penetration depth
$f_{h,i,k}$ = characteristic embedment strength in timber member i
d = fastener diameter
$M_{y,Rk}$ = characteristic yield moment in fastener
β = ratio between embedment strengths of the members
$F_{ax,Rk}$ = characteristic withdrawal capacity of the fastener

Equation 2.51a represent the failure mode *a* illustrated in Figure 2.37 and likewise with the remaining three equations and figures.

If the timber members have the same density and fasteners have the same diameter, the timber elements will also have the same embedment strength and therefore β will be equal to one.

The withdrawal strength $F_{ax,Rk}$ is the contribution from rope effect. The contribution from rope effect depends on which type of fastener it is and is limited according to Table 2.24 in relation to the shear capacity. If the contribution is unknown this factor should be taken as zero.

Table 2.24: *Maximum contribution to the load-carrying capacity from rope effect.*

Fastener type	Percentage
Round nails	15 %
Square and grooved nails	25 %
Other nails	50 %
Screws	100 %
Bolts	25 %
Dowels	0 %

The design value of the load-carrying capacity $F_{v,Rd}$ is determined according to Equation 2.52, where γ_M is a partial factor for a material property that is chosen from Table 2.22. The modification factor k_{mod} is chosen from Table 2.23.

$$F_{v,Rd} = k_{mod} \frac{F_{v,Rk}}{\gamma_M} \tag{2.52}$$

2.9.6 Slip modulus of fasteners

The slip modulus K_{ser} per shear plane per fastener for dowel-type fasteners should according to CEN (2004) be taken as presented in Table 2.25. These values should be used for Serviceability Limit State (SLS).

Table 2.25: *Slip modulus K_{ser} for fastener in timber structures.*

Fastener type	K_{ser} [N/mm]
Dowels Bolts with or without clearance Screws Nails (with pre-drilling)	$\rho_m^{1.5} d/23$
Nails (without pre-drilling)	$\rho_m^{1.5} d^{0.8}/30$

where:

$$\rho_m = \text{mean density of the timber in kg/m}^3$$
$$d = \text{outer diameter of the fastener in mm}$$

If the structure instead is in Ultimate Limit State (ULS) the slip modulus should be calculated according to Eurocode 5 as:

$$K_u = \frac{2}{3} K_{ser} \tag{2.53}$$

The reason to why the slip modulus in ULS is only 2/3 of the slip modulus in SLS is because in SLS there is a linear relationship between load and deformation, while in ULS there is a nonlinear stress-strain behaviour. This will lead to plastic deformation and therefore the approach of an ideal stress-strain relationship up to the maximum load, which will increase the angle underneath the curve and reduce the slip modulus.

3 Finite Element model and methodology

In this chapter the finite element model is presented together with how the input parameters have been defined. The first part of the chapter consists of a description of the applied software along with an explanation of how the processes have been carried out. In the analyses, both linear and nonlinear behaviour of the connections are included. Finally, to validate the results from the FE-model, these were compared to hand calculations and tests performed according to Flatscher (2017) which are presented in this chapter.

3.1 FE software Abaqus/CAE

The finite element model was developed in the software Abaqus/CAE (henceforth simply referred to as "Abaqus"), which is suitable for simulations and visualisation of FE-models. The modelling in this thesis were performed in version 2017 of Abaqus. The FE analyses consist of three different steps, where the first step is pre-processing or modelling, the second step is processing or FE-analysing, and the last step is post-processing. The software is written in the programming language Python, which is an open-source language. Therefore, the input file can easily be created or altered by Python scripting instead of making changes in the visual model, e.g. the pre-processing step can be created in Python instead of Abaqus. This allows for a faster and more manageable option when executing several different analyses where only minor modifications are made before each run.

3.2 Abaqus model

The model analysed in Abaqus was developed according to Figure 3.1. The size of the CLT wall element is 3 000 mm in both x- and y-direction, while the thickness of the element is 100 mm. The dimensions of the CLT element were chosen to be the same as the ones applied in the model of Flatscher (2017) to be able to compare with the tests and simulations performed in that thesis.

Since the focus is set on laterally loaded CLT wall systems, a horizontal force or displacement was applied at the top left corner of the element. To prevent the entire CLT element from moving, the lower right corner was assigned a boundary condition as illustrated in Figure 3.1. Thereby, movement is prohibited in all directions except rotation around that point. This means that the displacement due to sliding v_{sl} is avoided and the total displacement v_{tot} will only consist of the contributions from rocking v_{rg} and the deformations of the CLT v_{CLT}. To avoid the effect of eccentricity also in the FE-model, a symmetry plane was made, creating symmetry on both sides of the x- and y-axis in the z-direction. To model the connections, springs have been used, which would only take load in axial direction. The node from the springs that is not attached to the CLT element is locked in all directions to symbolise connections that are fixed to the concrete floor element. The connections were modelled, first with linear behaviour and then with nonlinear behaviour. This procedure was followed due to the possibility it brings, to step-wise being able to verify the accuracy of the model while continuously evolving it. The properties of the CLT wall element and the connections are further described in Section 3.2.1 and 3.2.2.

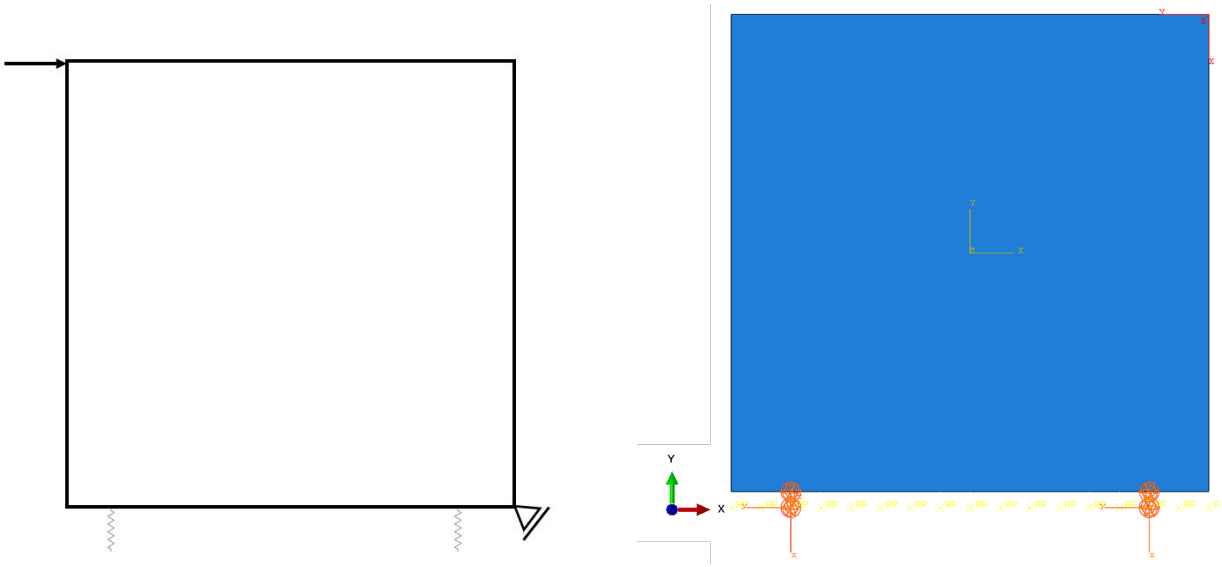

(a) (b)

Figure 3.1: *Model of system with two hold-downs - (a) illustration of applied load and boundary condition, (b) appearance of the FE-model in Abaqus.*

3.2.1 Modelling CLT wall element

Linear behaviour

For the linear analysis, the CLT element was assumed to behave isotropic. An isotropic material only has two elastic constants, one elastic modulus that is assumed to be the same in all directions of the material, and one Poisson ratio. The elastic modulus of the isotropic CLT element was set to 11 kN/mm^2, a value corresponding to the elastic modulus parallel to the grain of structural timber C24. A Poisson ratio of 0.3 was assumed since that is a value commonly used for structural timber.

Nonlinear behaviour

For modelling the CLT wall element in the nonlinear analysis, the orthotropic model was chosen since that is the most representative description of the behaviour of the CLT element. An orthotropic material has nine independent elastic constants: three elastic modulus, three shear modulus and three Poisson ratios.

The elastic modulus, also known as the Young's modulus, are locally defined in the axial, tangential and radial direction. The axial direction corresponds to the direction parallel to the grain direction. The tangential direction refers to the direction perpendicular to the grain direction and transverse to the growth rings. The radial axis is perpendicular to the grain direction and normal to the growth rings. For a composite element such as a CLT panel, the stiffness properties need to be defined globally. By having layers oriented in different directions, the grain direction in each axis is no longer only parallel or perpendicular to an applied load.

For determining the stiffness properties of an orthotropic material in the global x, y and z-direction there are several methods. A common method to verify the properties is to follow the rules in product standards when evaluating test specimen cut out from the CLT panel. While test specimen is not available in this case, a more theoretical approach is chosen. Thereby, the elastic modulus and the shear modulus in each direction of the CLT panel is calculated by considering every single layer according to the compound theory developed by Bodig and Jayne (1982). Since the layers in the CLT panel are assumed to consist of C24 timber, the stiffness properties parallel and perpendicular to the grain are based upon the material properties for structural timber C24 given in SS-EN 338:2016. The mean values will be used for both elastic modulus and shear modulus since the deformations will be studied.

As the mean value of the shear modulus is the same for both xy-direction and xz-direction, the compound theory does not influence those values. For structural timber according to SS-EN 338:2016, the shear modulus in yz-direction, called rolling shear modulus, is usually calculated as twice the tension strength perpendicular to the grain $f_{t,90,k}$. This method would give a rolling shear modulus of 0.0008 kN/mm^2, a very low value. The rolling shear modulus in CLT depends on the ratio between the width of each "wood panel" and the thickness of the layer. According to Schickhofer, Brandner, and Bauer (2016), in technical assessment documents, the rolling shear modulus is calculated as 10 % of the mean value of the shear modulus, for a ratio above 4 between the wood panel width and layer thickness. The production of CLT elements in Europe is, since a while back, showing an increase in the use of base material taken closer to the pith (Schickhofer et al., 2016). In the past, the base material was mainly taken from the side-boards, something that induced lower values for the shear modulus. The improved quality of the base material in today's CLT panels argues in favour of calculating the shear modulus in yz-direction as 10 % of G_{mean}.

The final three parameters, the Poisson ratios, are locally defined in the same directions as the shear modulus: xy-, xz- and yz-direction. Due to the layers of the CLT being crosswise arranged, the Poisson ratio is assumed to have a minor importance considering the load-deformation behaviour of the CLT wall element. The Poisson ratio is therefore assumed to be equal for all directions. For structural timber, which is the base-material of the CLT layers in this thesis, the Poisson ratio is usually assumed to be 0.3. Thereby, the Poisson ratio is set to 0.3 for every direction.

In Abaqus, the elastic modulus for an orthotropic material in the different directions are separated by the index numbers 1,2 and 3, where 1 represents the global x-direction, 2 stands for the global y-direction and 3 denotes the global z-direction. For the surface layers, the boards are oriented with the grain direction perpendicular to the load. Regarding the intermediate layer, the grain direction is parallel to the global x-axis and thereby parallel to the lateral load acting in the same direction.

The values of the stiffness properties that have been used in the FE-model are displayed in Table 3.1 and the calculations behind the values are attached in Appendix A.

Table 3.1: *Stiffness properties of CLT element used in FE-model.*

Material Parameters	Abaqus Notation	Value	Unit
Young's Modulus	$E_1 = E_x$	4.62	kN/mm^2
	$E_2 = E_y$	6.75	kN/mm^2
	$E_3 = E_z$	0.37	kN/mm^2
Shear Modulus	$G_{12} = G_{xy}$	0.69	kN/mm^2
	$G_{13} = G_{xz}$	0.69	kN/mm^2
	$G_{23} = G_{yz}$	0.069	kN/mm^2
Poisson Ratio	$\nu_{12} = \nu_{xy}$	0.3	-
	$\nu_{13} = \nu_{xz}$	0.3	-
	$\nu_{23} = \nu_{yz}$	0.3	-

Since the nonlinear FE-analysis is carried out with incremental steps, that is step-wise extracting the results, the force needs to be predicted if using a force-based method. If a too high force is given, the FE-analysis will be aborted as soon as the analysis reaches a force where the system no longer can undergo the corresponding deformations. If a too low force is assumed, the full load-displacement behaviour is not shown. To avoid errors in the FE-analysis, a backward method has been used, i.e. a displacement-based method. This was done by applying a lateral displacement at the top left corner of the CLT element, acting in the global x-direction. Then, the corresponding forces could be obtained.

3.2.2 Modelling connections

To model the hold-downs and angle brackets, springs were used. The springs were modelled to only take load in one direction, the axial direction of the spring. Since hold-downs only carry load in tension, they are modelled with one spring in y-direction. Angle brackets, however, carry both vertical and horizontal loads. To account for that in the model, the angle brackets are modelled as two springs, one acting in x-direction and the other in y-direction.

In Abaqus, three different types of springs can be modelled. The one used in this thesis was *Spring2*, which is an axial spring acting in a fixed direction. The force in the spring is positive in tension and the *Spring2* element has up to six degrees of freedom in contrast to the other types of springs that can have three degrees of freedom. In this thesis the degrees of freedom are set to 1 in each node and the direction of this is set to have the same direction as the spring. The first node in each spring connection is set as fully restrained, to model the concrete foundation. Therefore, the relative displacement of the spring will be equal to the relative displacement of the second node, which are connected to the CLT element.

Linear behaviour

When studying the linear behaviour, two types of systems were considered, one with hold-downs as the connections between the CLT wall element and the concrete foundation, and the other with angle brackets as connections. Moreover, these systems were divided into three set-ups each, one where two connections were applied, one with four connections applied and a last, with eight connections

applied. This is resulting in a total of six systems studied, all of which are subjected to a lateral load $F = 10$ kN, acting in the upper corner of the CLT wall element.

For the systems with hold-downs, one type of hold-down was studied, that is the HTT22E hold-down, described in Chapter 2.2.2. The reason for choosing that hold-down is that it is commonly used in CLT structures, additionally, the HTT22E hold-down has been studied by Flatscher (2017), something that is to an advantage when comparing results. The fasteners chosen for the HTT22E hold-down are 24 nails of the type CNA 4.0x60 mm, which is in line with the recommendations from the manufacturer SIMPSON Strong-Tie, see Chapter 2.2.2.

As for the systems with hold-downs, only one type of angle bracket is considered for the systems with angle brackets. The angle bracket that have been studied in the linear analysis is the AE116 angle bracket, described in Chapter 2.2.3. This angle bracket is included in the studies by Flatscher (2017) which is the main reason for the choice of the AE116 angle bracket. Also, here, the CNA 4.0x60 mm nails have been chosen. The minimum number of nails for this angle bracket according to SIMPSON Strong-Tie (2019) is 11. In the linear analysis, 12 nails have been considered for each angle bracket.

To model the connections in Abaqus, the linear spring behaviour needs to be defined, i.e. a constant spring stiffness should be specified. The stiffness of the hold-downs and the angle brackets that have been used as input data in the model are presented in Table 3.2. The values are determined by multiplying the slip modulus K_{ser} of each individual fastener with the number of fasteners in the connection, i.e. 24 for the hold-down and 12 for the angle bracket. The calculation is made by hand and follows Eurocode 5 where the stiffness assumes that there are pre-drilled holes for the fasteners in the CLT element. In Appendix B, the calculations are provided.

Table 3.2: *Input data for connections in the linear analyses in Abaqus.*

Connection type	Stiffness of spring
Hold-down	36 kN/mm
Angle bracket	18 kN/mm

For the hold-downs, that simply carry vertical loads, the stiffness of 36 kN/mm was only assigned in the vertical direction, the y-direction. Since the angle brackets resist both uplift forces and shear forces, the stiffness of the 12 nails was assigned in two different springs, one acting only in x-direction and one only in y-direction, each with the same stiffness of 18 kN/mm.

Nonlinear behaviour

When studying the nonlinear behaviour, only the systems with hold-downs were considered with the same properties as described in the linear behaviour section above. This is resulting in a total of three systems studied, all of which are subjected to a lateral displacement acting in the upper corner of the CLT wall element.

To model the nonlinearity of connections the load deformation curves were adapted to fit the model described in Section 2.7, developed by Foschi. The values for the input parameters were taken from Flatscher (2017, p.157-161) and refers to a HTT22E hold-down loaded in tension. These values can be found in Table 3.3.

Table 3.3: *Mean input parameters for nonlinear load deformations curves.*

Connection	F_{max} [kN]	v_{max} [mm]	K_{ini} [kN/mm]	F_t [kN]	v_u [mm]
HTT22E	49.80	18.30	36.10	40.10	27.00

The input parameters F_{max} and K_{ini} were varied according to coefficients of variations described in Section 2.4.3 and the lower and upper limits from this along with the mean curve are illustrated in Figure 3.2.

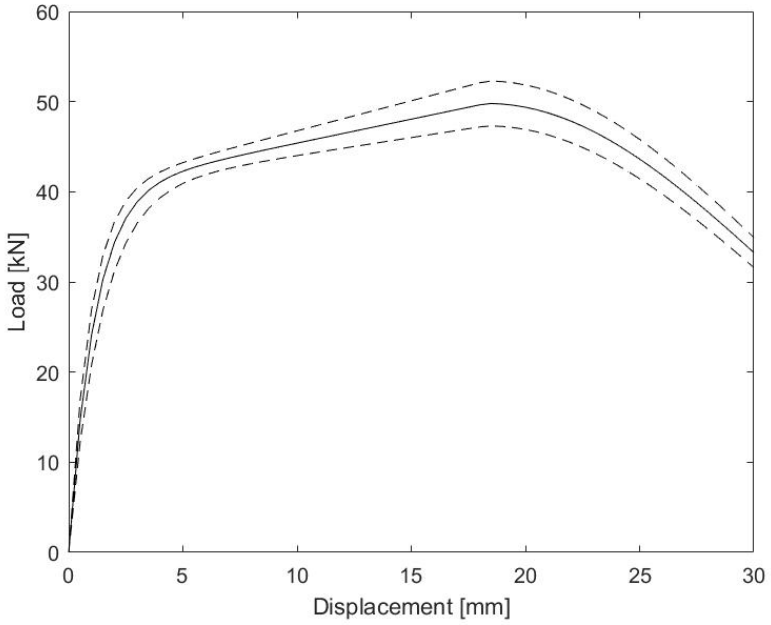

Figure 3.2: *Load deformation curve for one hold-down loaded in tension.*

To generate this nonlinear behaviour of springs in Abaqus, the input file had to be altered by adding *nonlinear, dependencies=2* after the other properties for the spring. After this line *1,1* is added to set how many degrees of freedom each node in the spring has. On the lines following this command, the load and displacement are given as a table. The load-deformation behaviour could also depend on other parameters such as temperature, which could be accounted for by increasing the number of dependencies. Since those parameters are excluded in this thesis, the dependencies are set equal to two. Following is an example with a spring modelled with bi-linear behaviour:

*SPRING, ELSET=.., ORIENTATION=.., NONLINEAR, DEPENDENCIES=2
1,1
F_0, u_0
F_1, u_1
F_2, u_2
*ELEMENT, TYPE=SPRING2, ELSET=...

3.2.3 Monte Carlo simulations

To be able to calculate the structural reliability of an entire structure, Monte Carlo simulations were performed on the nonlinear FE-analyses. Monte Carlo simulations are based on random sampling within a domain of possible values. In this thesis the random sampling is from creating different load-displacement curves within the area in Figure 3.2 with varying the maximum capacity F_{max} and initial stiffness K_{ini}. In total 1 000 simulations were carried out separately for each model, with two, four and eight hold-down connections. A Matlab script for creating these input files can be found in Appendix C. After creating the input files, these were executed in Abaqus through the command prompt by running a Python script, which can be found in Appendix D. The data from the simulations in Abaqus were saved in a .dat-file, which then was read by a Matlab code in order to extract the relevant data. The Matlab code can be found in Appendix E.

Monte Carlo simulations were also performed with varying ductility ratio with the purpose to determine how much influence the ductility of connections has on the global load-carrying capacity. The analyses were done with two, four and eight connections with varying ductile behaviour along with varying the maximum capacity F_{max} and initial stiffness K_{ini} as described in the paragraph above. For each connection type and ductility ratio; 500 simulations were performed. The different input load-displacement curves were modelled according to Figure 3.3.

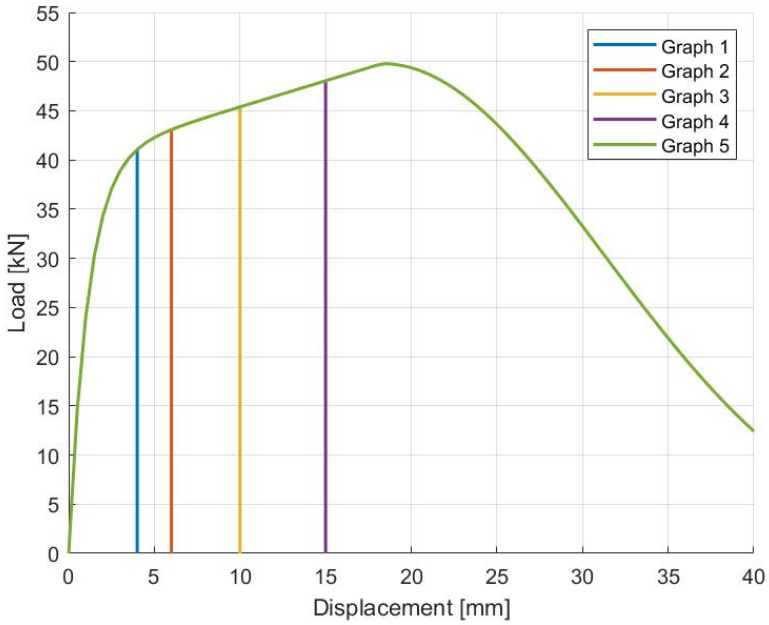

Figure 3.3: *Load-displacement curves for connections modelled with different level of ductility.*

3.3 Verification of FE-model

A verification of the FE-model was necessary to evaluate the reliability of the model. This was done by hand calculations and comparison with test data evaluated by Flatscher (2017). The hand calculations are based on Eurocode 5. The theory behind the equations are explained in Chapter 2.9, whereas in this chapter, the calculation process and the decisions behind it, are in focus.

3.3.1 Linear analysis

The stiffness K_{ser} of the connections were varied with ± 10 % in the FE-model and the spatial displacement U1, the global x-direction, in the upper corner of the element, on the opposite side of the applied load, were read off for each K_{ser}. The applied load of 10 kN were divided with the spatial displacement U1 to receive the global stiffness of the wall element $K_{ser,wall}$.

The percentage change between the varied K_{ser} were compared to the percentage change of the global wall stiffness $K_{ser,wall}$ in order to investigate the relationship between the connection stiffness and the global stiffness of the wall system.

Then, the global wall stiffness $K_{ser,wall}$ was calculated by hand according to Eurocode considering linear-elastic behaviour. Through condition of equilibrium, the expression stated in Equation 3.1 could be derived as shown in Appendix F.

$$K_{ser,wall} = K_{ser} \cdot \frac{\sum b_i^2}{h^2} \tag{3.1}$$

where:

b_i = distance between connection i and Point of Rotation (PoR)
h = height of CLT wall element

The hand calculated global stiffness $K_{ser,wall}$ for systems with two, four and eight connections were compared with the global stiffness values obtained from the FE-model. This was only done for the hold-downs since it was assumed that, if the hold-downs in the FE-model correspond well to the hand calculations, the angle brackets would also correspond well to the hand calculations. This due to the fact that both type of connections are modelled in the same way, with the only difference that there are horizontal springs included in the model with angle brackets.

3.3.2 Nonlinear analysis

To verify the nonlinear FE-model, the results from the model are compared with results from hand calculations. More specifically, the load-carrying capacity of the connections, and the global load-carrying capacity of the wall system with the applied connections are calculated by hand according to Eurocode 5 and thereafter compared with the corresponding results from the FE analyses.

Load-carrying capacity per connection

Here follows the process of how the design value of the load-carrying capacity $F_{v,Rd}$ for each connection was calculated. Firstly, the characteristic load-carrying capacity per fastener $F_{v,Rk}$ was determined considering fasteners in double shear, since the studied wall consists of a three-layered CLT panel. This was done by taking the minimum value in the equation of load-carrying capacity, presented in Chapter 2.9.5, where the sub-equations are representing the different failure modes that can occur. In this way, the load-carrying capacity of the fastener is governed by the load-carrying capacity of the failure mode that is most likely to occur first.

The ring shank nail from SIMPSON Strong-Tie that has been used in the FE-model is also the one that the calculations have been based on. The nail, CNA 4.0x60, introduced in Table 2.2 and Figure 2.3 in Chapter 2.2.1, has a diameter d of 4.0 mm, a length l of 60 mm and an characteristic axial withdrawal capacity $F_{ax,Rk}$ of 1.25 kN. The nail is made of stainless steel 304 and the characteristic tensile strength f_u is set to 0.51 kN/mm^2. The calculations assume that there are no pre-drilled holes. The contribution to the load-carrying capacity due to the rope effect have been taken into account and the contribution was limited to 15 % of the rope effect according to Table 2.24 for round nails.

When the characteristic value of the load-carrying capacity per fastener is determined, the design value can be calculated. This has been done according to Equation 2.52 in Chapter 2.9.5 where the partial factor γ_M for connections have been applied. The modification factor k_{mod} is based upon the assumptions that the wall belongs to service class 1 and the load-duration class is short-term, corresponding to e.g. wind load. Finally, the design value per fastener is multiplied with the number of fasteners in the hold-down, that is 24 nails, and thereby, the design value of the load-carrying capacity per hold-down connection is received. The calculations can be found in Appendix F.

Global load-carrying capacity of wall system

Similar to the calculations for the global wall stiffness, the global load-carrying capacity of the wall system was calculated by hand according to Eurocode considering linear-elastic behaviour. Through condition of equilibrium, the expression stated in Equation 3.2 could be derived as shown in Appendix F. The calculation is performed for both the characteristic values and the design values.

$$F_{v,R,wall} = F_{v,R} \cdot \frac{\sum \left(\frac{b_i^2}{b_1} \right)}{h} \tag{3.2}$$

where:

b_1 = distance between connection 1 and PoR
b_i = distance between connection i and PoR
h = height of CLT wall element

The design value for the hand calculated global load-carrying capacity $F_{v,Rd,wall}$ and the characteristic value $F_{v,Rk,wall}$ for systems with two, four and eight connections were compared with the global load-carrying capacity values obtained from the nonlinear FE-analyses. By doing so, one could study the differences between; designing completely according to Eurocode 5 for linear-elastic behaviour, and designing according to nonlinear FE-analyses with analytical approximation of connection properties, based on test data. This comparison was done regarding load distribution.

Next, the 0.05-quantile values for the global load-carrying capacity $F_{0.05}$ obtained from the nonlinear FE-analyses were divided with the design values for the global load-carrying capacity $F_{v,Rd,wall}$, creating a factor η that is representing the extra capacity that is left in the wall system if designing according to Eurocode 5. This factor could be seen as a safety factor and it is used to compare the design approach in Eurocode 5 with the nonlinear FE-analyses in terms of effect of ductility. Since ductility is not considered in Eurocode 5, the factor η is plotted against different ductility ratio for the wall systems with two, four and eight connections to study how large the differences is between Eurocode 5 and the nonlinear analyses.

4 Linear FE-analyses

The first part of the FE-analysis was when the connections were modelled with linear behaviour. The results from these analyses are presented and discussed in this chapter.

4.1 Hold-down connections

The stiffness K_{ser}, that was assigned to the hold-downs was initially 36 kN/mm. Then the stiffness was decreased with 10 % but also increased with 10 %, resulting in a stiffness K_{ser} of 32.4 kN/mm and 39.6 kN/mm, respectively. The resulting global wall stiffness $K_{ser,wall}$ from the linear FE-analysis are presented in Table 4.1 together with the percentage change of the global wall stiffness. The results from the hand calculations are presented in the same table, where the global wall stiffness $K_{ser,wall}$ have been calculated considering the same variation of connection stiffness as in the FE-model.

Table 4.1: *Stiffness of connections and wall element with hold-downs from linear analyses.*

Number of connections	K_{ser} [kN/mm]	$K_{ser,wall}$ [kN/mm]	change in K_{ser} [%]	change in $K_{ser,wall}$ [%]	calculated $K_{ser,wall}$ [kN/mm]
2	32.4	17.13	-10	-7	25.31
	36	18.39	-	-	28.13
	39.6	19.57	+10	+6	30.94
4	32.4	22.79	-10	-6	42.53
	36	24.16	-	-	47.25
	39.6	25.42	+10	+5	51.98
8	32.4	34.12	-10	-5	86.06
	36	35.77	-	-	95.63
	39.6	37.26	+10	+4	105.19

When looking at the percentage change in the global stiffness of the wall $K_{ser,wall}$ in Table 4.1, it is clear that the wall system does not behave quite linear. With an increase of the connection stiffness K_{ser} by 10 %, the global wall stiffness $K_{ser,wall}$ is expected to follow the pattern of 10 % increase. For two hold-downs, the global stiffness of the wall increases by 6 %, for four hold-downs, there is an increases of 5 % and for eight hold-downs, the global stiffness of the wall only increases by 4 %. This indicates that the connection stiffness is not the governing factor for the global stiffness of the studied wall systems.

The results of the global wall stiffness from the FE-analyses were expected to be very similar to the values obtained from the linear-elastic hand calculations, since both analyses are based on linear behaviour. As can be confirmed by the results presented in Table 4.1, the FE-values are smaller than the calculated ones. In fact, the more connections and the higher the connection stiffness, the larger the gap gets between the FE-values and the calculated values. To investigate this deviation, the deformed CLT wall element in the FE-model is studied in Figure 4.1, for the wall system with two hold-downs.

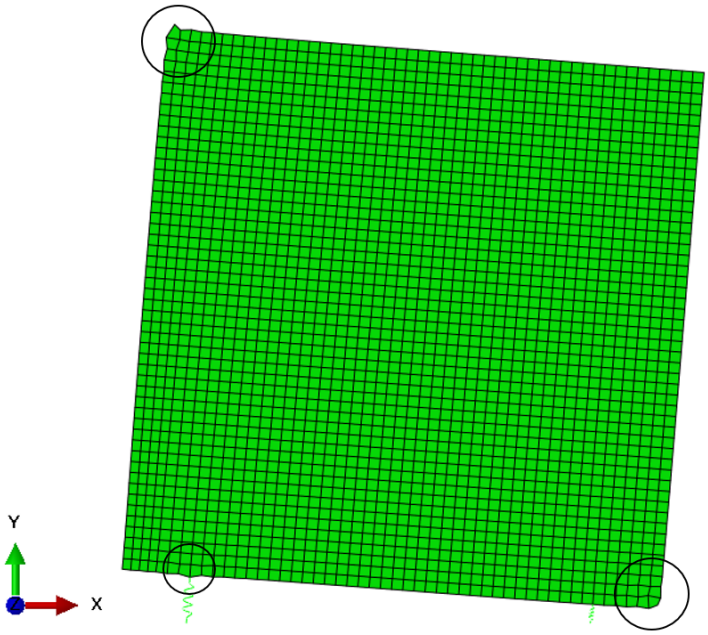

Figure 4.1: *Displacements of CLT wall system in FE-model with two hold-downs under lateral load F=10 kN and an elastic modulus of the CLT of 11 kN/mm^2 - disturbances marked with black circles.*

As the area in the black circles demonstrate in Figure 4.1, there is disturbance in the material in the upper left corner, where the lateral load of 10 kN is applied, but also by the left hold-down modelled as a spring, and in the lower right corner. This indicates that, either the load is too large, or the stiffness of the CLT wall element is too small. The lower global stiffness as a result of the larger displacements, that is the outcome of the linear FE-analysis could be caused by deformations of the CLT element. In the FE-model, the CLT wall element is assigned with a Young's modulus of 11 kN/mm^2, whereas the wall element in the linear-elastic hand calculations according to Eurocode are assumed to be rigid, i.e. very stiff. To be able to verify the linear FE-analysis, the CLT element was assigned with a very high stiffness, specifically, a Young's modulus of 1 100 000 kN/mm^2. The deformed CLT wall system with two hold-downs and a rigid CLT wall panel is shown in Figure 4.2. There, it can be noticed that there are no longer any deformations in the CLT element.

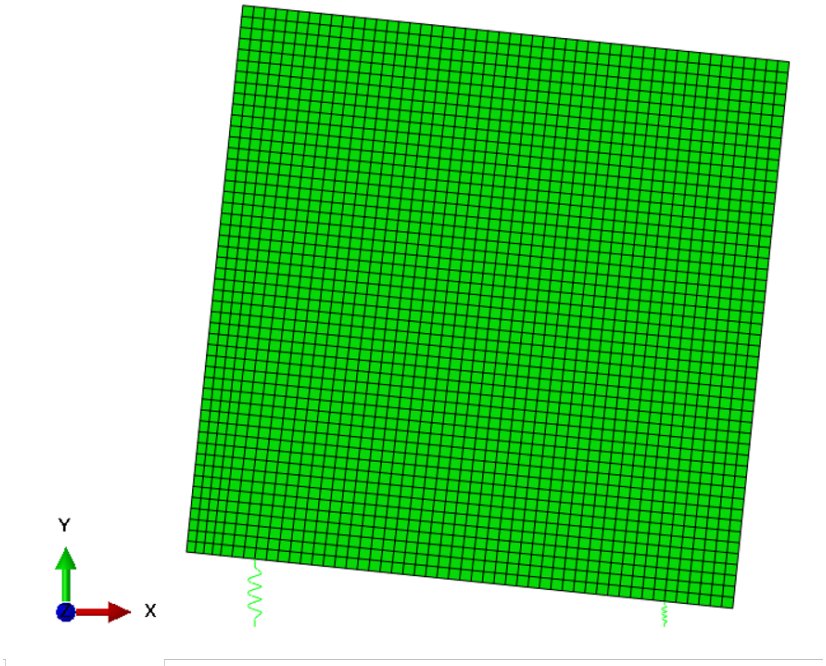

Figure 4.2: *Displacements of CLT wall system in FE-model with two hold-downs under lateral load F=10 kN and an elastic modulus of the CLT of 1 100 000 kN/mm^2.*

The global wall stiffness $K_{ser,wall}$ was once again extracted from the FE-results. The global wall stiffness $K_{ser,wall}$, together with its percentage change and the calculated global wall stiffness $K_{ser,wall}$ is displayed in Table 4.2.

Table 4.2: *Stiffness of connections and wall element with hold-downs from linear analyses with high initial stiffness.*

Number of connections	K_{ser} [kN/mm]	$K_{ser,wall}$ [kN/mm]	change in K_{ser} [%]	change in $K_{ser,wall}$ [%]	calculated $K_{ser,wall}$ [kN/mm]
2	32.4	25.31	-10	-10	25.31
	36	28.12	-	-	28.13
	39.6	30.94	+10	+10	30.94
4	32.4	42.52	-10	-10	42.53
	36	47.25	-	-	47.25
	39.6	51.97	+10	+10	51.98
8	32.4	86.06	-10	-10	86.06
	36	95.62	-	-	95.63
	39.6	105.19	+10	+10	105.19

Now, the global stiffness of the wall system $K_{ser,wall}$ from the FE-analysis correspond very well with the calculated values. As can be seen in Table 4.2, most values are the exact same, and for those which are not identical, there is a marginally difference of one hundredth. Thereby, the linear FE-analysis for the hold-downs is verified.

4.2 Angle bracket connections

For the angle brackets, the same check was made as for the systems with hold-downs. The stiffness K_{ser} for the angle brackets was initially assigned with the value 18 kN/mm. The resulting global wall stiffness $K_{ser,wall}$ from the linear FE-analyses are presented in Table 4.3 together with the percentage change of the global wall stiffness.

Table 4.3: *Stiffness of connection and wall element with angle brackets from linear analyses.*

Number of connections	K_{ser} [kN/mm]	$K_{ser,wall}$ [kN/mm]	change in K_{ser} [%]	change in $K_{ser,wall}$ [%]
2	16.2	10.22	-10	-8
	18	11.12	-	-
	19.8	11.99	+10	+8
4	16.2	14.71	-10	-7
	18	15.83	-	-
	19.8	16.89	+10	+7
8	16.2	24.06	-10	-6
	18	25.63	-	-
	19.8	27.10	+10	+6

The same pattern can be seen regarding the percentage change in stiffness of the global wall system $K_{ser,wall}$ in Table 4.3 as earlier seen for the system with hold-downs in Table 4.1 with only small differences in percentage. It is expected that the CLT wall element in the FE-model with angle brackets suffer from disturbances similar to those seen in the system with hold-downs, since the elastic modulus of 11 kN/mm^2 is the same for both systems. To confirm this theory, the deformed wall element, presented in Figure 4.3, was studied also for the system with angle brackets.

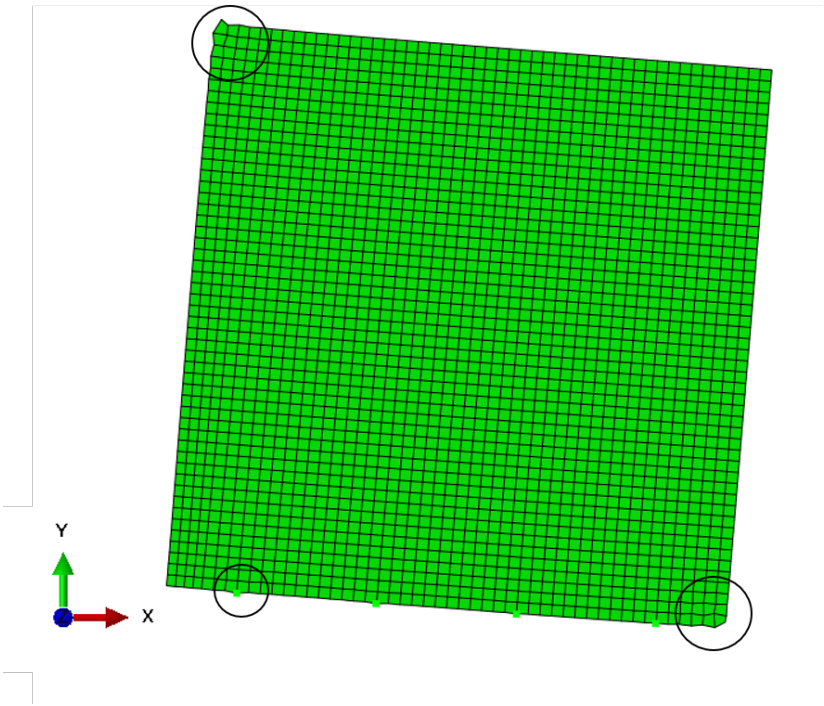

Figure 4.3: *Displacements of CLT wall system in FE-model with four angle brackets under lateral load F=10 kN and an elastic modulus of the CLT of 11 kN/mm^2.*

The figure confirms what was earlier predicted, that deformations in the CLT occur for an elastic modulus of 11 kN/mm^2. To be able to validate the linear behaviour of the connections also for the wall system with angle brackets, the CLT was made very stiff by increasing the elastic modulus to 1 100 000 kN/mm^2. The deformed wall system for the stiff CLT element can be seen in Figure 4.4.

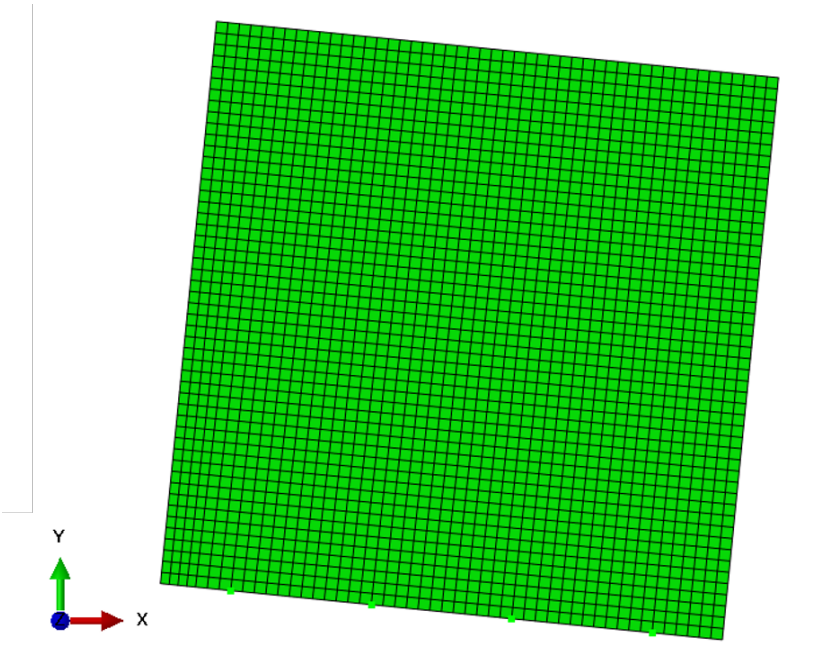

Figure 4.4: *Displacements of CLT wall system in FE-model with four angle brackets under lateral load F=10 kN and an elastic modulus of the CLT of 1 100 000 kN/mm^2.*

Now, the behaviour of the wall system appears as anticipated and the global stiffness values were extracted once again by the same procedure as described earlier. The values for the stiff wall system with two, four and eight angle brackets are displayed in Table 4.4. There, the percentage change in global wall stiffness $K_{ser,wall}$ is shown. Hand calculations are not made for the angle brackets due to the reason explained in Chapter 3.3.1.

Table 4.4: *Stiffness of wall element from linear analyses with angle brackets with high initial stiffness.*

Number of connections	K_{ser} [kN/mm]	$K_{ser,wall}$ [kN/mm]	change in K_{ser} [%]	change in $K_{ser,wall}$ [%]
2	16.2	10.22	-10	-10
	18	11.12	-	-
	19.8	11.99	+10	+10
4	16.2	14.71	-10	-10
	18	15.83	-	-
	19.8	16.89	+10	+10
8	16.2	24.06	-10	-10
	18	25.63	-	-
	19.8	27.10	+10	+10

Since the percentage change in connections stiffness K_{ser} is the same as the percentage change in global wall stiffness $K_{ser,wall}$, the linear behaviour is validated also for the systems with angle brackets. With the linear behaviour verified, the FE-model could be evolved by considering nonlinear behaviour.

5 Nonlinear FE-analyses

The second step of the FE-analyses were when the springs were modelled with nonlinear behaviour. Before these simulations some alterations were made after the linear analyses. Since the results from the linear simulations from hold-downs and angle bracket connections indicate the same, i.e. linear relation and no change in global stiffness compared to initial connection stiffness, the nonlinear analyses will only be performed with hold-downs. This chapter will present the results from the nonlinear FE-simulations along with a discussion about the results and a comparison with hand calculations.

5.1 Load distribution

In Figure 5.1, 5.2 and 5.3 the load displacement curves for two, four and eight hold-downs are presented with a clearer picture of the load distribution next to it. The forces in each connection element are also displayed against the deformation, as dotted lines. All the figures in this section were modelled with the mean value of each input parameter in the behaviour of each connection and both connections were modelled with the same values.

In the case of only two hold-downs, Figure 5.1, the first connection reaches its maximum load-carrying capacity, then also the entire structure is at the maximum load-carrying capacity. Therefore, each connection is of great importance for the load-carrying capacity. During the first 10 mm displacement only the first connection is carrying the load. The second connection starts contributing to taking the load when the first one has reached yielding. However, the first connection continues to contribute but the load is spread more evenly between the two connections.

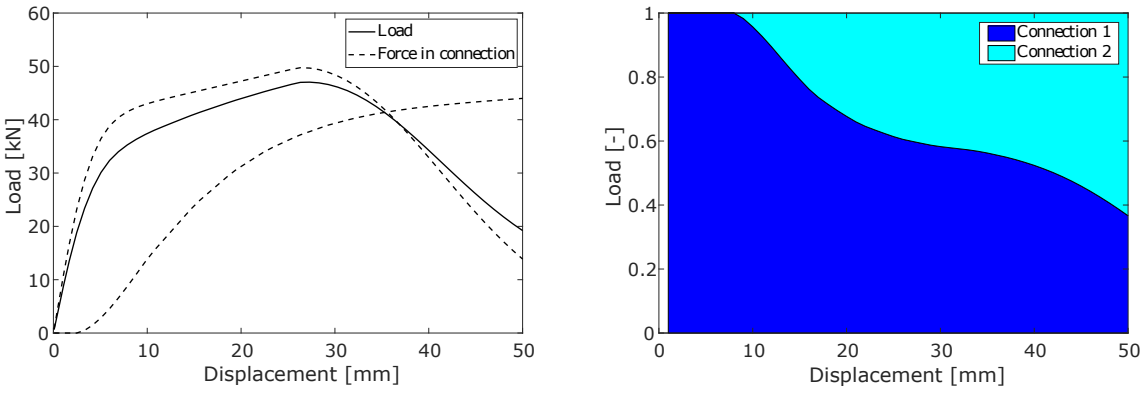

(a) **(b)**

Figure 5.1: *Load-displacement curves for each connection and load distribution for two connections.*

When modelled with four connections, Figure 5.2, the maximum load-carrying capacity for the entire structure is reached after the two first connections have reached its maximum capacity. The last connection is hardly contributing to carry any of the load, only starting to contribute after a displacement of 20 mm. In the beginning, the load is carried by each connection linearly until almost 10 mm, since at this point the first two connections have reached their yield point. After this point the first two connections are losing its capacity to take as much load as before.

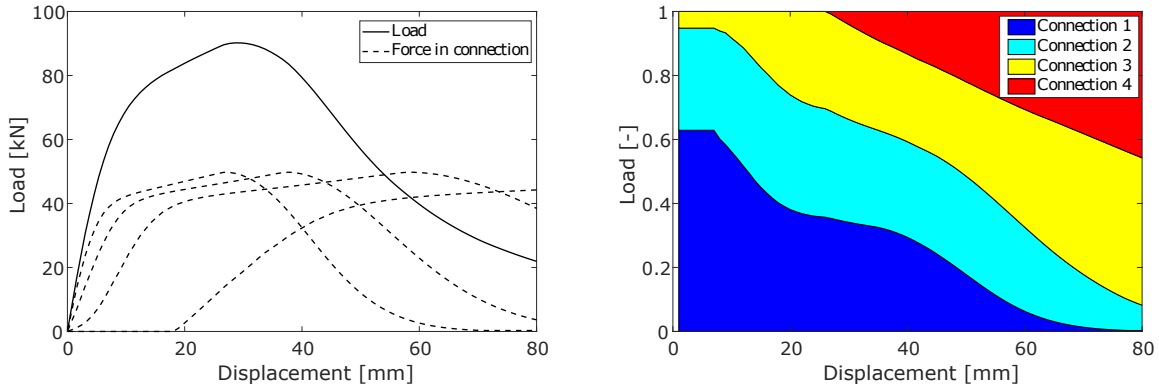

(a) **(b)**

Figure 5.2: *Load-displacement curves for each connection and load distribution for four connections.*

In the case of eight connections, Figure 5.3, not all connections will take any load before the structure has reached its maximum capacity. This capacity is first achieved when three connections are beyond the maximum capacity and seven connections are to some extent contributing to the distribution of the load. From Figure 5.3b, it is clear that mostly the first five connections will contribute to carry the load.

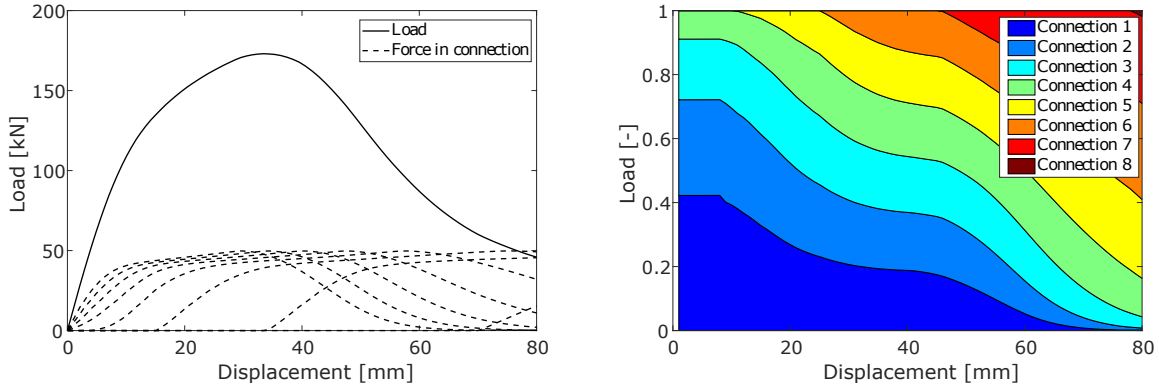

(a) **(b)**

Figure 5.3: *Load-displacement curves for each connection and load distribution for eight connections.*

5.2 Structural reliability

As mentioned in Section 3.2.3, about Monte Carlo simulations, multiple simulations were carried out while varying the initial stiffness and maximum load-carrying capacity of the connections. From these simulations; the mean, standard deviation (std), coefficient of variation, 0.05-quantile and 0.95-quantile for the maximum load-carrying capacity were calculated and are presented in Table 5.1. The distribution is also illustrated as probability density function (pdf) and cumulative distribution function (cdf) in Figure 5.4. From the cdf figure the different quantiles and mean can easily be determined. The pdf for two connections would have a higher peak but since the mean is lower than for four connections the coefficient of variation is lower for four than for two connections. The pdf with eight connections has a larger spread but a higher mean and therefore a lower coefficient of variation.

Table 5.1: *Statistical values for the maximum load-carrying capacity.*

Number of connections	Mean [kN]	Std [kN]	CoV [%]	0.05-quantile [kN]	0.95-quantile [kN]
2	47.07	2.02	4.29	43.79	50.35
4	90.12	2.27	2.52	86.29	93.63
8	172.69	3.35	1.94	167.61	178.51

Since there is a doubling in number of fasteners between each simulation there also is an increase in the mean value. However, the mean is not twice as high if the number of fasteners is doubled. As one would expect, the coefficient of variation is lowered the more fasteners that are added. The difference between the 0.05-quantile and mean value along with the 0.95-quantile mean value is also decreased if the number of fasteners is increased. The coefficient of variations of the global system, Table 5.1, are significantly lower than the input coefficient of variation of initial stiffness and maximum load-carrying capacity. This indicates there is a lower variation in global stiffness than the variation in the input material parameter.

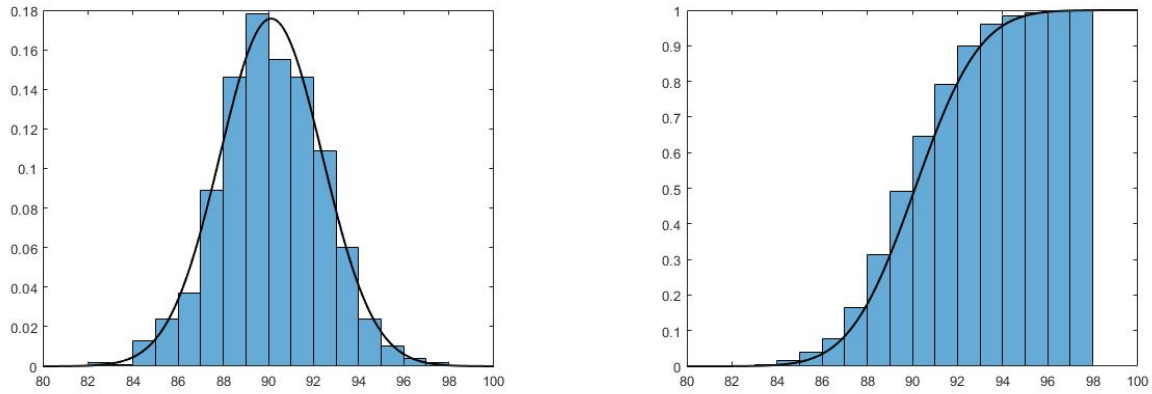

(a) *pdf* **(b)** *cdf*

Figure 5.4: *Distribution of maximum load-carrying capacity in the case of four connections in parallel with varying material parameters.*

5.3 Ductility

To be able to determine the contribution of the ductile behaviour of a connection, Monte Carlo simulations were performed with varying ductility ratio. The ductility ratios were calculated according to Equation 2.7 and are presented in Table 5.2. According to Table 2.20, the first graph has either low ductility or brittle according to all references, while the last one has high ductility in all references. The graphs in between these two have different classifications according to different references.

When the connections have different ductility, the maximum load-carrying capacity of the entire structure differ from each other, as can be seen in Table 5.2. The larger the ductile behaviour of a connection, the higher the mean maximum load-carrying capacity as well as the 0.05-quantile of the maximum load-carrying capacity for the global structure. Therefore, to secure a more reliable structure, an increase in ductile behaviour of connections would be of great interest.

Table 5.2: *Ductility ratio and maximum load-carrying capacity for different graphs from Figure 3.3 along with varying the initial stiffness and load-carrying capacity of each connection.*

		2 hold-downs		4 hold-downs		8 hold-downs	
Graph	D	$F_{0.05}$	F_{Mean}	$F_{0.05}$	F_{Mean}	$F_{0.05}$	F_{Mean}
1	1.15	32.46	33.87	59.39	62.59	107.01	110.33
2	1.71	36.11	37.13	68.41	71.47	124.22	127.23
3	2.85	39.07	41.01	77.79	79.77	144.47	146.72
4	4.28	42.09	44.78	82.57	85.69	158.36	162.31
5	6.57	43.79	47.07	86.29	90.12	167.61	172.96

From the results, the ductility has a significant influence on the maximum load-carrying capacity. However, this is not something that is accounted for in Eurocode 5, where the capacity is not dependent on the ductile behaviour of the connection. Since the global load-carrying capacity can differ with more than 40 %, it would be valuable if this is regarded in Eurocode 5.

Another way of illustrating the result presented in Table 5.2, is through Figure 5.5, where it is clearer that the load-carrying capacity is significantly increasing with higher ductility. The figures are similar for both two and eight connections in terms of load-carrying capacity, which is increasing when there are an increase in ductility ratio. The coefficient of variation of the load-carrying capacity for each ductility ratio are similar to those presented in Table 5.1. Because they are similar, the differences between mean and 0.05-quantile values, are of the same range for all ductility ratios.

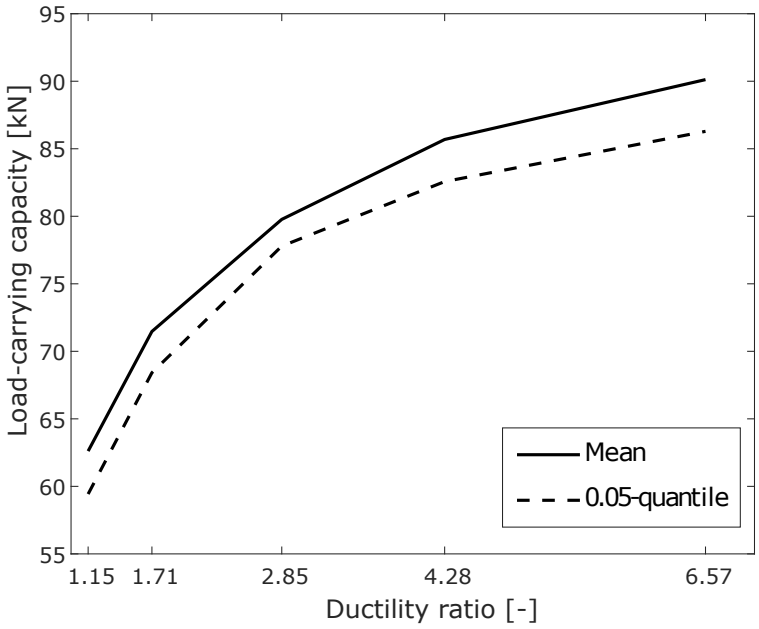

Figure 5.5: *Maximum load-carrying capacity versus ductility ratio for four connections.*

However, the input maximum load-carrying capacity of the fasteners in the simulations above are different depending on the ductility ratio. This is something that also will influence the global load-carrying capacity. To see how much this influences the capacity, a second smaller study were done where the maximum load-carrying capacity were constant but the level of an elastic branch differs, as can be seen in Figure 5.6a. As one would expect, also the maximum load-carrying capacity have an influence on the global capacity, which is shown in Figure 5.6b. This influence is, however, lower than the influence the ductility ratio has, around 20 %. A reduction of the safety factor, which SIA 265 (2012) mentions, would deal with some of the issue with ductility, since lowering the safety factor from 1.7 to 1.5 would lower the capacity with more than 10 %.

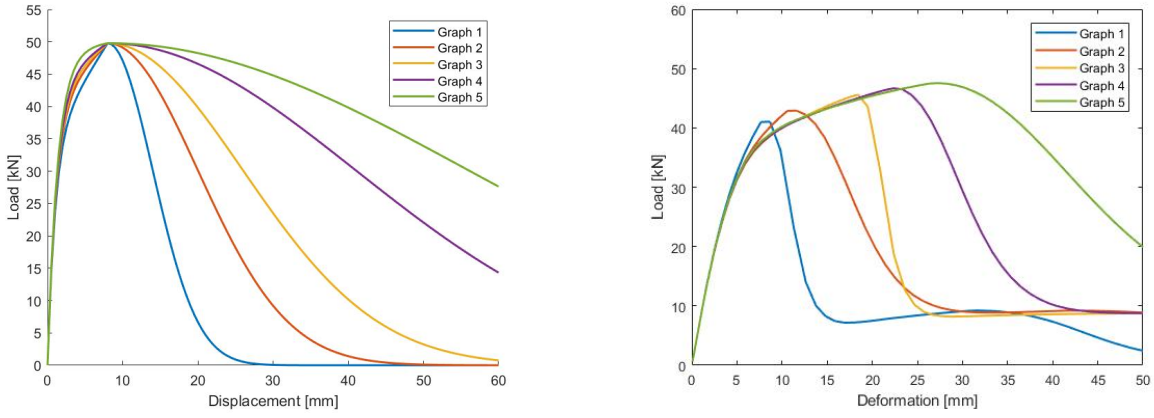

(a) **(b)**

Figure 5.6: *Load-deformation curves with different ductility level. The left figure represent the input load-carrying capacity of connections, while the right figure represent the global load-carrying capacity of the entire wall element.*

5.4 Hand calculations

The characteristic value of the load-carrying capacity $F_{v,Rk}$ of one hold-down with 24 nails is according to the hand calculations based on Eurocode 5 equal to 28.53 kN, whereas the design value $F_{v,Rd}$ is equal to 19.75 kN. The characteristic value $F_{v,Rk,wall}$ and the design value $F_{v,Rd,wall}$ of the global load-carrying capacity for a wall system consisting of two, four and eight hold-downs are presented in Table 5.3.

Table 5.3: *Global theoretical load-carrying capacity for a wall system consisting of two, four and eight connections.*

	Global load-carrying capacity [kN]	
Number of connections	Characteristic $F_{v,Rk,wall}$	Design value $F_{v,Rd,wall}$
2	25.47	17.63
4	42.80	29.63
8	80.84	55.96

When comparing the calculated characteristic values to the values from the nonlinear FE-modelling, the calculated values are significantly lower. However, the values are similar until the yield point are reached in the nonlinear cases. The reason they differ after the yield point is that in the hand calculations, linear behaviour have been considered, while in the FE-modelling, the connections have a nonlinear behaviour after reaching the yield point.

The calculated design values are all within the elastic branch of the load-deformation curves obtained from the nonlinear FE-analyses, compare Figure 5.1, 5.2 and 5.3 with Table 5.3. This is reasonable since Eurocode is using a design approach based on linear-elastic behaviour. By designing according to Eurocode, the first connection in the system is decisive. When the load-carrying capacity of that connection is reached, the system is considered to have reached its maximum capacity. In this way, redistribution of the load is not accounted for, as it is in the nonlinear FE-analyses. As can be seen in Figure 5.3, only five out of eight hold-downs have had the chance to contribute before the load-carrying capacity according to Eurocode, seen in Table 5.3, is achieved.

If comparing the calculated values with the nonlinear FE-modelling with low ductility ratio, see Table 5.2, there is a larger correlation. This can also be seen in Figure 5.7, where the ductility ratio are presented versus the η value, which defined as the 0.05-quantile value from nonlinear FE-modelling value divided by the calculated design value, see Equation 5.1.

$$\eta = \frac{F_{0.05}}{F_{v,Rd,wall}} \tag{5.1}$$

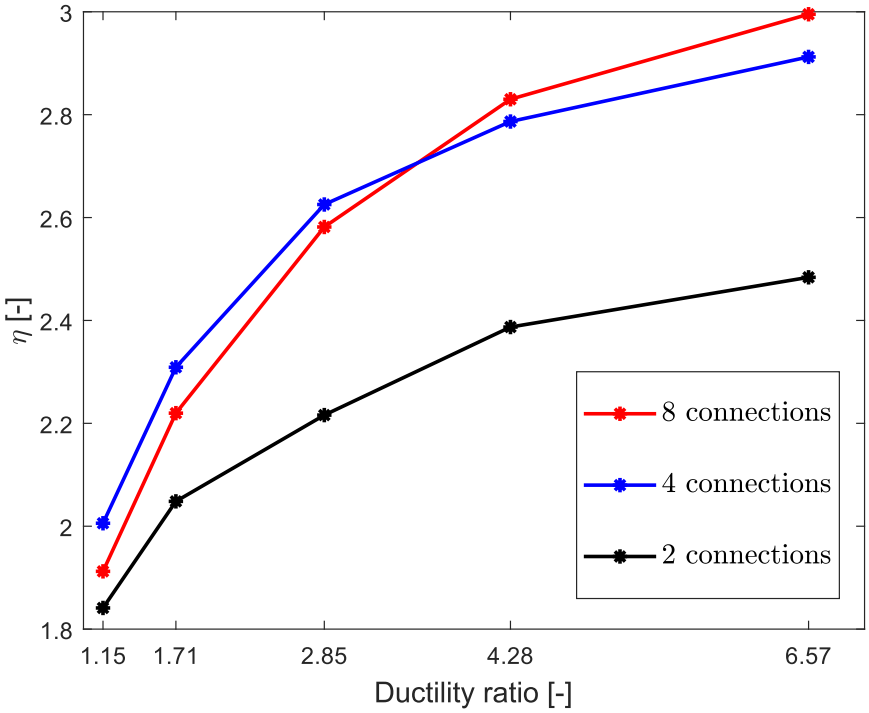

Figure 5.7: *Extra capacity for each system when varying the ductility ratio.*

When the ductility ratio is low, there is a small difference in global load-carrying capacity between the nonlinear FE-values and the hand calculated values as apparent in Figure 5.7. This indicates that the extra capacity that can be accounted for, is very limited in case of a low ductility ratio. For a high ductility ratio, on the other hand, the FE-values for the global load-carrying capacity are from 2.4, up to 3.0 times higher than the calculated values based on Eurocode 5. It was expected that the curve representing eight connections would be above the curve symbolising four connections. As can be seen in the figure, the curves are deviating from what was expected. For a low ductility ratio, the curve for four connections actually show a higher ratio η than the curve for eight connections. This, however, shifts at a ductility ratio between 2.85 and 4.28. Since the only thing that differs between the two systems, except for the amount of connections, is the distance from the most outer connections to the edge of the wall and the spacing between the connections, the shift most likely depends on the distances between the connections in the systems. This is only a speculation though, and the exact cause would need to be further investigated, something that is not done here.

6 Conclusion

The aim in this thesis was to develop guidance for a more robust and reliable design of CLT systems, focusing on the stiffness and load-deformation behaviour of connections in a laterally loaded CLT wall system. Initially, linear FE-analyses were carried out for two types of connections, i.e. hold-downs and angle brackets, for three set-ups of the wall systems; system with two connections, four connections and eight connections. Then, nonlinear analyses were performed to study the load-carrying capacity and the load distribution in the wall systems, this time only considering hold-downs as connections. For the FE-results, comparisons were made with hand calculations according to Eurocode 5. Monte Carlo simulations were then applied on the nonlinear FE-analyses, taking the variability of the connections into account in order to be able to evaluate the structural reliability of the entire structure. Additionally, the ductility ratio in the connections were varied, making it possible to study the influence of the ductile behaviour on the global load-carrying capacity.

In general, both the nonlinear analyses and the design approach according to Eurocode 5 show that the first connection in the wall system is the most important one in terms of global load-carrying capacity. The nonlinear analyses show that when the maximum load is reached in the first connection, the load is redistributed to the other connections through parallel action, and the global load-carrying capacity of the wall system is not reached until several of the connections have come beyond their maximum load-carrying capacity point. While, in Eurocode 5, the global load-carrying capacity of the wall system is attained when the load-carrying capacity of the first connection is reached.

The effects the coefficient of variation of initial material parameters has on the global structure in the nonlinear analyses will decrease with an increase of number of elements in the structure. The coefficient of variation is also lower in the global structure than the variation in each input element in the nonlinear cases. Indicating that the structure in the nonlinear case is not as dependent on the coefficient of variation of the initial material parameter.

The results from FE-analyses regarding ductility is that the more ductile behaviour the connection has, the larger is also the load-carrying capacity of the entire structure. If a connection has a highly ductile behaviour instead of a brittle behaviour, the global load-carrying capacity will increase significantly. Additionally, the comparison with hand calculations when the ductility ratio was varied, show that the capacity in the nonlinear FE-analyses are in the range from 1.8, up to 3.0 times higher than the design values according to Eurocode 5. Thus, this should be considered in Eurocode, maybe by including a ductility factor? Details regarding how ductility should be considered and where in the standards it should be introduced is however, a topic for further discussion.

None of the hand calculated values for the global load-carrying capacity of the wall system exceeded the corresponding nonlinear load-carrying capacity obtained from the FE-analyses, indicating that the design of large CLT wall systems are reliable in terms of load-carrying capacity. This is a result of the linear-elastic approach in Eurocode 5, where design values, including safety factors, are leading to conservative load-carrying capacities. There are probably many systems with low ductility that endure thanks to this conservative approach. From the results of the nonlinear analyses, it can be concluded that, the laterally loaded CLT wall system allows for redistribution of loads via parallel action in the connections, which is improving the structural robustness of the system. If this would be included in Eurocode 5, the design value for the load-carrying capacity of the system could be increased, resulting in a more efficient structural design. Nevertheless, for insufficient load distribution between the elements, the variation of the connections can lead to unpredictable

global failure. This also needs to be accounted for in Eurocode 5. Since parallel action between the connections is currently not considered in Eurocode 5 and ductility is not part of the design, it is not possible to assure robustness of CLT wall systems as it is today.

Further work within the topic described in this thesis would revolve mostly on how the issues that have arisen herein could be assessed in Eurocode 5. More detailed, a way to account for the ductile behaviour in the standards would be of great interest along with the influence of applying variation in material parameters. Furthermore, this thesis only dealt with hold-downs and CLT in the nonlinear analyses. Therefore, analyses with other connection types and other timber materials would be suitable for further studies. Finally, since the simplicity of the model in this thesis could have an impact on the results, it is suggested for further studies, to create a more advanced model to be able to make a more detailed investigation and evaluate how this effects the results.

References

American Forest & Paper Association. (1999). TECHNICAL REPORT 12 General dowel equations for calculating lateral connection values. *12*, 24.

Bodig, J. & Jayne, B. (1982). *Mechanics of Wood and Wood Composites*. Van Nostrand Reinhold Company Inc.

Brandner, R. (2013). Production and Technology of Cross Laminated Timber (CLT): A state-of-the-art Report. *Focus Solid Timber Solutions - European Conference on Cross Laminated Timber (CLT)*, (May 2013), 3–36. doi:10.1093/geronb/gbr157

Brandner, R., Ringhofer, A., & Dietsch, P. (2017). Design approaches for dowel-type connections in CLT structures and their verification. In *Fp1402*. Graz, Austria. doi:10.3217/978-3-85125-553-9

Brühl, F. & Kuhlmann, U. (2017). Consideration of Connection Ductility within the Design of Timber Structures. In *International conference on connections in timber engineering – from research to standards* (Pages 32–45).

CEN. (2004). *Eurocode 5* (technical report Number 138227).

Chen, Z., Chui, Y., Ni, C., Doudak, G., & Mohammad, M. (2014). Load distribution in timber structures consisting of multiple lateral load resisting elements with different stiffnesses. *Journal Performance of Constructed Facilities*, *28*(6).

Faber, M. H. (2005). Risk and Safety in Civil, Surveying and Environmental Engineering. *Lecture Notes*.

Flatscher, G. (2017). *Evaluation and approximation of timber connection properties for displacement-based analysis of CLT wall systems (Doctoral Thesis)* (Doctoral dissertation, Graz University of Technology).

Foschi, R. O. (2000). Determining embedment response parameters from connector tests. In *World conference on timber engineering*. Whistler, B.C., Canada.

Gavric, I., Fragiacomo, M., & Ceccotti, A. (2015). Cyclic behaviour of typical metal connectors for cross-laminated (CLT) structures. *Materials and Structures/Materiaux et Constructions*, *48*(6), 1841–1857. doi:10.1617/s11527-014-0278-7

ISO/TC165. (2018). Timber structures — Timber connections and assemblies — determination of yield and ultimate characteristics and ductility from test data. *2018*.

Jockwer, R., Fink, G., & Köhler, J. (2017). Assessment of Existing Safety Formats for Timber Connections – How Probabilistic Approaches can Influence Connection Design in Timber Engineering. In *Connections in timber engineering – from research to standards* (Pages 16–31).

Joint Committee on Structural Safety. (2000). *Probabilistic Model Code, Part I*.

Joint Committee on Structural Safety. (2006). 3.5 PROPERETIES OF TIMBER. In *Jcss probabilistic model code*. doi:10.1017/S1047951106000655

Köhler, J., Fink, G., & Brandner, R. (2016). Basis of Design Principles – Application to CLT. In *Cost actions fp1402 & fp1404* (Pages 45–61).

Köhler, J., Sørensen, J. D., & Faber, M. H. (2007). Probabilistic modeling of timber structures. *Structural Safety*, *29*(4), 255–267. doi:10.1016/j.strusafe.2006.07.007

Leijten, A., Köhler, J., & Jorissen, A. (2004). Review of probability data for timber connections with dowel-type fasterners. In *Cib w18*. Edinburgh.

Lukacs, I., Björnfot, A., & Tomasi, R. (2018). State-of-the-art: Cross Laminated Timber shear wall capacity and stiffness assessment methods. In *Cost action fp1402* (Pages 203–216).

Lukacs, I., Pradel, C., Björnfot, A., & Tomasi, R. (2018). State-of-the-art: Timber floor diaphragms. In *Cost action fp1402* (Pages 217–230).

Muñoz, W., Mohammad, M., Salenikovich, A., & Quenneville, P. (2008). Determination of yield point and ductility of timber assemblies: A need for a harmonised approach. *Proceedings, Annual Conference - Canadian Society for Civil Engineering*, *2*, 1146–1155.

ON EN 12512. (2002). *Timber structures – Test methods – Cyclic testing of joints made with mechanical fasteners* (technical report Number december 2002).

Pozza, L., Ferracuti, B., Massari, M., & Savoia, M. (2018). Axial – Shear interaction on CLT hold-down connections – Experimental investigation. *Engineering Structures*, *160*(January), 95–110. doi:10.1016/j.engstruct.2018.01.021

Ringhofer, A., Brandner, R., & Blass, H. J. (2018). Design approaches for dowel-type connections in CLT structures and their verification. In *Design of connections in timber structures* (Pages 161–192).

Sassu, M., Puppio, M. L., Awad, V., Giresini, L., & Koshihara, M. (2017). Experimental Analyses and Numerical Models of CLT Shear Walls under Cyclic Loading. *Wood in Civil Engineering*, (March). doi:10.5772/65024

Schickhofer, G., Brandner, R., & Bauer, H. (2016). Introduction to CLT, Product Properties, Strength Classes. *Joint Conference of COST Actions FP1402 and FP1404*, (1), 1–22.

SIA 265. (2012). Timber Structures (in German).

Sigrist, C. (2018). CLT - Considerations Regarding Denomination and Testing. In *Cost action fp1402* (Pages 128–141).

SIMPSON Strong-Tie. (2019). Connectors for Cross-Laminated Timber & Glulam Timber. *44*(0).

Smith et al. (2006). Possible Canadian / ISO approach to deriving design values from test data. In *39th cib w18 meeting - cib-w18/39-17-1*. Florence, Italy.

Smith et al. (2015). The reality of seismic engineering in a modern timber world. In *2nd inter meeting - inter/48- 102-3',* Sibenik, Croatia.

Swedish Wood. (2016). *Design of timber structures - Volume 1: Structural aspects of timber construction*.

A Calculation of CLT stiffness properties

Input parameters:

$t_{CLT} := 100mm$ total thickness of CLT wall element

$t_{outer} := 30mm$ thickness of outer layers of CLT wall element

$t_{inner} := 40mm$ thickness of inner layer of CLT wall element

$E_{0.mean} := 11\frac{kN}{mm^2}$ mean value of elastic modulus parallel to grain, C24 timber

$E_{90.mean} := 0.37\frac{kN}{mm^2}$ mean value of elastic modulus perpendicular to grain, C24 timber

$G_{mean} := 0.69\frac{kN}{mm^2}$ mean value of shear modulus, C24 timber

Calculation of elastic properties in each direction according to the compound theory:

$$E_1 := \frac{1}{t_{CLT}}\cdot\left(2\cdot E_{90.mean}\cdot t_{outer} + E_{0.mean}\cdot t_{inner}\right) = 4.62\cdot\frac{kN}{mm^2}$$

$$E_2 := \frac{1}{t_{CLT}}\cdot\left(2\cdot E_{0.mean}\cdot t_{outer} + E_{90.mean}\cdot t_{inner}\right) = 6.75\cdot\frac{kN}{mm^2}$$

$$E_3 := \frac{\left(E_{90.mean}^{\ 2}\cdot t_{CLT}\right)}{\left(2\cdot E_{90.mean}\cdot t_{outer} + E_{90.mean}\cdot t_{inner}\right)} = 0.37\cdot\frac{kN}{mm^2}$$

$$G_{12} := \frac{1}{t_{CLT}}\cdot\left(2\cdot G_{mean}\cdot t_{outer} + G_{mean}\cdot t_{inner}\right) = 0.69\cdot\frac{kN}{mm^2}$$

$$G_{23} := 0.1\cdot G_{mean} = 0.069\cdot\frac{kN}{mm^2}$$

B Calculation of connection stiffness properties

Input parameters:

$\rho_m := 420 \frac{kg}{m^3}$ mean density of timber

$d := 4mm$ outer diameter of fastener

$n_{HD} := 24$ number of nails in hold-down

$n_{AB} := 12$ number of nails in angle bracket

$u_1 := \frac{m^{4.5}}{kg^{1.5}} \cdot \frac{N}{mm}$ correction factor

Calculation of stiffness (slip modulus) according to Table 2.25, for nails with pre-drilling:

Table 2.25: *Slip modulus K_{ser} for fastener in timber structures.*

Fastener type	K_{ser} [N/mm]
Dowels Bolts with or without clearance Screws Nails (with pre-drilling)	$\rho_m^{1.5} d/23$
Nails (without pre-drilling)	$\rho_m^{1.5} d^{0.8}/30$

$K_{ser} := \rho_m^{1.5} \cdot \frac{4}{23} \cdot u_1 = 1.5 \cdot \frac{kN}{mm}$ stiffness of 1 fastener with the assumption of pre-drilled holes

$K_{ser.HD} := K_{ser} \cdot n_{HD} = 36 \cdot \frac{kN}{mm}$ stiffness of 1 hold-down

$K_{ser.AB} := K_{ser} \cdot n_{AB} = 18 \cdot \frac{kN}{mm}$ stiffness of 1 angle bracket

C Matlab code for creating abaqus input files

```
clc
clear all

%Number of input files
numbers=1000;

% Input parameters
v_max=18.3;
K_ini=36.1;
F_t=40.1;
v_B=27;
i=1;
% K_ini
mean_K=36.1;
cov_K=0.2;
var_K=(mean_K*cov_K)^2;
mu_K=log((mean_K^2)/sqrt(var_K+mean_K^2));
sigma_K=sqrt(log(var_K/(mean_K^2)+1));
% F_max
mean_F=49.8;
cov_F=0.05;
var_F=(mean_F*cov_F)^2;
mu_F=log((mean_F^2)/sqrt(var_F+mean_F^2));
sigma_F = sqrt(log(var_F/(mean_F^2)+1));

Name1=sprintf('Input_part_1.inp'); %Part 1 of input file
Name3=sprintf('Input_part_3.inp'); %Part 3 of input file

% Create input file
for run=1:numbers
    Name2=sprintf('Input_number_%d.inp',run);
    copyfile(Name1,'workfile.inp','f');
    fid=fopen('workfile.inp','a');

    % Spring 1
    fprintf(fid,'\n*Spring, elset=Springs/Dashpots-1-spring, orientation=
    "Datum csys-2", nonlinear, dependencies=2\n1,1\n');
    F_max=lognrnd(mu_F,sigma_F,1,1);
    K_ini=lognrnd(mu_K,sigma_K,1,1);
    K_p=((F_max/(1-exp(-K_ini*v_max/F_t))-F_t)/v_max);
    F_u=0.8*F_max;
    C=log(F_u/F_max)/((v_max*(v_B/v_max-1))^2);
    for v=0:0.5:60
        if v <= v_max
```

```
            F=(F_t+K_p*v)*(1-exp(-K_ini*v/F_t));
            fprintf(fid,'%10.7f,',F);
        else
            F=F_max*exp(C*(v-v_max)^2);
            fprintf(fid,'%10.7f,',F);
        end
        fprintf(fid,'%10.7f\n',v);
    end
    fprintf(fid,'*Element, type=Spring2, elset=Springs/Dashpots-1-spring\n1,
    Part-2-1.1, Part-1-1.1678\n');

    % Spring 2
    fprintf(fid,'*Spring, elset=Springs/Dashpots-2-spring, orientation=
    "Datum csys-2", nonlinear, dependencies=2\n1,1\n');
    F_max=lognrnd(mu_F,sigma_F,1,1);
    K_ini=lognrnd(mu_K,sigma_K,1,1);
    K_p=((F_max/(1-exp(-K_ini*v_max/F_t))-F_t)/v_max);
    F_u=0.8*F_max;
    C=log(F_u/F_max)/((v_max*(v_B/v_max-1))^2);
    for v=0:0.5:60
        if v <= v_max
            F=(F_t+K_p*v)*(1-exp(-K_ini*v/F_t));
            fprintf(fid,'%10.7f,',F);
        else
            F=F_max*exp(C*(v-v_max)^2);
            fprintf(fid,'%10.7f,',F);
        end
        fprintf(fid,'%10.7f\n',v);
    end
    fprintf(fid,'*Element, type=Spring2, elset=Springs/Dashpots-2-spring \n2,
    Part-3-1.1, Part-1-1.388\n');

    % Creates file
    fclose(fid);
    copyfile(Name3,'workfile2.inp');
    dos('copy workfile.inp +workfile2.inp workfile.inp');
    copyfile('workfile.inp',Name2);
end
```

D Python script

```
import sys
import os
#
i=0
run=[]
#
COMMAND = os.environ['ABA_COMMAND']
print
print 'NOTE all input files in this directory will be executed with ',COMMAND
files = os.listdir('.')
print
#
while i < len(files):
    nameall = files[i]
    ext = nameall[(len(nameall)-3):]
    if ext == 'inp':
      run.append(nameall[:(len(nameall)-4)])
    i=i+1
#
i=0
#
while i < len(run):
    name = run[i]
    cmd = COMMAND+' -j '+str(name)+' inter'+' cpus=4'
    print 'Executing '+cmd
    os.system(cmd)
    i=i+1
#
print
print '***'
print '**Completed all analysis runs**'
```

E Matlab code for reading .dat-files from Abaqus

```
fclose('all')
clear all; close all; clc;
tic;    % to calculate the calculation time

files=dir('*.dat');
numbers=length(files);
for i1=1:numbers
    Name_file=sprintf('Input_number_%d',i1)

    fid = fopen([ Name_file '.dat'], 'r');
    Data = textscan(fid, '%s', 'delimiter', '\n');
    Data_String = Data{1};
    fclose(fid);

    e1=regexp(Data_String, {'N O D E   O U T P U T';});
    elt=regexp(Data_String, {'E L E M E N T   O U T P U T';});
    count=0;
    count1=0;
    for i=1:size(e1,1)
        if e1{i,1}==1
            count=count+1;
            Set_Force_position(count)=i;
            Set_Disp_position(count)=i;
        end
    end
    for i=1:size(elt,1)
        if elt{i,1}==1
            count1=count1+1;
            Set_Spring_position(count1)=i;
        end
    end

    number_increments=size(Set_Force_position,2);

    for n=1:number_increments   % Force
        Data_Value_F=Data_String(Set_Force_position(n)+25);
        V_opp = textscan(Data_Value_F{1,1}, '%f %f %f');
        V_opp_output1(n,1)=V_opp{1,2};
        V_opp_output1(n,2)=V_opp{1,3};
        clear V_opp Data_Value_F
    end
    for n=1:number_increments   %Disp right corner
        Data_Value_D=Data_String(Set_Disp_position(n)+10);
        H_opp = textscan(Data_Value_D{1,1}, '%f %f %f');
```

```
        H_opp_output(n,1)=H_opp{1,2};
        H_opp_output(n,2)=H_opp{1,3};
        clear H:opp Data_Value_D
    end
    for n=1:number_increments   %Spring 1
        Data_Value_S=Data_String(Set_Spring_position(n)+12);
        Spring1 = textscan(Data_Value_S{1,1}, '%f %f %f %f');
        Spring1_output(n,1)=Spring1{1,2};
        Spring1_output(n,2)=Spring1{1,3};
        Spring1_output(n,3)=Spring1{1,4};
        clear Spring1 Data_Value_S
    end
    for n=1:number_increments   %Spring 2
        Data_Value_S2=Data_String(Set_Spring_position(n)+28);
        Spring2 = textscan(Data_Value_S2{1,1}, '%f %f %f %f');
        Spring2_output(n,1)=Spring2{1,2};
        Spring2_output(n,2)=Spring2{1,3};
        Spring2_output(n,3)=Spring2{1,4};
        clear Spring2 Data_Value_S2
    end

    for n=1:number_increments
        Force(n,i1)=V_opp_output1(n,1);
        Deformation(n,i1)=H_opp_output(n,1);
        Spring1_strain(n,i1)=Spring1_output(n,2);
        Spring1_stress(n,i1)=Spring1_output(n,3);
        Spring2_strain(n,i1)=Spring2_output(n,2);
        Spring2_stress(n,i1)=Spring2_output(n,3);
    end
    Spring_stress=[Spring1_stress,Spring2_stress];
    clear Set_Force_position Set_Disp_position Set_Spring_position
    count count1 number_increments Data_String

    % Excel filer
    dataname01 =['Results_F.xlsx'];
    dataname02 =['Results_d.xlsx'];
    dataname03 =['Results_spring1stress.xlsx'];
    dataname04 =['Results_spring2stress.xlsx'];
    xlswrite(dataname01,Force(:,:),1);
    xlswrite(dataname02,Deformation(:,:),1);
    xlswrite(dataname03,Spring1_stress(:,:),1);
    xlswrite(dataname04,Spring2_stress(:,:),1);
end

% time
Time=toc; disp 'Time for calculation'; disp(Time)
```

F Calculation of global stiffness of wall system, load-carrying capacity of connections and global load-carrying capacity of wall system

State of equilibrium:

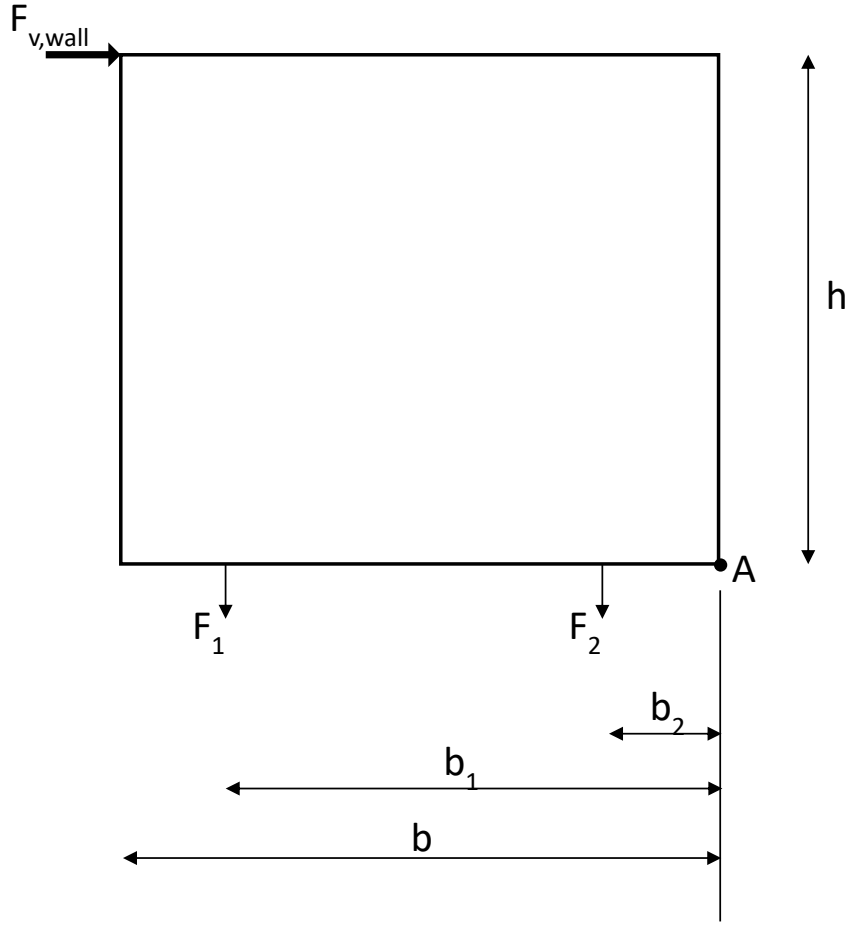

$$\sum M_A = 0$$

$$F_{v,wall} \cdot h = F_1 \cdot b_1 + F_2 \cdot b_2 \qquad (F1)$$

$$F_{v,wall} = \frac{F_1 \cdot b_1 + F_2 \cdot b_2}{h} \qquad (F2)$$

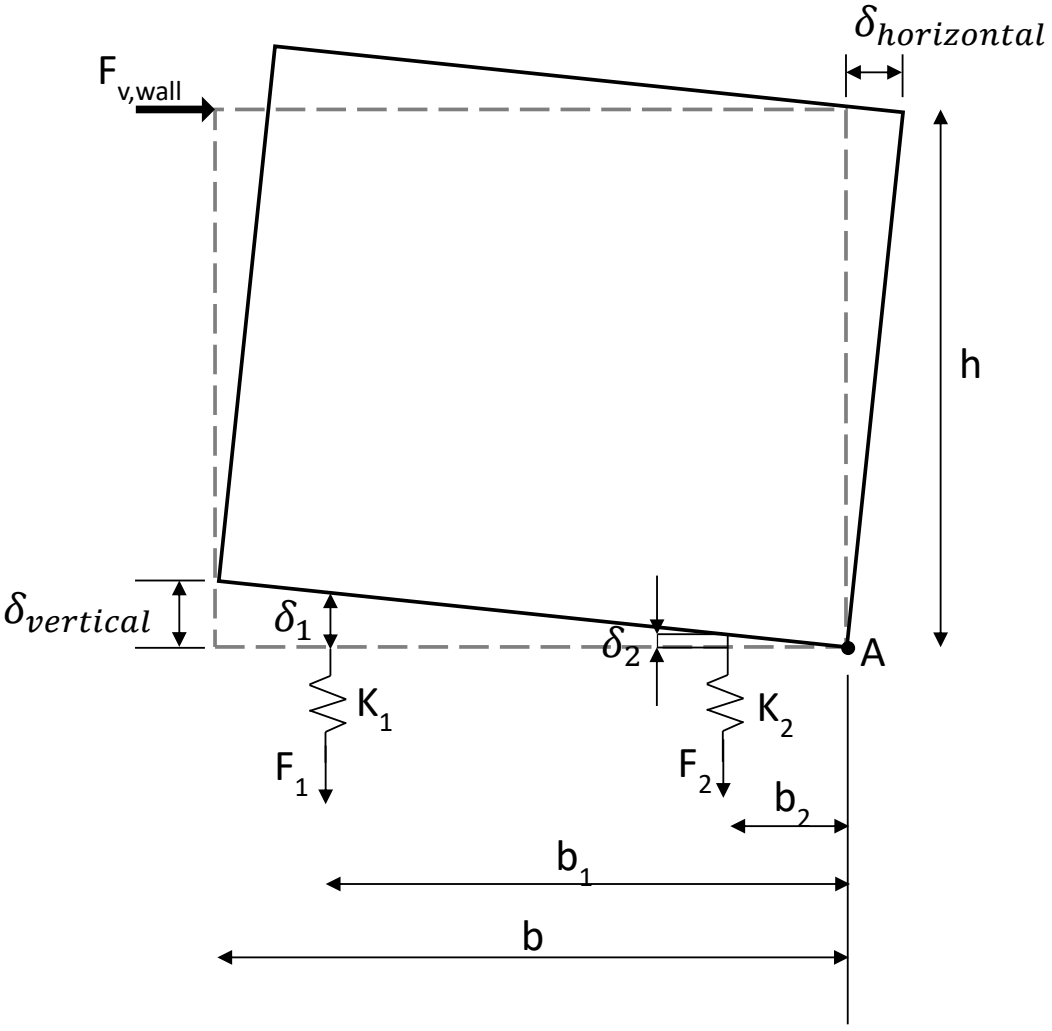
$\delta_{horizontal}$
F v,wall
h
$\delta_{vertical}$
δ_1
δ_2
A
K 1
K 2
F 1
F 2
b 2
b 1
b

Relationship between $\delta_{horizontal}$ and $\delta_{vertical}$ according to Figure 2.18 and Equation 2.2 in this thesis:

$$\frac{\delta_{horizontal}}{h} = \frac{\delta_{vertical}}{b} \quad \Rightarrow \quad \delta_{horizontal} = \frac{h \cdot \delta_{vertical}}{b} \qquad (F3)$$

$$\frac{\delta_{vertical}}{b} = \frac{\delta_1}{b_1} = \frac{\delta_2}{b_2} \qquad (F4)$$

Forces and stiffness in connections:

$$F_1 = K_1 \cdot \delta_1 = K_1 \cdot \frac{\delta_{vertical}}{b} b_1 \Rightarrow \quad K_1 = F_1 \cdot \frac{b}{\delta_{vertical} \cdot b_1} \qquad (F5)$$

$$F_2 = K_2 \cdot \delta_2 = K_2 \cdot \frac{\delta_{vertical}}{b} b_2 \Rightarrow \quad K_2 = F_2 \cdot \frac{b}{\delta_{vertical} \cdot b_2} \qquad (F6)$$

Due to assumption of equal stiffness in all connections:

$$K_1 = K_2 \qquad (F7)$$

$$\Rightarrow F_2 = K_2 \cdot \frac{\delta_{vertical}}{b} b_2 = \left(F_1 \cdot \frac{b}{\delta_{vertical} \cdot b_1}\right) \cdot \frac{\delta_{vertical}}{b} b_2 \qquad (F8)$$

$$F_2 = F_1 \cdot \frac{b_2}{b_1} \qquad (F9)$$

GLOBAL STIFFNESS OF WALL SYSTEM

Derivation of global wall stiffness through Equation (F2), together with Equation (F5) and (F6):

$$K_{ser,wall}\delta_{horiz} = \frac{\left(K_1 \cdot \frac{\delta_{vert}}{b} b_1\right) \cdot b_1 + \left(K_2 \cdot \frac{\delta_{vert}}{b} b_2\right) \cdot b_2}{h} \quad \textit{(F10)}$$

$$K_{ser,wall}\delta_{horiz} = \frac{\delta_{vert}}{h \cdot b}(K_1 \cdot b_1^2 + K_2 \cdot b_2^2) \quad \textit{(F11)}$$

$$K_{ser,wall} = \frac{\delta_{vert}}{\delta_{horiz} \cdot h \cdot b}(K_1 \cdot b_1^2 + K_2 \cdot b_2^2) \quad \textit{(F12)}$$

With Equation (F3) in Equation (F12):

$$K_{ser,wall} = \frac{\delta_{vert}}{\left(\frac{h \cdot \delta_{vert}}{b}\right) \cdot h \cdot b}(K_1 \cdot b_1^2 + K_2 \cdot b_2^2) \quad \textit{(F13)}$$

$$K_{ser,wall} = \frac{b \cdot \delta_{vert}}{\delta_{vert} \cdot h^2 \cdot b}(K_1 \cdot b_1^2 + K_2 \cdot b_2^2) \quad \textit{(F14)}$$

Due to assumption of equal stiffness in all connections, stated in (F7), the final global wall stiffness becomes:

$$K_{ser,wall} = K_{ser} \cdot \frac{b_1^2 + b_2^2}{h^2} \quad \textit{(F15)}$$

GLOBAL LOAD-CARRYING CAPACITY OF WALL SYSTEM

Equation (F2) together with Equation (F9) gives:

$$F_{v,wall} = \frac{F_1 \cdot b_1 + F_1 \cdot \frac{b_2}{b_1} \cdot b_2}{h} = F_1 \frac{\left(b_1 + \frac{b_2^2}{b_1}\right)}{h} \qquad (F16)$$

That leads to the expression for the global load-carrying capacity of a wall system with 2 hold-downs:

$$F_{v,R,wall,2HD} = F_{v,R} \frac{\left(b_1 + \frac{b_2^2}{b_1}\right)}{h} \qquad (F17)$$

Finally, a general expression for the global load-carrying capacity of a wall system can be stated as follows:

$$F_{v,R,wall} = F_{v,R} \frac{\Sigma\left(\frac{b_i^2}{b_1}\right)}{h} \qquad (F18)$$

Global stiffness of wall system

Input parameters:

$b := 3000mm = 3\,m$ width of CLT wall

$h := 3000mm = 3\,m$ height of CLT wall

Distances between connections:

System with 2 hold-downs:

$b_{1.2HD} := 2625mm = 2.625\,m$

$b_{2.2HD} := 375mm = 0.375\,m$

System with 4 hold-downs:

$b_{1.4HD} := 2625mm = 2.625\,m$

$b_{2.4HD} := 1875mm = 1.875\,m$

$b_{3.4HD} := 1125mm = 1.125\,m$

$b_{4.4HD} := 375mm = 0.375\,m$

System with 8 hold-downs:

$b_{1.8HD} := 2812.5mm = 2.813\,m$

$b_{2.8HD} := 2437.5mm = 2.438\,m$

$b_{3.8HD} := 2062.5mm = 2.063\,m$

$b_{4.8HD} := 1687.5mm = 1.688\,m$

$b_{5.8HD} := 1312.5mm = 1.313\,m$

$b_{6.8HD} := 937.5mm = 0.938\,m$

$b_{7.8HD} := 562.5mm = 0.563\,m$

$b_{8.8HD} := 187.5mm = 0.188\,m$

Stiffness per hold-down, K.ser:

$K_{ser} := 36 \frac{kN}{mm}$

$K_{ser.inc} := K_{ser} \cdot 1.1 = 39.6 \frac{kN}{mm}$ stiffness of hold-down increased with 10 %

$K_{ser.dec} := K_{ser} \cdot 0.9 = 32.4 \frac{kN}{mm}$ stiffness of hold-down decreased with 10 %

Calculation of global wall stiffness, K.ser.wall for systems with 2, 4 and 8 hold-downs, for different connection stiffness, according to equation below:

$$K_{ser,wall} = K_{ser} \cdot \frac{\sum b_i^2}{h^2}$$

2 hold-downs:

$K_{ser.wall.2HD} := K_{ser} \cdot \frac{\left(b_{1.2HD}^{\ 2} + b_{2.2HD}^{\ 2}\right)}{h^2} = 28.13 \frac{kN}{mm}$

$K_{ser.wall.2HD.inc} := K_{ser.inc} \cdot \frac{\left(b_{1.2HD}^{\ 2} + b_{2.2HD}^{\ 2}\right)}{h^2} = 30.94 \frac{kN}{mm}$

$K_{ser.wall.2HD.dec} := K_{ser.dec} \cdot \frac{\left(b_{1.2HD}^{\ 2} + b_{2.2HD}^{\ 2}\right)}{h^2} = 25.31 \frac{kN}{mm}$

4 hold-downs:

$$K_{ser.wall.4HD} := K_{ser} \cdot \frac{\left(b_{1.4HD}^{2} + b_{2.4HD}^{2} + b_{3.4HD}^{2} + b_{4.4HD}^{2}\right)}{h^{2}} = 47.25 \frac{kN}{mm}$$

$$K_{ser.wall.4HD.inc} := K_{ser.inc} \cdot \frac{\left(b_{1.4HD}^{2} + b_{2.4HD}^{2} + b_{3.4HD}^{2} + b_{4.4HD}^{2}\right)}{h^{2}} = 51.98 \frac{kN}{mm}$$

$$K_{ser.wall.4HD.dec} := K_{ser.dec} \cdot \frac{\left(b_{1.4HD}^{2} + b_{2.4HD}^{2} + b_{3.4HD}^{2} + b_{4.4HD}^{2}\right)}{h^{2}} = 42.52 \frac{kN}{mm}$$

8 hold-donws:

$$K_{ser.wall.4HD} := K_{ser} \cdot \frac{\left(\begin{matrix} b_{1.8HD}^{2} + b_{2.8HD}^{2} + b_{3.8HD}^{2} + b_{4.8HD}^{2} \ldots \\ + b_{5.8HD}^{2} + b_{6.8HD}^{2} + b_{7.8HD}^{2} + b_{8.8HD}^{2} \end{matrix}\right)}{h^{2}} = 95.63 \frac{kN}{mm}$$

$$K_{ser.wall.4HD.inc} := K_{ser.inc} \cdot \frac{\left(\begin{matrix} b_{1.8HD}^{2} + b_{2.8HD}^{2} + b_{3.8HD}^{2} + b_{4.8HD}^{2} \ldots \\ + b_{5.8HD}^{2} + b_{6.8HD}^{2} + b_{7.8HD}^{2} + b_{8.8HD}^{2} \end{matrix}\right)}{h^{2}} = 105.19 \frac{kN}{mm}$$

$$K_{ser.wall.4HD.dec} := K_{ser.dec} \cdot \frac{\left(\begin{matrix} b_{1.8HD}^{2} + b_{2.8HD}^{2} + b_{3.8HD}^{2} + b_{4.8HD}^{2} \ldots \\ + b_{5.8HD}^{2} + b_{6.8HD}^{2} + b_{7.8HD}^{2} + b_{8.8HD}^{2} \end{matrix}\right)}{h^{2}} = 86.06 \frac{kN}{mm}$$

Load-carrying capacity per connection

Input parameters:

$d := 4.0mm = 4 \times 10^{-3}\,m$ — diameter of nail

$d_2 := 4$

$\rho_k := 420\,\frac{kg}{m^3}$ — characteristic density of timber

$l_{nail} := 60mm = 0.06\,m$ — length of nail

$u_1 := \frac{m^3}{kg}\cdot MPa\cdot mm^{0.3}$ — correction factor for embedment strength

$u_2 := mm^{0.4}$ — correction factor for yield moment

$f_{h.1.k} := 0.082\cdot\rho_k\cdot d^{(-0.3)}\cdot u_1 = 22.722\cdot\frac{N}{mm^2}$ — characteristic embedment strength in timber members, assumed without pre-drilled holes

$f_{h.2.k} := f_{h.1.k} = 22.722\cdot\frac{N}{mm^2}$

$\beta := \frac{f_{h.2.k}}{(f_{h.1.k})} = 1$

$f_u := 510MPa = 510\cdot\frac{N}{mm^2}$ — characteristic tensile strength, SS 304 steel

$M_{y.Rk} := 0.3\cdot f_u\cdot d^{2.6}\cdot u_2 = 5.624\cdot N\cdot m$ — yield moment

$t_1 := 30mm = 0.03\,m$ — thickness of outer layer of CLT wall element

$t_2 := l_{nail} - t_1 = 0.03\,m$ — penetration depth

Contribution from rope effect:

$F_{ax.Rk} := 1.25kN$ characteristic axial withdrawal capacity of fastener acc. to performance values of CNA nails from SIMPSON Strong-Tie

$limit := 15\% = 0.15$ limit for round nails' contribution to load-carrying capacity due to rope effect

Characteristic load-carrying capacity per fastener for fasteners in double shear:

$$F_{v.Rk.1} := f_{h.1.k} \cdot t_1 \cdot d = 2.727 \cdot kN$$

$$F_{v.Rk.2} := 0.5 \cdot f_{h.2.k} \cdot t_2 \cdot d = 1.363 \cdot kN$$

$$ratio := \frac{\left(f_{h.1.k} \cdot t_1 \cdot d\right)}{(2 + \beta)} = 908.877\,N$$

$$F_{v.Rk.3} := (1.05 \cdot ratio) \cdot \left[\sqrt{2 \cdot \beta \cdot (1 + \beta) \frac{4 \cdot \beta \cdot (2+\beta) \cdot M_{y.Rk}}{f_{h.1.k} \cdot d \cdot t_1^{\,2}}} - \beta \right] + \frac{F_{ax.Rk}}{4} \cdot limit = 1.189 \cdot kN$$

$$F_{v.Rk.4} := 1.15 \cdot \sqrt{\frac{2 \cdot \beta}{1 + \beta}} \cdot \sqrt{2 \cdot M_{y.Rk} \cdot f_{h.1.k} \cdot d} + \frac{F_{ax.Rk}}{4} \cdot limit = 1.21 \cdot kN$$

$$F_{v.Rk} := \min\left(F_{v.Rk.1}, F_{v.Rk.2}, F_{v.Rk.3}, F_{v.Rk.4}\right) = 1.19 \cdot kN$$

$F_{v.Rk.HD} := F_{v.Rk} \cdot 24 = 28.53 \cdot kN$ Characteristic load-carrying capacity of a hold-down (24 nails)

Design value of load-carrying capacity:

$k_{mod} := 0.9$ assumed service class 1 and short term action (wind)

$\gamma_M := 1.3$ partial factor for connections (Table 2.3)

$$F_{v.Rd} := k_{mod} \cdot \frac{F_{v.Rk}}{\gamma_M} = 0.823 \cdot kN$$

$F_{v.Rd.HD} := F_{v.Rd} \cdot 24 = 19.75 \cdot kN$ load-carrying capacity of a hold-down (24 nails)

Global load-carrying capacity of wall system

System with 2 hold-downs:

Characteristic:

$$F_{v.Rk.wall.2HD} := F_{v.Rk.HD} \cdot \left[\frac{\left(\frac{b_{1.2HD}^{2}}{b_{1.2HD}} + \frac{b_{2.2HD}^{2}}{b_{1.2HD}} \right)}{h} \right] = 25.47\,kN$$

Design value:

$$F_{v.Rd.wall.2HD} := F_{v.Rd.HD} \cdot \left[\frac{\left(\frac{b_{1.2HD}^{2}}{b_{1.2HD}} + \frac{b_{2.2HD}^{2}}{b_{1.2HD}} \right)}{h} \right] = 17.64\,kN$$

System with 4 hold-downs:

Characteristic:

$$F_{v.Rk.wall.4HD} := F_{v.Rk.HD} \cdot \left[\frac{\left(\frac{b_{1.4HD}^{2}}{b_{1.4HD}} + \frac{b_{2.4HD}^{2}}{b_{1.4HD}} + \frac{b_{3.4HD}^{2}}{b_{1.4HD}} + \frac{b_{4.4HD}^{2}}{b_{1.4HD}} \right)}{h} \right] = 42.8\,kN$$

Design value:

$$F_{v.Rd.wall.4HD} := F_{v.Rd.HD} \cdot \left[\frac{\left(\frac{b_{1.4HD}^{2}}{b_{1.4HD}} + \frac{b_{2.4HD}^{2}}{b_{1.4HD}} + \frac{b_{3.4HD}^{2}}{b_{1.4HD}} + \frac{b_{4.4HD}^{2}}{b_{1.4HD}} \right)}{h} \right] = 29.63\,kN$$

System with 8 hold-downs:

Characteristic:

$$F_{v.Rk.wall.8HD} := F_{v.Rk.HD} \cdot \left[\frac{\left(\frac{b_{1.8HD}^{2}}{b_{1.8HD}} + \frac{b_{2.8HD}^{2}}{b_{1.8HD}} + \frac{b_{3.8HD}^{2}}{b_{1.8HD}} + \frac{b_{4.8HD}^{2}}{b_{1.8HD}} \ldots + \frac{b_{5.8HD}^{2}}{b_{1.8HD}} + \frac{b_{6.8HD}^{2}}{b_{1.8HD}} + \frac{b_{7.8HD}^{2}}{b_{1.8HD}} + \frac{b_{8.8HD}^{2}}{b_{1.8HD}} \right)}{h} \right] = 80.84\,kN$$

Design value:

$$F_{v.Rd.wall.8HD} := F_{v.Rd.HD} \cdot \left[\frac{\left(\frac{b_{1.8HD}^{2}}{b_{1.8HD}} + \frac{b_{2.8HD}^{2}}{b_{1.8HD}} + \frac{b_{3.8HD}^{2}}{b_{1.8HD}} + \frac{b_{4.8HD}^{2}}{b_{1.8HD}} \ldots + \frac{b_{5.8HD}^{2}}{b_{1.8HD}} + \frac{b_{6.8HD}^{2}}{b_{1.8HD}} + \frac{b_{7.8HD}^{2}}{b_{1.8HD}} + \frac{b_{8.8HD}^{2}}{b_{1.8HD}} \right)}{h} \right] = 55.97\,kN$$